AD NUMBER

AD852788

LIMITATION CHANGES

TO:

Approved for public release; distribution is unlimited.

FROM:

**Distribution authorized to U.S. Gov't. agencies and their contractors;
Administrative/Operational Use; APR 1969. Other requests shall be referred to Air Force Weapons Lab., Kirtland AFB, NM.**

AUTHORITY

AFWL ltr 30 Nov 1971

AFWL-TR-
67-95,
Vol II

COMPENSATION AND AVALANCHE TECHNIQUES FOR TREE HARDENING

Volume II

Nuclear Damage on Avalanche Transistors and Diodes

Harold T. Cates L. T. Boatwright
W. W. Grannemann Goebel Davis, Jr.

University of New Mexico
Bureau of Engineering Research
Albuquerque, New Mexico 87106

Contract F29601-67-C-0017

TECHNICAL REPORT NO. AFWL-TR-67-95, Vol II

April 1969

AIR FORCE WEAPONS LABORATORY
Air Force Systems Command
Kirtland Air Force Base
New Mexico

DISCLAIMER NOTICE

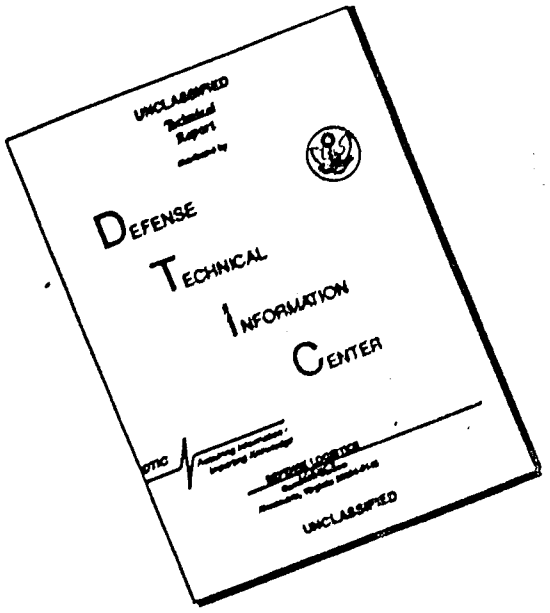

THIS DOCUMENT IS BEST QUALITY AVAILABLE. THE COPY FURNISHED TO DTIC CONTAINED A SIGNIFICANT NUMBER OF PAGES WHICH DO NOT REPRODUCE LEGIBLY.

COMPENSATION AND AVALANCHE TECHNIQUES FOR TREE HARDENING

Volume II

Nuclear Damage on Avalanche Transistors and Diodes

Harold T. Cates L. T. Boatwright
W. W. Grannemann Goebel Davis, Jr.

University of New Mexico
Bureau of Engineering Research
Albuquerque, New Mexico 87106
Contract F29601-67-C-0017

TECHNICAL REPORT NO. AFWL-TR-67-95, Vol II

FOREWORD

This report was prepared by the University of New Mexico, Bureau of Engineering Research, Albuquerque, New Mexico, under Contract F29601-67-C-0017. The research was performed under Program Element 6.16.46.01.D, Project 5710, Subtask 16.027, and was funded by the Defense Atomic Support Agency (DASA).

Inclusive dates of research were 15 November 1966 through 14 September 1967. The report was submitted 13 March 1969 by the Air Force Weapons Laboratory Project Officer, Dr. Julian S. Nichols (WLDE).

The principal investigator was Dr. W. W. Grannemann. Other investigators on the project were Dr. Lewellyn T. Boatwright, Dr. Harold Cates, and Dr. Goebel Davis, Jr.

Information in this report is embargoed under the US Export Control Act of 1949, administered by the Department of Commerce. This report may be released by departments or agencies of the US Government to departments or agencies of foreign governments with which the United States has defense treaty commitments, subject to approval of AFWL (WLDE), Kirtland AFB, NM, 87117.

This technical report has been reviewed and is approved.

Julian S. Nichols

JULIAN S. NICHOLS
Project Officer

Carl F. Davis

CARL F. DAVIS
Lt Colonel, USAF
Chief, Electronics Branch

George C. Darby, Jr.

GEORGE C. DARBY, JR.
Colonel, USAF
Chief, Development Division

ABSTRACT

(Distribution Limitation Statement No. 2)

An analytical model to describe the behavior of a forward biased or reverse biased (including avalanche breakdown) diode in a transient X-ray environment is developed. The calculated results are compared with experimental results. The avalanche multiplication phenomenon is related to the physical parameters of the device. Equivalent circuits for the device under irradiation are developed. The basic theory of avalanche transistor operation is reviewed and the critical design factors for operation of an avalanche circuit in a radiation environment are discussed. The circuits were tested in the range from 10^6 R/sec to over 10^{10} R/sec. Circuits were tested with and without different types of junction compensations. Avalanche diodes and transistors were also irradiated in a neutron environment. Some of the diodes and transistors were still functioning properly at doses of 8.6×10^{15} nvt. An avalanche circuit was shown to be relatively insensitive to a neutron environment after exposure to neutron fluence in excess of 10^{15} n/cm^2.

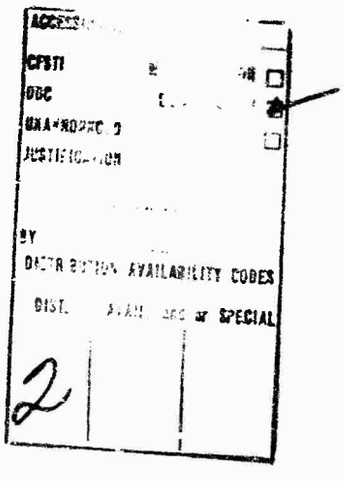

AIR FORCE WEAPONS LABORATORY
Air Force Systems Command
Kirtland Air Force Base
New Mexico

CONTENTS

CONTENTS (cont'd)

ILLUSTRATIONS

ILLUSTRATIONS (Cont'd)

ILLUSTRATIONS (cont'd)

ILLUSTRATIONS (cont'd)

ILLUSTRATIONS (cont'd)

ILLUSTRATIONS (cont'd)

TABLES

LIST OF PRINCIPAL SYMBOLS

A	junction area in cm^2
BV_{CBO}	collector to base voltage with the emitter lead open circuited
BV_{CEX}	collector to emitter breakdown voltage with a specified circuit from base to emitter
C_D	diode depletion capacitance
D_1	the base emitter idealized diode
D_n	electron diffusion constant, (cm^2/sec)
D_p	hole diffusion constant (cm^2/sec)
d_n	depletion width in n-region
d_p	depletion width in p-region
E	electric field
e	$\frac{n_i^2-np}{\tau_{pr}(n+n_r) + \tau_{nr}(p+p_r)}$ = carrier emission or generation
erf	error function or probability integral where $\text{erf } x = \frac{2}{\sqrt{\pi}} \int_o^x e^{-x^2} dx$
$\bar{e}$	average energy in electron volts to form one hole-electron pair
f_t	gain-bandwidth product frequency
f_α	alpha cutoff frequency
g	electron hole pair generation rate = pairs/sec-cm^3

$I(t)$	external circuit transient photocurrent
I_B	base current
i_C	collector current
I_{COl}	transistor T_1 collector to base leakage current when the emitter to base junction is reverse biased
I_{DS}	bulk diffusion saturation current
I_G	charge generation current in the depletion layer (I_{rg})
I_{ppl}	the X-ray induced transient primary photocurrent produced in T_1
I_R	reversed diode current
I_{SL}	surface leakage current
$i^*_{pp}(t)$	radiation induced avalanche multiplied primary photocurrent
$i_{pp}(t)$	radiation induced primary photocurrent
j_n	electron current density (ampere/cm^2)
j_p	hole current density (ampere/cm^2)
K	proportionality constant; approaches unity for a reverse bias greater than one volt
k	Boltzmann constant (1.380×10^{-23} pulses/^oK)
K_τ	lifetime damage constant
$\frac{kT}{q}$	0.026 v at room temperature ($T = 300^oK$)
M	the avalanche multiplication factor

M_1	$\frac{1}{1 - \left(\frac{V_{CE}}{BV_{CBO}}\right)^{n'}}$ the avalanche multiplication factor for transistor T_1
M_2	avalanche multiplication factor associated with transistor T_2
$Mi_{pp}(t)$	avalanche multiplied primary photocurrent
N_A	acceptor concentration in n-region
N_D	donor concentration in p-region
N_i	majority carrier concentration
$\frac{\Delta N_i}{\Delta \Phi}$	carrier removal rate
n'	empirical constant that varies from approximately 2 to 10
p	hole concentration
post-test	electrical testing of the device after exposure to nuclear radiation
pre-test	electrical testing of the device prior to any irradiation
q	electron charge $= 1.6 \times 10^{-19}$ coulomb
R_A	avalanche collector to emitter resistance
R_{AV}	avalanche diode resistance
R_L	load resistor
R_ℓ	resistance of lightly doped region
R_S	shunt leakage resistance around the junction

R_{se}	the input signal source equivalent output resistance
R_V	viewing resistor
r_b	total diode bulk and spreading resistance
r_{bb}	the transistor base spreading and bulk resistance
r'_{be}	the transistor base emitter junction equivalent internal resistance
r_s	the transistor collector bulk series resistance
T	absolute temperature
T_b	transit time
$V_{\alpha M}$	collector-emitter breakdown voltage when $\alpha M=1$
V_B	breakdown voltage
V_{CE}	the collector to emitter voltage
V_{CP}	the base emitter contact potential $\cong$ 0.6 volt for silicon
V_D	total voltage across diode
V_j	reverse voltage across junction
W	depletion width
W_b	base thickness
α_n	ionization coefficient for an electron
α_o	h_{fb}, the low frequency common base forward transfer ratio
α_p	ionization coefficient for a hole
β_{M_1}	$\frac{M_1\alpha_o}{1-M_1\alpha_o}$

β_o	initial gain of common emitter
β_Φ	gain at some fast-neutron fluence
μ_n	electron mobility (cm^2/volt-sec)
μ_p	hole mobility (cm^2/volt-sec)
σ_i	crystal conductivity (i = n or p)
τ_n	lifetime in seconds for the minority carrier electrons in the p-material
τ_o	carrier lifetime before irradiation (Φ = o)
τ_p	lifetime in seconds for the minority carrier electrons in the n material
Φ	fast neutron fluence

SECTION I

INTRODUCTION

At the present time, various circuits utilizing semiconductor devices are being incorporated into sophisticated military weapon systems which might be subjected to severe radiation environments. Previous research efforts have resulted in the evaluation of various semiconductor circuits and devices in a nuclear environment. These efforts have shown the need for further theoretical investigation and experimental evaluation of these circuits and new circuits to develop additional hardening criteria and compensation techniques.

The present understanding of the basic mechanisms involved in the production of undesirable radiation induced transient and permanent effects in avalanche semiconductor devices is still in the evolutionary stage. As semiconductor devices and circuits become more and more complex, the need also arises for equivalent circuit models of these devices and circuits. These device models can be used in computer programs for complex circuits to predict the approximate total circuit responses and correlate these responses with the actual experimental results.

An experimental and theoretical study of the basic aspects of avalanche breakdown was made so that a comparison of theoretical model responses and actual device

responses under radiation could be made. Models for avalanche diodes and transistors were developed for both the cutoff and avalanche regions of operation.

The avalanche diodes investigated were p+n silicon alloy diodes with breakdown voltages in the range of 8 to 22 volts. The significant effect of X-ray radiation on these devices is the production of electron-hole pairs which results in the production of a transient photocurrent. The photocurrent is shown to be multiplied by the device's avalanche multiplication factor M, which enhances the normally observed photocurrents. As the external voltage across the device approaches the breakdow· voltage, the photocurrent increases about an order of magnitude above that observed at low voltage. Beyond breakdown, the photocurrent tends to decrease again. This is a basic phenomenon which is characteristic of the avalanche device. When the device is in the breakdown region, a longer tail (or slower decay) is observed on the resulting radiation induced photocurrent. This behavior is caused by the buildup of an electric field inside the lowly doped n-region of the diode.

The basic theory of avalanche transistor operation was reviewed and the critical design factors were discussed. Simplified equivalent circuits were developed for avalanche transistor operation under transient X-ray irradiation. Since avalanche transistor circuits are normally sensitive to transient radiation, methods of circuit design and hardening techniques were developed. Using these methods,

optimum designs for radiation-hardened-avalanche-transistor circuits were established and were tested in a transient radiation environment.

Basic theory of neutron degradation of semiconductors was reviewed, and critical design factors of semiconductors in relation to neutron damage were discussed. Avalanche diodes and transistors were irradiated in a neutron environment, and pre- and post-data were taken. Using these results, the theory of operations of avalanche devices and basic neutron degradation of semiconductors, upper limits of exposure were established that still permitted the devices to operate satisfactorily.

SECTION II

THEORY OF AVALANCHE SEMICONDUCTOR DEVICES

1. Avalanche Devices and Phenomena

In most p-n junctions, the predominant physical mechanism which gives rise to reverse breakdown is called the avalanche effect. Many times the avalanche effect is confused with the Zener effect, but these effects are two entirely different phenomena. The avalanche diode or Zener diode is a solid state semiconductor device which uses certain features of the reverse electrical characteristics of a p-n junction. Also the forward characteristic of these devices can be used for low voltage reference or as temperature compensation for the reverse-biased junction (reference 1).

The avalanche effect is a nondestructive carrier multiplication that occurs in the depletion region. When the voltage across a reverse-biased p-n junction is increased, it is found that the current will gradually increase. As the voltage approaches the breakdown voltage of the junction, the current increases very rapidly, and it is only limited by the external circuit resistance. This phenomenon occurs because the minority carriers, which are thermally or otherwise generated, diffuse to the junction, and they are acc .erated by the high field region of the reverse-biased junction. If the free electron or hole drifting through the depletion region acquires sufficient

energy from the field, it can ionize the atoms in the depletion region by collision with them. This collision ionizes the atom and produces a free electron-hole pair. The ionized electron-hole pair, upon gaining sufficient energy, is capable of repeating the above process, and so on, resulting in an avalanche multiplication. Thus, the process is cumulative and may result in a tremendous increase in current, depending on the voltage across the device.

In making diodes with low breakdown voltage, large doping levels N_A and N_D are required. But as the doping levels get too large, another breakdown phenomenon called Zener breakdown takes over for an electric field of 10^6 volts/cm or greater. The Zener breakdown is a direct rupture of the valance bonds, caused by the large field developed across the depletion region. This field is sufficiently large to liberate electrons from the covalent bond producing free electron-hole pairs with the direct excitation of electrons from the valence band to the conduction band (reference 2).

The liberated electron-hole pair acts as a charge carrier, and thus increases the current. Therefore, in the Zener breakdown, an energetic ionizing carrier is not required, as the Zener mechanism is quantum mechanical in nature (analogous to tunneling). For instance, in a field of 10^6 volts/cm extending over a distance of 10 Å, a carrier would only gain a maximum energy of 0.1 volt. For

avalanche breakdown to take place, approximately 3.6 electron volts per electron-hole pair must be produced. Thus, the above field is not enough for ionizing collision, but this field would still produce Zener breakdown (reference 2). Consequently, the attempt to make a p-n junction with a breakdown voltage below 5 volts requires heavier doping of the p and n region. This reduces the width of the depletion region in which a particle can gain energy for an ionizing collision, and the Zener mechanism becomes the predominant cause of breakdown.

At voltages less than the Zener or avalanche breakdown, another form of breakdown may occur because of the heat produced by the current flowing through the depletion region. The heat increases the thermal generation of free electron-hole pairs. This effect is cumulative, and if the temperature of the junction becomes sufficiently high, a large current increase will be observed. But this effect is small in comparison to the Zener or avalanche and usually can be ignored. There is also the possibility of surface breakdown, but devices are available that minimize this effect.

A typical current-voltage characteristic of a diode is shown in figure 1. When the diode forward current becomes sufficiently large, a deviation in plotting the universal diode equation is observed. This deviation is caused by a significant voltage drop produced in the contacts and semiconductor material. Also, when the diode reaches breakdown, the diode equation no longer applies. The reverse breakdown

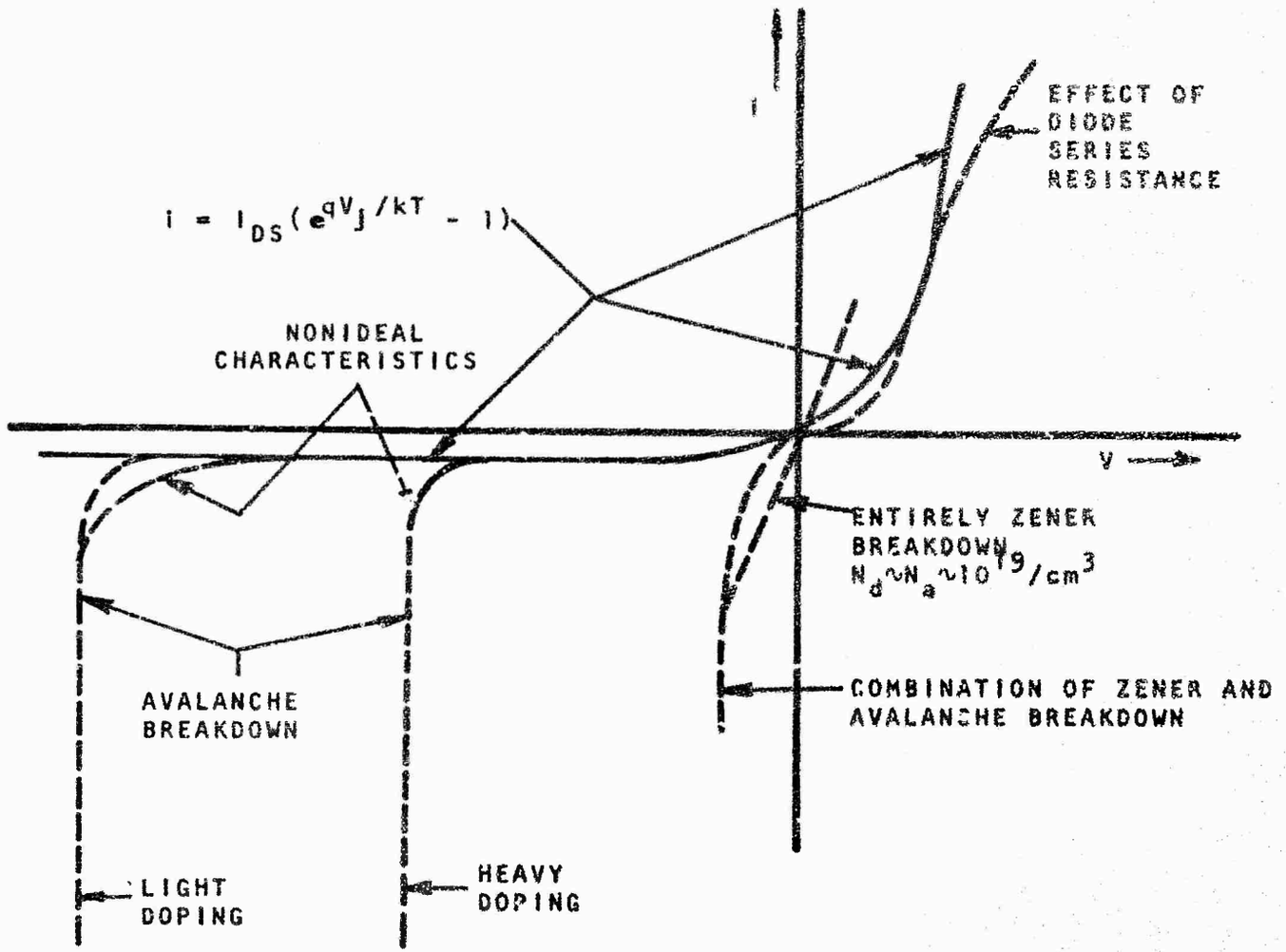

Figure 1. Current-Voltage Characteristic of a Diode

voltage may be anywhere from a few volts to around 1,000 volts, depending mainly on the conductivity of the various regions (increasing the temperature also will increase the conductivity) and the type of material. The reverse breakdown does not have to be destructive, as some diodes are purposely made to operate in this region. If the diode is operated in this region, an external circuit is used to limit the current to prevent appreciable heating and permanent damage to the junction. However, by using an appropriate heat sink, it is possible to make and use diodes which can dissipate watts at their breakdown voltage. The Zener diodes, avalanche diodes, or breakdown diodes can be used in the fields of voltage regulation and clipping, and for voltage reference purposes.

The universal diode equation for an ideal reverse-biased diode below breakdown is given by

$$I_R = I_{DS}(e^{qv_j/kT} - 1) \cong - I_{DS} \qquad (1)$$

where

I_R = reverse diode current

I_{DS} = bulk diffusion saturation current

q = electron charge (1.6019×10^{-19} coulomb)

v_j = voltage across junction (negative for reverse bias)

k = Boltzmann constant (1.380×10^{-23} J/°K)

T = absolute temperature

$\frac{kT}{q}$ = 0.026 v at room temperature ($T = 300°K$)

In reality, the total reverse current for a p-n junction is the sum of three components, namely

$$I_R = I_{DS} + I_{SL} + I_G \tag{2}$$

where

I_{DS} = bulk diffusion saturation current

I_{SL} = surface leakage current

I_G = charge generation current in the depletion layer

Neglecting I_{SL}, experimental measurements reveal that at room temperature and above I_{DS} is much greater than I_G in germanium, but in silicon I_{DS} is so small that the generation current I_G predominates. I_G has been shown by Pell (reference 3) to vary as

$$I_G = KqWAe \tag{3}$$

where

K = proportionality constant which approaches unity for a reverse bias greater than one volt

W = depletion width

A = junction area

$e = \dfrac{n_i^2 - np}{\tau_{pr}(n + n_r) + \tau_{nr}(p + p_r)}$ = carrier emission or generation.

From the above discussion on avalanche, one would expect the reverse bulk current in the diode to exhibit a multiplication effect, that is

$$I_R = - M(I_{DS} + I_G) \tag{4}$$

where the negative signs indicate conventional current is flowing from the n to the p side of the junction and M represents the multiplication factor.

It is well known that the number of minority carriers which are multiplied may be controlled by means of an emitter junction which is positioned in close proximity to the reverse-biased, multiplying collector junction (reference 4). This type of behavior is often referred to as an n-p-n or p-n-p avalanche mode of operation or as an avalanche transistor. The device is capable of exhibiting emitter current multiplication greater than one, and it is used mainly in the field of switching (pulse generators, counter circuit, regenerative pulse amplifier) and transmission application. For switching application, it can have an alpha greater than one and a negative resistance, as do point-contact or hook-collector transistors. The negative resistance region can be used to reduce losses in transmission systems. But the design of circuits using avalanche transistors is quite difficult as the devices may be unstable and/or display a high degree of distortion due to the alteration of the collector characteristics from avalanche multiplication.

In most transistors the switching speed is limited because of storage of minority carriers. However, in bistable type circuits using avalanche transistors, the collector junction never becomes forward biased (transistor never goes

into the current saturation region) and the problem of the usual storage of minority carriers does not occur. The multiplication process is extremely fast and in most transistors this is on the order of nanoseconds. Thus, any significant charge storage effect caused from radiation would not seem to occur. Depending on the operating location of this device, it is perhaps possible to pick out an operating point that would minimize the change in output voltage under radiation. This section will discuss the avalanche breakdown theory and its application in circuits employing diodes and transistors operating in their avalanche regions.

2. Diode Avalanche Breakdown Theory

McKay (references 5 and 6) used a modified form of the Townsend discharge theory for gases to explain the avalanche mechanism responsible for breakdown in reverse-biased p-n junctions. In our derivation we will modify McKay's derivation, and we will define an ionization coefficient α_n as the number of electron-hole pairs/cm^3 produced by an ionizing electron per unit distance traveled, and an ionization coefficient α_p as the number of electron-hole pairs/cm^3 produced by an ionizing hole per unit distance traveled. As shown in figure 2, the space charge region of a reverse-biased p-n junction has a width W and plane parallel geometry. In a step p+n junction, the n-region resistivity is much higher than the p-region resistivity so that the depletion region spreads almost entirely into the n-region. Also the

reverse diffusion current and/or any diffusion primary photocurrent consists mainly of minority holes p_o/cm^3 that diffuse from the n-region. We assume that the number of holes/cm^3 injected into the space charge region at $x = 0$ is p_o, and these holes are capable of producing more electron-hole pairs in the region from $x = 0$ to $x = W$. We assume that the number of holes/cm^3 created in the space charge region by electrons and/or holes is p_c. Then the number of holes generated between x and $x + \Delta x$ can be expressed as

$$p(x + \Delta x) = p(x) + p_{generated} - p_{recombined} \qquad (5)$$

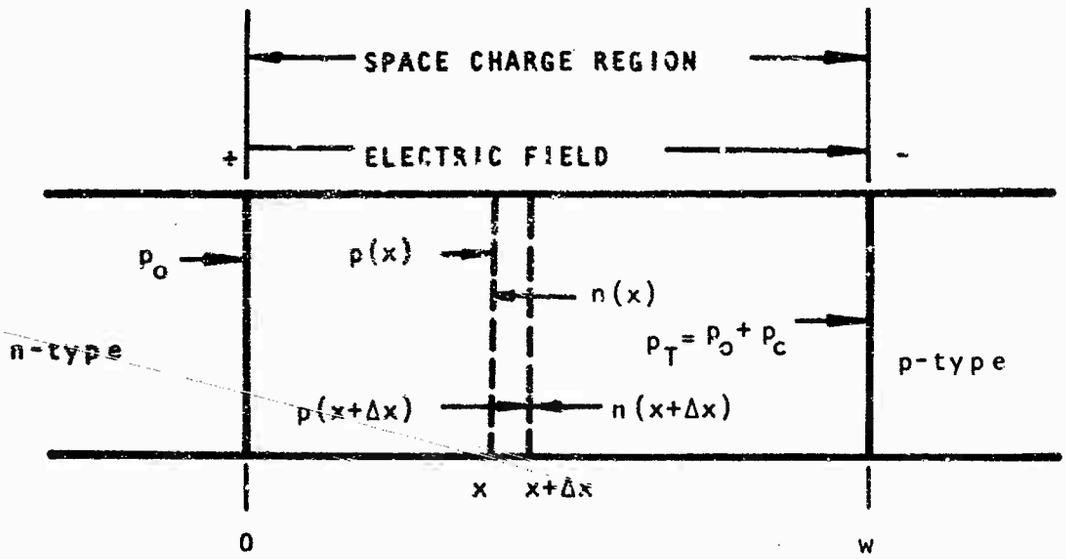

Figure 2. Avalanche Multiplication Region

We know that the time required for an ionized carrier to cross the high field-space region of a typical diode is about 10^{-9} second or less, but the recombination times are of the order of 10^{-6} second (reference 6). Therefore, if we assume that the loss of carriers by recombination in the depletion region is negligible, then the neglecting of the recombination term in the above equation should not introduce any noticeable error. Assuming that the generation of a carrier/cm^3 is proportional to the total number of carriers/cm^3 there, equation (5) becomes

$$p(x + \Delta x) - p(x) = p(x)\alpha_p \Delta x + n(x + \Delta x)\alpha_n \Delta x \qquad (6)$$

Dividing by Δx and taking the limit as $\Delta x \to 0$ we get

$$\frac{dp(x)}{dx} = p(x)\alpha_p + n(x)\alpha_n = [p_T - n(x)]\alpha_p + n(x)\alpha_n \qquad (7)$$

where p_T is the total number of holes/cm^3 at $x = W$.
The change in holes/cm^3 (hole generation) must equal the change in electron/cm^3 (electron generation) or, in equation form, we say

$$\frac{dn(x)}{dx} = -\frac{dp(x)}{dx} = -(\alpha_n - \alpha_p)n(x) - p_T\alpha_p \qquad (8)$$

or

$$\frac{dn(x)}{dx} + (\alpha_n - \alpha_p)n(x) = -p_T\alpha_p \qquad (9)$$

Solving the above first order differential equation, we obtain

$$n(x) = e^{-\int_o^x (\alpha_n - \alpha_p)dx'} \left[c - \int_o^x p_T \alpha_p e^{\int_o^\eta (\alpha_n - \alpha_p)dx'} d\eta \right] \quad (10)$$

Putting in the boundary conditions that $n(x = W) = 0$ and $n(x = 0) = p_T - p_o$ and simplifying,

$$1 - \frac{1}{M} = \int_o^W \alpha_p e^{\int_o^x (\alpha_n - \alpha_p)dx'} dx \quad (11)$$

where $M = p_T/p_o$, the multiplication factor. If $\alpha_n = \alpha_p = \alpha_e$, an effective ionization factor, the above equation reduced to

$$1 - \frac{1}{M} = \int_o^W \alpha_e dx \quad (12)$$

which is McKay's result. An analogous expression holds for electrons if the initiating carriers are electrons. As the integral in equation (12) approaches unity, M approaches infinity; and when the integral attains unity, M equals infinity and breakdown has occurred.

In the above derivation we have neglected the past history of the ionizing carrier and have assumed that α_n or α_p is solely a function of the electric field E. We have also assumed that at any instant of time the number of electrons/cm^3 and holes/cm^3 in the space charge region is relatively low and that we can neglect their mutual and self-interaction. In the above analysis we have essentially followed only the history of one carrier. The other carrier will automatically

be taken care of in order to record that one carrier has completely crossed the space charge region.

We can support the previous derivation by a simplified mathematical treatment of avalanche multiplication. We know that the carrier and those created within the depletion region have a distribution of energies, a distribution of time between collisions, and a distribution of direction (reference 2). Therefore, not all the carriers that enter the depletion region nor those created will be capable of producing new carrier pairs. We can say then that there is a probability that a given carrier or those created will produce an electron-hole pair as it crosses the depletion region.

Suppose that n_o electrons/cm^3 enter the depletion region such that P percent of them suffer an ionizing collision in crossing the space-charge region. In an ionizing event an electron-hole pair is created, but the pair together move the same distance that one electron would move in crossing the entire region. Therefore, if the electron and hole have the same probability for ionizing, we can assume that each pair created has the same probability P of creating another pair. That is, n_o electrons/cm^3 produce Pn_o pairs/cm^3; these Pn_o pairs/cm^3 can produce $P(Pn_o/cm^3)$ more pairs, etc.; or the number of electrons/cm^3 leaving the transition region under these conditions is given by

$$n_{out} = n_o + Pn_o + P(Pn_o) + P(P)(Pn_o) + \ldots = n_o \sum_{k=o}^{\infty} P^k \quad (13)$$

If we define the multiplication factor as the ratio of the number of electrons/cm^3 leaving the region to the number which enter, we can solve the previous equation for M and obtain

$$M = \frac{n_{out}}{n_o} = \sum_{k=0}^{\infty} P^k = \frac{1}{1 - P} \text{ when } |P| < 1 \qquad (14)$$

using the properties of a geometric series. P in the above theory can be related to previous discussion by

$$P = \int_o^W \alpha_e(E)dx = 1 - \frac{1}{M} \qquad (15)$$

which is less than one except at breakdown where $M \to \infty$, $P \to 1$, and

$$\int_o^W \alpha_e(E)dx = 1 \qquad (16)$$

If P is equal to 1/2, M is 2 and only half of the primary electrons on the average have ionizing collisions. Similarly, only half of the first generation pairs can produce ionizing collisions to form second generation pairs; only half of the second generation pairs can produce ionizing collisions to form third generation pairs; etc. This form of behavior is illustrated in figure 3 for n_o equal to four. It must be kept in mind in this diagram that each ionized pair is treated as one carrier having the ionizing probability

P of 1/2. The subscript o in the figure indicates an initial carrier entering the region, and the subscript i indicates an ionized carrier.

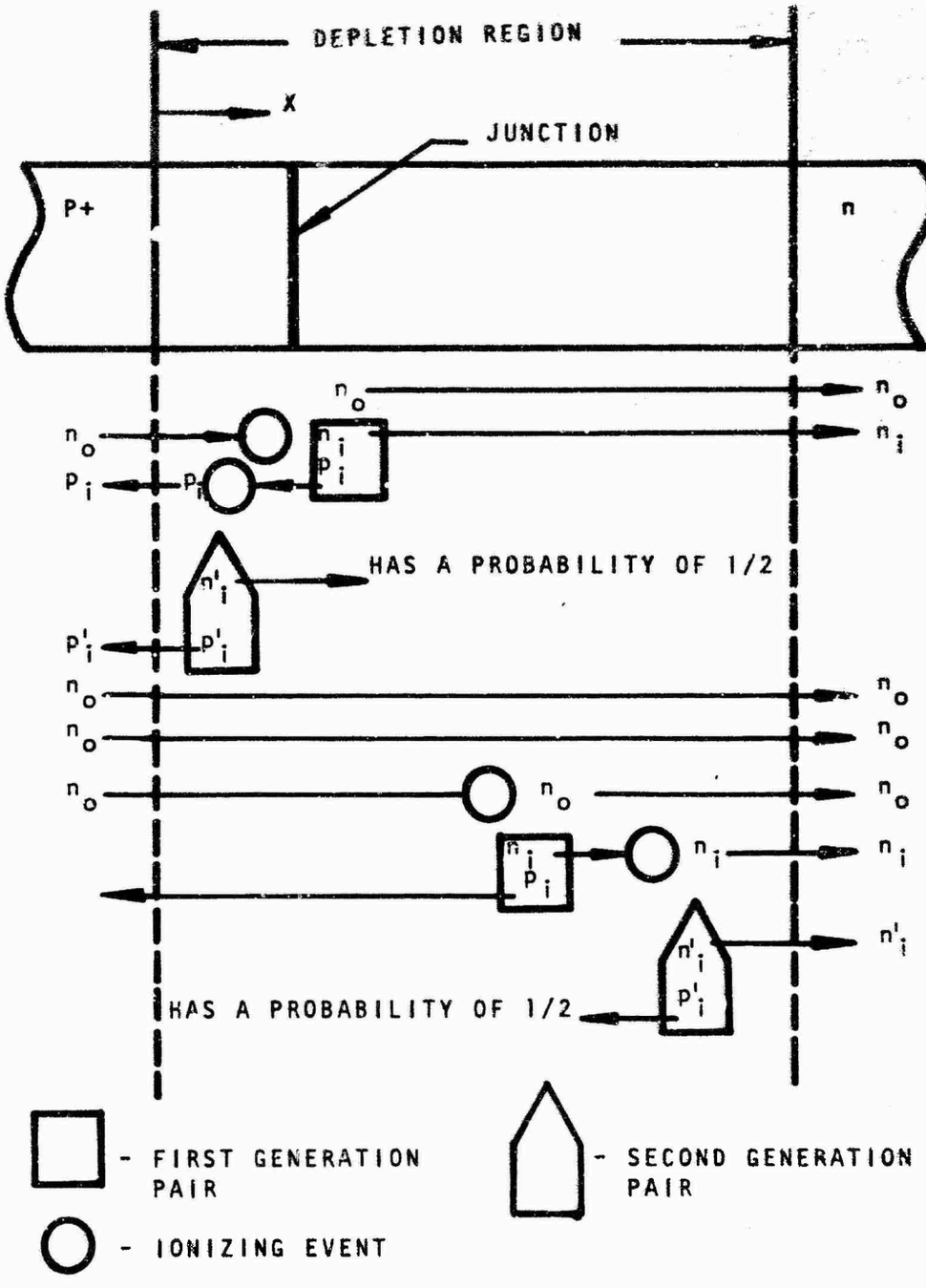

Figure 3. Pictorial Representation of Avalanche Multiplication for P=1/2

It has been shown by Miller (references 7 and 8) that P and M depend on the reverse bias, V_j, applied across the depletion region. When $V_j = 0$, $M = 1$, and $P = 0$, and, when $V_j \rightarrow$ the avalanche breakdown voltage V_B, $M \rightarrow \infty$, and $P \rightarrow 1$. A reasonable fit to experimental data which also satisfies the above properties is given by

$$P = \left(\frac{V_j}{V_B}\right)^{n'} \tag{17}$$

where n' is an empirical constant depending on geometrical factors and material constants. Substituting the above expression for P into equation (15), we obtain

$$M = \frac{1}{1 - \left(\frac{V_j}{V_B}\right)^{n'}} \tag{18}$$

A typical plot of M as a function of V_j/V_B is shown in figure 4 for different values of n'. From this plot one sees that the multiplication for low value of voltage is very small and can be approximated by one. However, depending on n', above a certain threshold voltage the multiplication effect takes over and becomes large.

As discussed in Appendix II, the depletion region of a p+n junction expands almost entirely into the lightly doped n-side, and the following approximations hold for the depletion width W, the electric field E, and the junction voltage V_j:

$$W = \sqrt{\frac{-\epsilon_r \epsilon_o V_j}{qN_D}} = W_1 \sqrt{-V_j} = \frac{W_1^2 E_o}{2} \tag{19}$$

$$E = \frac{qN_D W}{\epsilon_r \epsilon_o}\left(\frac{x}{W} + 1\right) = E_1\left(\frac{x}{W} + 1\right); -W \le x \le 0 \tag{20}$$

$$-V_j = \int_{-W}^{0} E \cdot dx = \frac{E_c W}{2} = \frac{E_o^2 W_1^2}{4} \tag{21a}$$

$$E_o = \frac{-2V_j}{W} = \frac{-2V_j\sqrt{qN_D}}{\sqrt{-2\epsilon_r \epsilon_o V_j}} = \sqrt{\frac{2q}{\epsilon_r \epsilon_o}}\left(|V_j| N_D\right)^{1/2} \tag{21b}$$

where W_1 is the junction width when the reverse bias is 1 volt, E_o is the maximum electric field, and V_j is the junction bias measured with respect to n side (i.e. for a reverse-biased condition as above, V_j is negative, and it includes the externally applied voltage and the built-in contact potential). In the Zener hypothesis, breakdown occurs when a critical field is reached anywhere in the junction. This critical field is a constant at a given temperature and would be reached at the breakdown voltage, hence,

$$(E_o) = \text{constant} = \sqrt{\frac{2q}{\epsilon_r \epsilon_o}}\ |V_B|^{1/2}\ N_D^{1/2} \tag{22}$$

or

$$V_B = \frac{(\text{constant})^2 \frac{\epsilon_r \epsilon_o}{2q}}{N_D} \tag{23}$$

Thus, the Zener theory predicts a breakdown voltage which is inversely proportional to the doping density of the lightly doped side or proportional to the resistivity of the lightly doped side. The Zener theory has been experimentally shown not to hold, but that breakdown can be described from the avalanche theory.

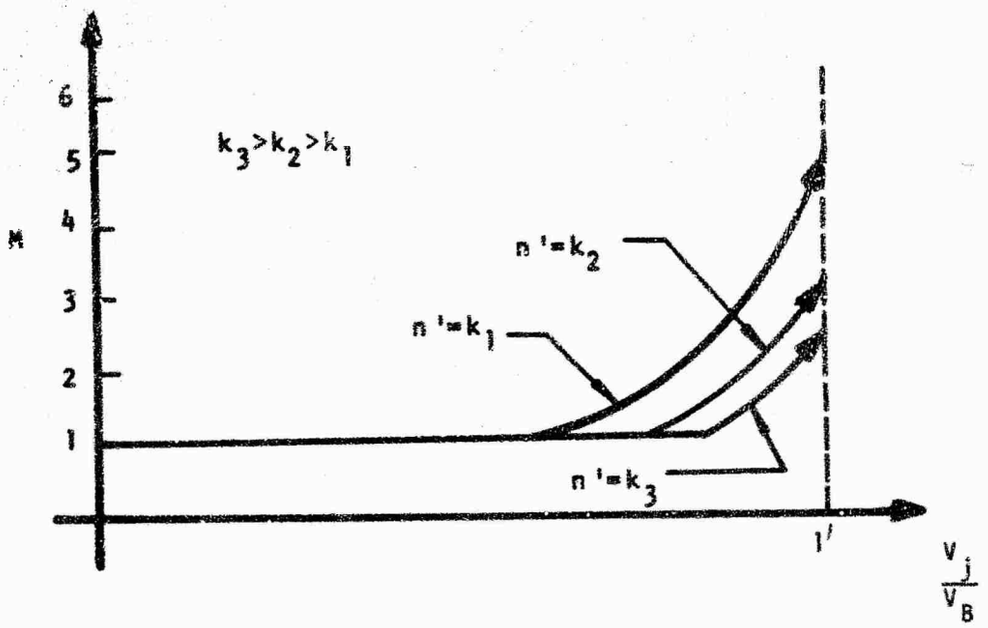

Figure 4. M as a Function of V_j/V_B for Different Values of n'

At very high multiplication rates, the number of electrons and holes participating in the avalanche process is essentially equal, and so one would expect the breakdown voltage of a p+n or an n+p junction to be approximately equal (reference 8).

In germanium the ionization rate for holes is greater than that for electrons by about a factor of two. This difference between the ionization rates is reflected in the empirical multiplication laws for p+n and n+p diodes. In an n+p junction the average ionization rate initially starts up the electron ionization curve for low voltages. As the voltage increases, a higher and higher percentage of the particles participating in the avalanche process is holes. Thus, the multiplication rises sharply with increasing voltages as the average particle ionization rate rises toward the hole ionization rate. A similar argument would tend to make the multiplication in a p+n junction more gradual.

3. Avalanche Transistor

Three basic modes of use for switching transistor circuits are the avalanche mode, saturation mode, and current mode. The area the switching transistor circuits fall into depends on the operation conditions and the portions of the transistor output characteristics utilized. In all three modes, the off region is characterized by the intersection of the load line with the cutoff region of the transistor. In a saturated mode switch the maximum voltage change which occurs at the collector with switching is approximately equal to the collector supply voltage. However, as we shall see later in this section, the maximum allowable

voltage swing in the avalanche mode depends not only on the characteristics of the transistor, but also on the transistor base circuitry. Basically, avalanche mode switching is nothing more than a rapid transition from collector base diode breakdown to the collector emitter type breakdown.

Transistors operating in the avalanche mode can give rise to nanoseconds rise time pulses by operation in the negative impedance area of the common-emitter-breakdown region. The area of operation of an avalanche transistor may be understood with the aid of figure 5, which shows an n-p-n transistor biased in the avalanche mode. Initially, we bias the base so that $I_{BR} = I_{BR_1}$ is a small reverse base current, which maintains the transistor operating at point A. If a positive pulse is applied so that the base current is reduced to zero, the transistor operating point shifts to point B' within a few nanoseconds (assuming V_{CC} can supply the current through R_C and the device can dissipate the power). After the trigger pulse is over, the operating point shifts to B and remains at that point. However, if a negative pulse is applied so that A is the only stable operating condition on the load line, then the transistor returns to A. Point A' is not a stable point because of the inherently negative resistance of the device at this point.

Some of the main advantages of avalanche circuitry are its extremely fast rise time, low cost due to few circuit components,

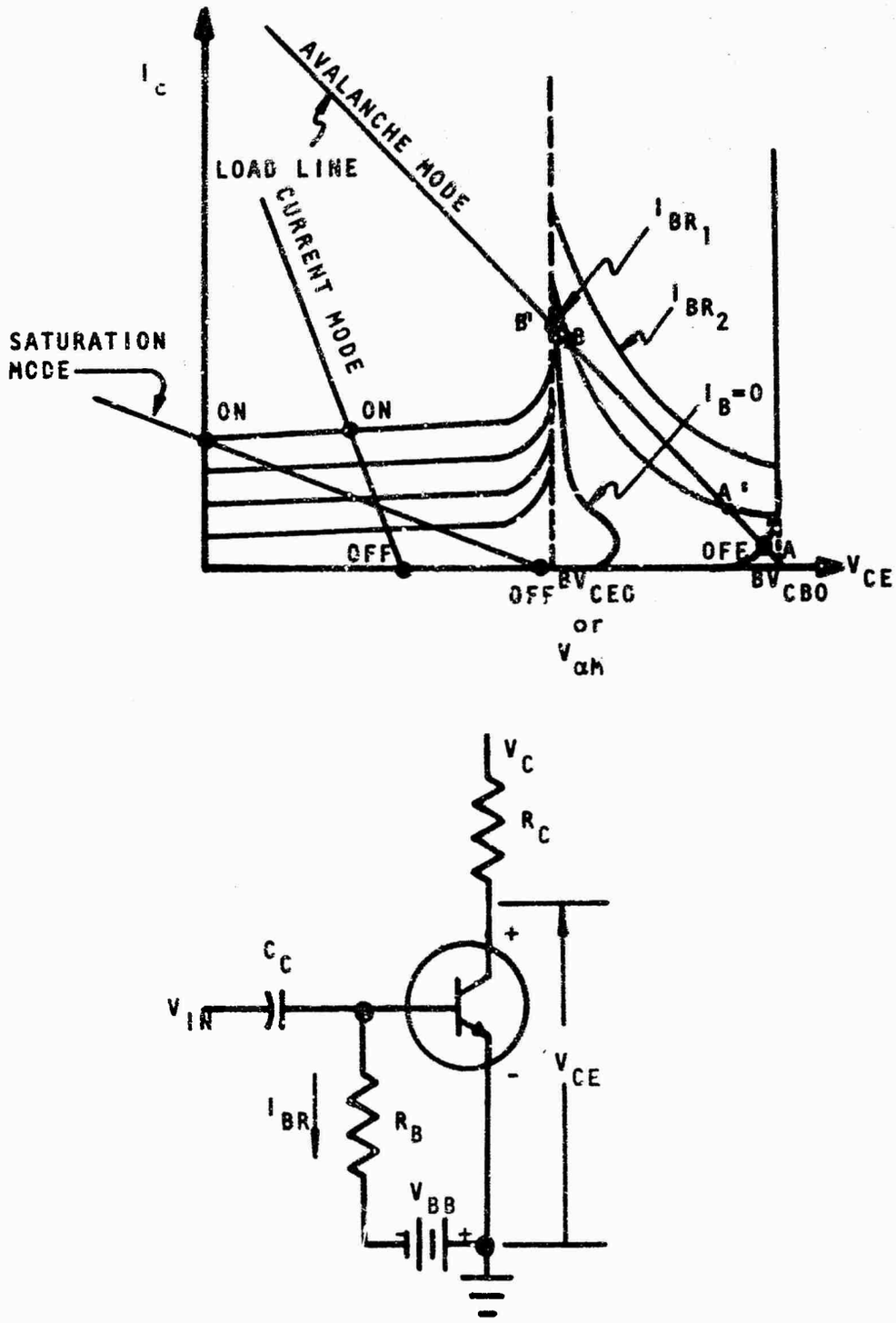

Figure 5. Typical Bias and Characteristic of a Transistor in a Basic Avalanche Mode Circuit

minimum temperature sensitivity, large voltage and current gain, and small delay time. However, associated with the advantages are disadvantages, such as large ratio of recovery time to rise time, a delay time associated with the input, limited repetition rate because of transistor power dissipation capability and circuit design, and possibility of transistor failure. However, not all the disadvantages listed have to be present in a particular application, as they may be minimized without compromising the advantages of avalanche circuitry.

It has been found possible to design an avalanche transistor pulse generator with peak power of about 500 W and voltage comparison circuits that have nanoseconds rise times. The shape of the voltage pulse can be changed by using charge lines, and the turn-off time can be decreased with the use of another avalanche transistor. Most of these circuits require some means of driving the transistor into avalanche and then bringing it out again, which can be accomplished by various methods. The circuits we will discuss have been designed for practicality and for understanding transient radiation effects rather than optimization of circuitry. Avalanche circuitry has not found too great an application in logic circuits as avalanche circuits are usually a-c coupled, which prevents the circuits from remaining in the "on state" for long periods of time.

As has been discussed earlier, avalanche multiplication occurs in a reverse biased p-n junction as a result of impact ionization produced by mobile charge carriers. As a result of this ionization, we defined a multiplication factor M as the number of electron-hole pairs produced per carrier entering the depletion layer. This increases the normal bulk leakage current by M. At high enough voltage, the multiplication factor becomes infinite, and breakdown is attained. In a silicon diode most of the ionizing carriers are thermally generated; however, in a transistor, both the injected carriers and thermally generated carriers will be multiplied. The injected carriers into the collector depletion region can be controlled by the emitter and base currents.

A good empirical fit to the breakdown characteristics of many transistor types is given by (reference 9)

$$M = \frac{1}{1 - \left(\frac{V_{CB}}{BV_{CBO}}\right)^{n'}} \qquad (24)$$

where

V_{CB} = collector to base voltage

BV_{CBO} = collector to base breakdown voltage with the emitter lead open-circuited

n' = empirical constant that varies from approximately 2 to 10

The parameter n' controls the sharpness of the onset of breakdown. The larger n' is, the sharper the onset of breakdown. That is, M continues at nearly unity until V_{CB} approaches very close to BV_{CBO} for large n' and then increases rapidly. If we multiply equation (24) by α(α is the common-base current gain which is less than one) and define $V_{CB}|_{\alpha M=1} = V_{\alpha M}$, we find that

$$\frac{V_{\alpha M}}{BV_{CBO}} = (1 - \alpha)^{1/n'} \tag{25}$$

The common emitter current gain β is equal to $\frac{\alpha}{1-\alpha}$, so the above expression reduces to

$$\frac{V_{\alpha M}}{BV_{CBO}} = (\beta + 1)^{-1/n'} \tag{26}$$

This result indicates that $V_{\alpha M}$ is some fraction of BV_{CBO}. The behavior is shown in figure 6. The figure indicates that the larger n' is, the less dependent $V_{\alpha M}$ is on β and the closer $V_{\alpha M}$ is to BV_{CBO}. It should be pointed out here that α and n' are a function of current. α increases to a peak at low currents and $V_{\alpha M}$ tends to decrease. However, as current levels increase, we also have the depletion region widening. The tendency here would be for multiplication to decrease or n' to increase with a resulting increase in $V_{\alpha M}$.

Since the two important parameters of avalanche circuits are $V_{\alpha M}$ and BV_{CBO}, circuit designers have been reluctant in the past to use avalanche circuitry in application where consistent results and reliability are required. However, in the last couple of years high speed transistors have become available on the market, which have a high degree of reliability and consistent values of $V_{\alpha M}$ and BV_{CBO} due to better manufacturing techniques.

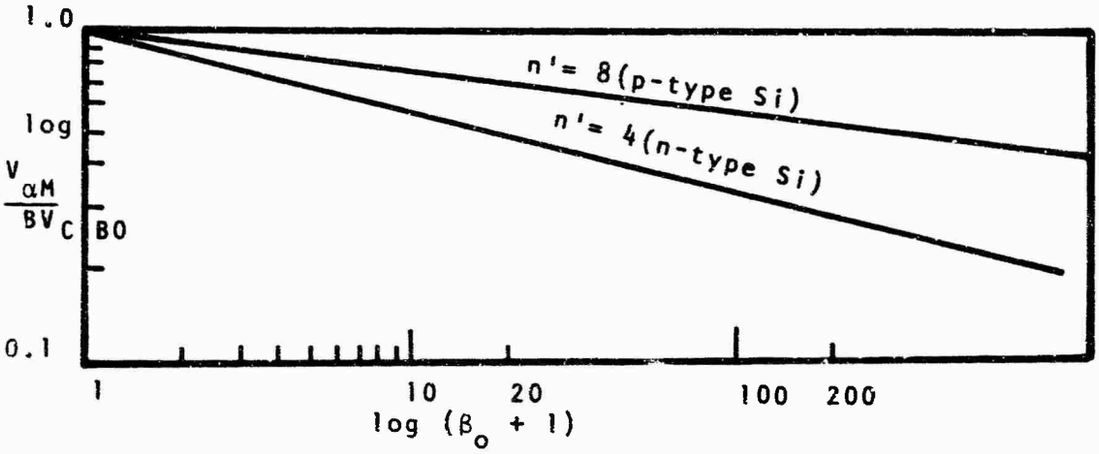

Figure 6. Behavior of $V_{\alpha M}/BV_{CBO}$ versus (β_o + 1)

If a current I_E flows through the emitter of a transistor, then αI_E reaches the collector junction. However, incorporating the multiplication factor into the current observed in the collector, we can express the total collector current with multiplication as

$$I_C = M(\alpha I_E + I_{CBO}) \qquad (27)$$

where I_{CBO} is the normal collector-base reverse leakage current due to diffusion or charge generation without the

presence of the multiplication effect. Here we are saying that in the presence of avalanche multiplication, the transistor behaves as if its common base current gain were α^* where

$$\alpha^* = M\alpha \tag{28}$$

Since $I_E = I_C + I_B$, equation (27) is solved for I_C, yielding

$$I_C = \frac{M}{1-\alpha M}(\alpha I_B + I_{CBO}) = \frac{1}{\frac{1}{M}-\alpha}(\alpha I_B + I_{CBO}) \tag{29}$$

If αM becomes greater than unity, the base current must reverse to satisfy the equation (29). Thus, any V_{CB} in excess of $V_{\alpha M}$ places operation of the transistor in the avalanche region. Designating $-I_{BR}$ as the reverse base current necessary to satisfy equation (29) when V_{CB} is greater than $V_{\alpha M}$ and substituting equation (24) into (29), we obtain

$$I_C = \frac{I_{CBO} - \alpha I_{BR}}{1 - \left(\frac{V_{CB}}{BV_{CBO}}\right)^{n'} - \alpha} \tag{30}$$

Assuming that $V_{CB} \approx V_{CE}$ and solving for the collector-emitter voltage V_{CE},

$$V_{CE} = BV_{CBO}\left[1 - \alpha + \frac{\alpha I_{BR}}{I_C} - \frac{I_{CBO}}{I_C}\right]^{1/n'} \tag{31}$$

As I_C becomes large in comparison to I_{BR} and I_{CBO}, V_{CE} becomes

$$V_{CE} = BV_{CBO}(1-\alpha)^{1/n'} \qquad (32)$$

This is the same result as the voltage $V_{\alpha M}$ which we obtain for the case $\alpha M = 1$. The implication here is that for high I_C, V_{CE} approaches $V_{\alpha M}$ regardless of the condition at the base (reference 9).

Consider the circuit in figure 7 where r_{bb} is the base spreading resistance. We will assume that until the base emitter voltage $V_{B'E}$ exceeds the contact potential V_{CP} of the base emitter junction, all of I_C flows through the base (reference 10). This is because the built-in contact potential of the base emitter junction causes this junction to be reverse biased. The flow of leakage current through r_{bb} and R_B produces a voltage that attempts to forward bias the base emitter junction. The current continues to flow out of the base as long as $V_{B'E}$ is less than V_{CP}.

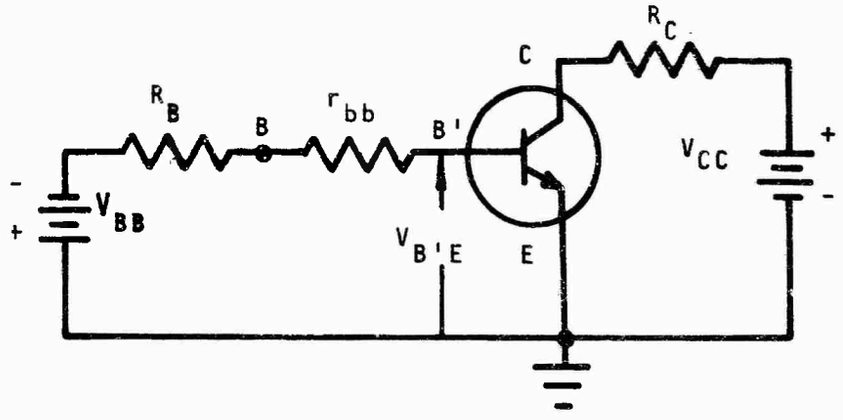

Figure 7. Variation of Breakdown Voltage Between Collector and Emitter by Base Circuit.

After $V_{B'E}$ exceeds the contact potential, the base emitter junction becomes forward biased and all the additional currents flow through the emitter. The resulting breakdown is labeled BV_{CEX}, where BV_{CEX} is defined as the breakdown voltage between collector to emitter with a specified circuit from base to emitter. Thus, for breakdown we require

$$V_{B'E} = MI_{CBO}[R_B + r_{bb}] - V_{BB} = V_{CP} \tag{33}$$

Solving equation (33) for M and setting it equal to equation (24) (assuming $V_{CB} \approx V_{CE}$) and solving for BV_{CEX}, we obtain

$$BV_{CEX} = BV_{CBO}\left(1 - \frac{I_{CBO}(R_B+r_{bb})}{V_{CP}+V_{BB}}\right)^{1/n'} \tag{34}$$

If $V_{BB} = 0$, this breakdown voltage is labeled BV_{CER} or

$$BV_{CER} = BV_{CBO}\left(1 - \frac{I_{CBO}(R_B+r_{bb})}{V_{CP}}\right)^{1/n'} \tag{35}$$

where BV_{CER} is the collector to emitter breakdown voltage with a specified resistance between base and emitter. Also if $R_B = 0$, the breakdown voltage is labeled BV_{CES} or

$$BV_{CES} = BV_{CBO}\left(1 - \frac{I_{CBO}r_{bb}}{V_{CP}}\right)^{1/n'} \tag{36}$$

where BV_{CES} is the measured collector to emitter breakdown voltage with the base shorted to the emitter. Equations (34), (35), (36), and (25) indicate that the breakdown voltage of the collector to emitter is somewhere between

$V_{\alpha M}$ and BV_{CBO}, depending on the condition of the base circuit. This typical behavior is illustrated in figure 8, but the exact shape depends on the variation of β with I_C. The variation of β with I_C depends on the transistor fabrication methods (alloy, planar, epitaxial, etc.) and thus, the breakdown characteristics can have a variety of shapes.

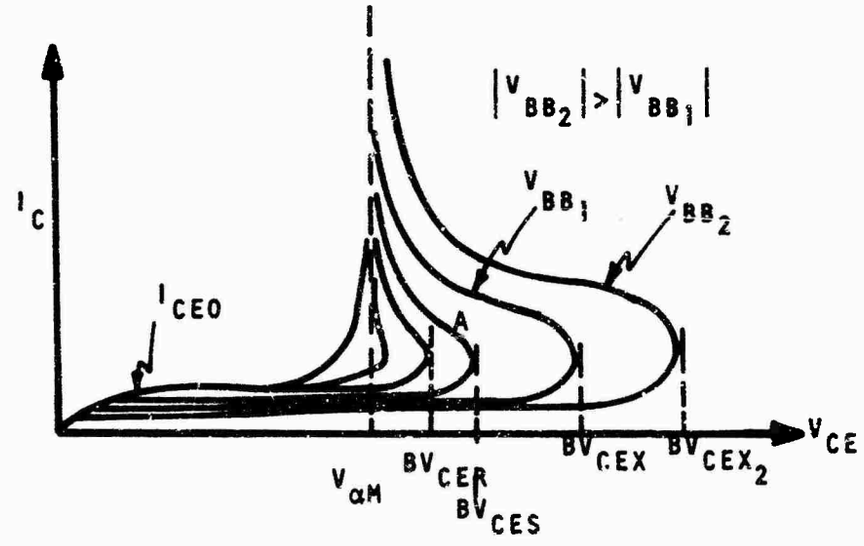

Figure 8. Typical Behavior of BV_{CE} with Base Circuitry

Once a transistor is operating in the avalanche region, a piecewise continuous model can be evaluated to determine the circuit stability. The collector to emitter incremental resistance r_A is defined as the differential change of voltage with respect to the collector current at a given operating point. From figure 8 and equation (31), this value is negative once the device triggers and approaches zero for high I_C.

The incremental capacitance is defined as $\frac{dq}{dV}$. If we assume we are at point A shown on the figure above and a

negative change in voltage $-\Delta V$ is applied to the collector emitter terminals, a resulting increase in current Δi occurs.

The stored charge must also increase by an amount Δq and the avalanche capacitance is given by

$$C_A = \frac{dq}{dV} = \frac{\Delta q}{-\Delta V} = -\left|\frac{\Delta q}{\Delta v}\right| \qquad (37)$$

The C_A as indicated in the previous equation (37) is a negative value throughout the negative resistance region. As point A moves to a higher current, the same $-\Delta V$ will result in a much larger Δi change.

The main point to be made in this short discussion is that at the collector emitter terminal a negative nonlinear output resistance and capacitance will be observed for a transistor operating in the avalanche mode as shown in the equivalent circuit in figure 9. At high I_C, $r_A \rightarrow 0$ and $C_A \rightarrow -\infty$; while at low I_C, $r_A \rightarrow \infty$ and $C_A \rightarrow C_{ob}$ (reference 9).

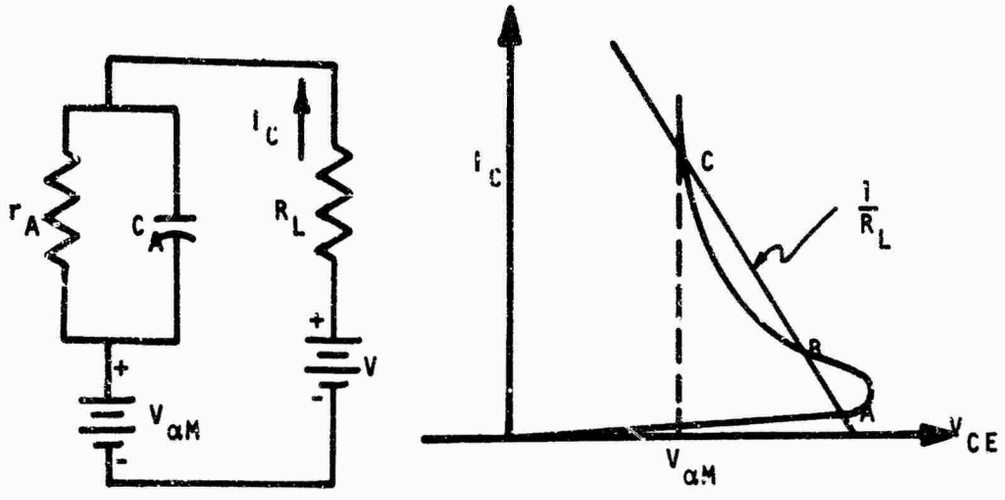

Figure 9. Equivalent Circuit of Collector Emitter Terminal with a Resistive Load and Static Characteristics

The single pole of the transistor equivalent circuit can be found by inspection and can be shown to be

$$S = -\frac{\frac{1}{R_L} + \frac{1}{r_A}}{C_A} \tag{38}$$

For the circuit to be stable, the above pole must be located in the left half of the complex plane. This requires that $\frac{1}{R_L} < \left|\frac{1}{r_A}\right|$ or $R_L > |r_A|$ for a stable point and thus the natural frequency corresponds to a decaying transient. However, if $R_L < |r_A|$, the operating point is unstable and the natural frequency corresponds to a growing transient. The operating point will then move in the direction of the disturbing signal until a stable point is established. Thus, for the characteristics shown in figure 9, point B is unstable ($R_L < |r_A|$) while point C is stable ($R_L > |r_A|$). Point A is stable as the device is not in the avalanche mode, and the transistor therefore has positive conductance and capacitance.

An avalanche circuit can then be triggered from the off state to the avalanche by making $|r_A| > R_L$. This can be accomplished by decreasing the magnitude of the base reverse current or increasing the collector voltage. To make the transistor return to the off state, $|r_A|$ must again be made greater than R_L which can be accomplished by the inverse of either of the above two methods (reference 9).

One of the circuits tested under nuclear radiation is the one shown in figure 10. The d-c load line was selected to yield a single stable point in the off state. The supply

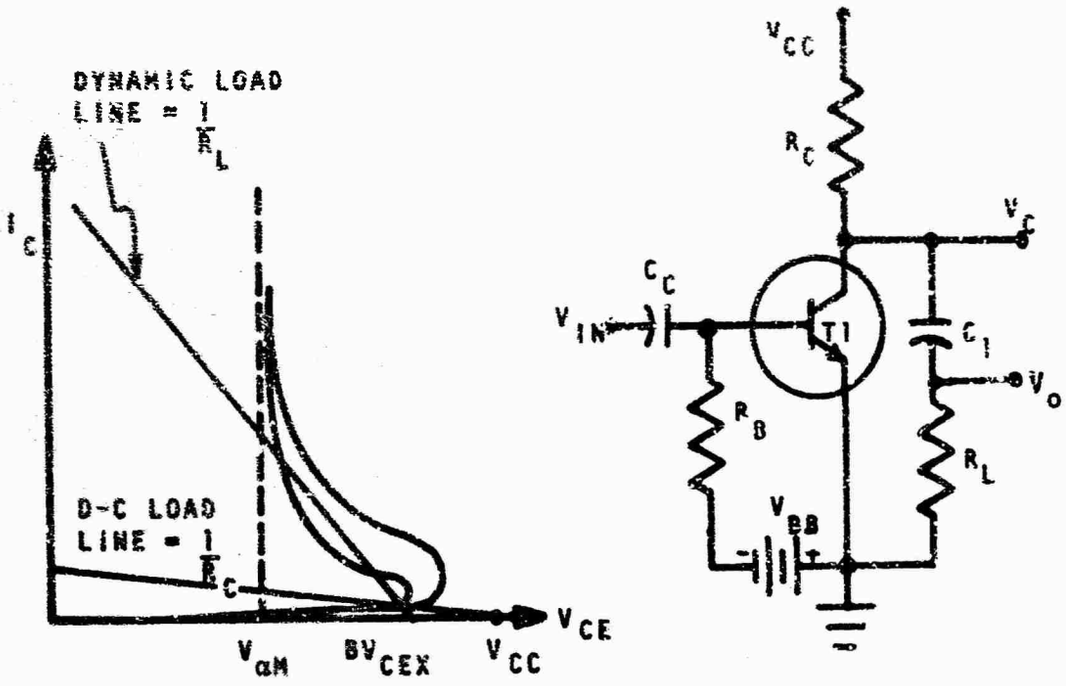

Figure 10. Basic Trigger Avalanche Circuit Employing a Capacitor for Energy Storage and Its Volt-Ampere Characteristics

voltage charges the capacitor through R_C to a voltage V_{CC} slightly less than the breakdown voltage BV_{CEX}. The static load line ($1/R_C$) is chosen so that it does not intersect the low voltage breakdown curve, and therefore, not give rise to latch-up and thermal destruction. The dynamic load is not too critical except that a minimum peak current should be obtained to have predictable avalanche switching. Since we were using a 50 Ω coaxial cable transmission system, R_L was chosen to be 50 Ω. As the circuit indicates, the base current is reversed and the base emitter junction may be slightly reversed biased. The multiplication factor at this point is large because V_{CC} is close to BV_{CBO}. If some

positive pulse of significant amplitude is applied to make the "off point" unstable and lower the breakdown voltage, the transistor essentially fires and switching occurs. However, as the transistor is switching to the on state , the transistor collector voltage is decreasing. This in turn decreases M, which makes the build-up proceed more slowly until equilibrium is reached. During this time we assume that the supply voltage cannot supply the current through R_C to maintain conduction in avalanche, and all the current must come from the capacitor. The capacitor then discharges rapidly through the transistor and the load resistor R_L. The voltage across R_L and the collector drops very rapidly and reaches a negative maximum peak in a few nanoseconds. After the voltage across R_L reaches a peak, it decays to zero as

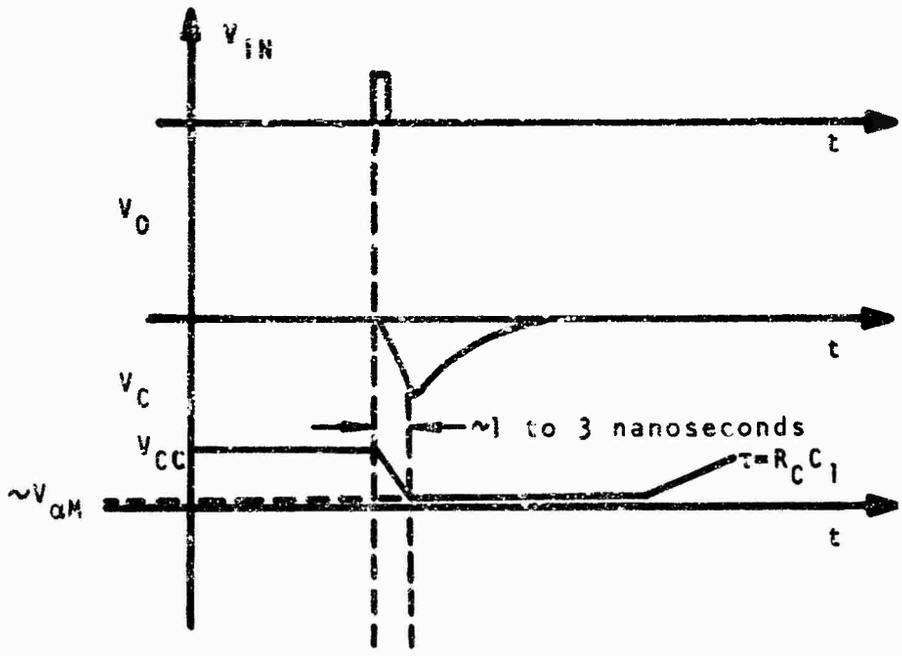

Figure . Typical Triggering Pulse, Output Waveform, and Waveform at Collector

the capacitor recharges. When the capacitor has discharged, the collector voltage, as shown in figure 11, remains for a time at the sustaining voltage, since the transistor takes a finite time to recover and return to the initial state. The pulse width depends upon R_L and C_1, and increases as C_1 increases. Assume that the pulse width recovery is primarily determined by the time required to recharge C_1. The recharge time is determined by $R_C C_1$ time constant which can be varied. However, R_C must not be made too small in order to prevent sustained conduction and remain permanently in avalanche. C_1 is usually fixed by the avalanche turn-on transient and pulse width requirements, and some different approach must be taken to reduce the repetition rate that avoids the danger of latching. Two possible solutions to this problem are illustrated in figure 12.

One circuit shows a diode returned to ground through V'_{CC} which is less than the breakdown voltage of the transistor. This allows the V_{CC} supply voltage to be increased beyond the breakdown voltage, and therefore decrease the required time to recharge C_1 and hence increase the repetition rate. The other circuit employs an emitter-follower action of T2 which reduces the charging time constant.

A single transistor operating in the avalanche mode which can be made to generate pulses (negative or positive) with controllable duration and amplitude is shown in figure 13 (references 9, 10, 11, 12).

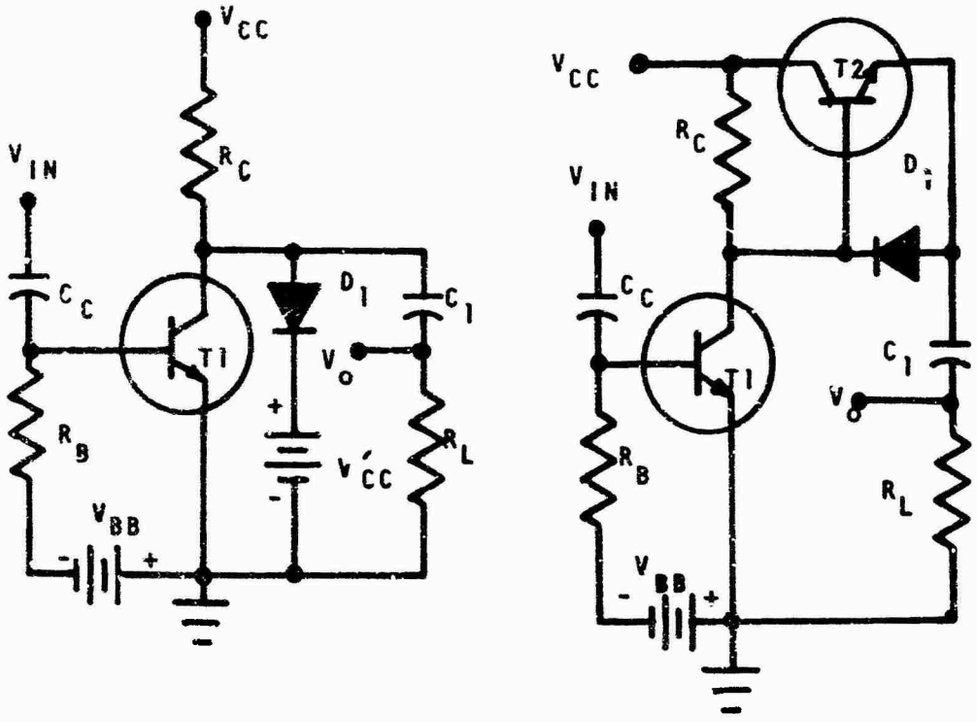

Figure 12. External Components Added to Basic Avalanche Circuit to Increase Repetition Rate

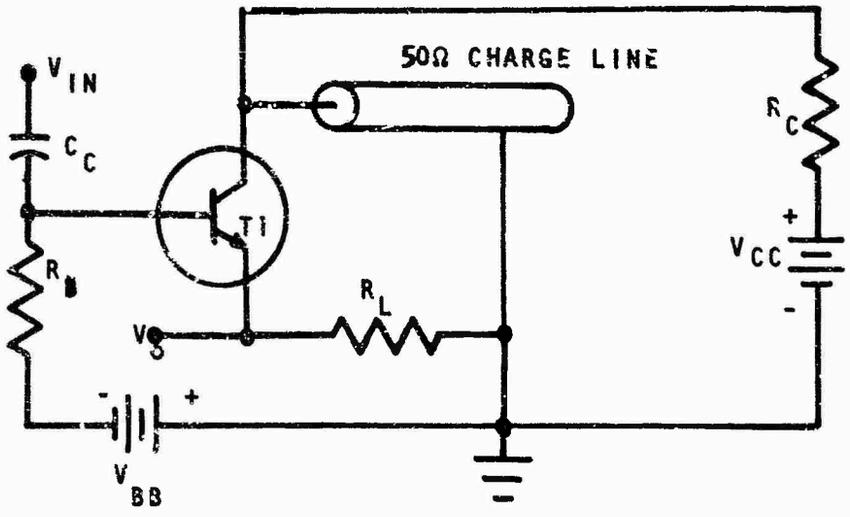

Figure 13. Avalanche Delay Line Generator

A negative pulse is obtained by placing R_L in series with the 50 Ω charge line to ground. For the purpose of calculating the output waveform, we will use the equivalent circuit shown in figure 14 where avalanche breakdown is indicated by closing of the switch S_2 and opening of switch S_1.

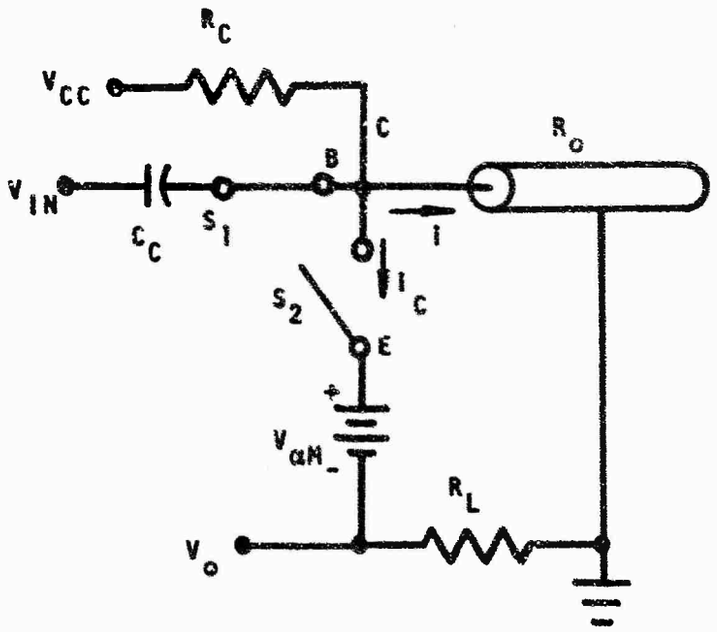

Figure 14. Equivalent Circuit of Avalanche Delay Line Generator in Avalanche Breakdown

During the transistor off cycle, the charge line essentially behaves as a capacitive load and charges to V_{CC} through R_C. If a positive pulse of significant amplitude is now applied to the input, the transistor breaks down and a

positive pulse appears at the output. This pulse has an amplitude $V = V_{CC} - V_{\alpha M}$. The initial charge line current was zero, so a step current starts down the line at t = 0+

$$i(0+) = \frac{-V}{R_0+R_L} \tag{39}$$

where the delay line appears to be a resistance equal to its characteristic impedance R_0. When this current reaches the end of the line at $t = T_d$ (where T_d is the one wave propagation time of the line), it is reflected as a current step by a reflection coefficient ρ given by

$$\rho = - \frac{R_T-R_0}{R_T+R_0} \tag{40}$$

where R_T is the terminated resistance of the charge line. In our case we are using an open line and the pulse is completely reflected with a change of polarity (i.e., $\rho = -1$). At $t = 2(T_d+)$ the pulse has reached the beginning of the line and has been reflected by

$$\rho' = - \frac{R_L-R_0}{R_L+R_0} \tag{41}$$

Therefore, the total line current at $t = 2T_d+$ is

$$i(2T_d+) = \frac{-V}{R_0+R_L} + \frac{V}{R_0+R_L} - \left(\frac{R_L-R_0}{R_L+R_0}\right) \frac{V}{R_0+R_L} = - \frac{(R_L-R_0)V}{(R_L+R_0)^2} \tag{42}$$

If we neglect the small current contributed by V_{CC} through R_C, the transistor current i_c will be positive at

$t = 2T_d$ for $R_L > R_0$. Hence the transistor would remain in avalanche and more reflection would occur. The output voltage across R_L would then consist of a staircase type waveshape with each level separated by $2T_d$ time intervals rather then a rectangular pulse output. If $R_L < R_0$, we would have a reversal of collector current at $t = 2T_d$ which would tend to turn the transistor off. Reflections may now occur on the line, but since the transistor is cut off and exhibits high impedance, they will not appear across R_L. However, if $R_L = R_0$, the transistor would go out of avalanche with the resulting opening of switch S_2, closing of switch S_1, and the dropping of the output voltage to zero. In either case, $R_L = R_0$ or $R_L < R_0$, there will appear across R_L at $t = 0+$ a positive pulse given by

$$V_0(0+) = i(0+)R_L \approx \frac{V_{CC}-V_{\alpha M}}{R_0 + R_L} R_L \qquad (43)$$

As shown in equation (43), the output voltage is adjustable through V_{CC}, R_L, and R_0. The pulse duration $2T_d$ can be controlled by the type and length of charge line. The output voltage is positive and can have a maximum amplitude of $V_{CC}-V_{\alpha M}$ for $R_L >> R_0$; however, this condition will result in reflections on the load. This occurs because the pulse amplitude V_L on the charge line is given by

$$V_L(0+) = (V_{CC}-V_{\alpha M}) \frac{R_0}{R_0+R_L} \qquad (44)$$

The pulse goes to the end of the charge line and is completely reflected without a change of polarity. At $t = 2T_d$ it returns to the collector and increases the voltage by the same amount as at $t = 0+$ with a reduction of the voltage across R_L. However, this reflected voltage would be too small to reduce the collector current significantly to terminate the pulse.

SECTION III

NUCLEAR RADIATION EFFECTS ON AVALANCHE p-n JUNCTIONS

1. Effects of Radiation on Semiconductor Components

When a burst of nuclear radiation, composed of both neutrons and gamma rays, is incident on a semiconductor component such as a diode, it is observed that the component rated value changes. The peak magnitude of the rated value change is a function of the intensity of the radiation, the time behavior of the pulse, and is dependent on both the material of which the semiconductor component is made and the surrounding environment of the component. But there is at least one fundamental difference in the phenomena generated by neutrons on the one hand, and X rays or gamma rays on the other hand. Roughly, neutrons primarily cause permanent damage to the material (physical properties change), while the effects of gamma rays or X rays are usually transient effects (reference 13). Some of the transient effects caused by the saturation of the circuit can last longer than the radiation pulse. For the most part, the neutrons interact with nuclei, causing, for example, dislocations within a crystal, transmutation of atoms, insertion of extraneous atoms or changing of chemical bonds, whereas photons are atomic interaction within materials and usually just produce free electron-hole pairs. In a nuclear weapon environment (fusion) most of the ionization produced

is due to the 14-Mev-neutrons and to the gamma rays of the radiation, but all nuclear particles can contribute. However, in this report, we will assume the neutrons cause just permanent damage and the X rays cause just transient effects.

Past experimental evidence has shown that semiconductor devices (diodes, transistors, etc.) are the components most sensitive to nuclear radiation and that reduction of the radiation sensitivity of these devices is necessary for a nuclear hardened system. Usually they are the devices which are responsible for most of the temporary short-time current and voltage signals that perturb an electronic system. The semiconductor devices also undergo significant degradation before other components, which leads to systems failure. In this section we will review experimental and theoretical aspects of radiation effects on semiconductor components caused by photons and neutrons.

2. Transient Effects

If a diode or transistor in a circuit is exposed to a pulse of X ray or gamma ray, the condition of the circuit will be modified by passing from its steady state condition before the radiation pulse to a state of excitation that will depend upon the intensity and duration of the pulse. When the radiation pulse has ceased, the circuit will then relax to its previous condition of equilibrium within a characteristic time. This effect is due to the creation of excess electron-hole pairs from ionization. These effects

usually do not directly cause permanent damage to the material, but because of a current overload the ionized carriers they produce may cause permanent changes to the semiconductor. However, high-energy gamma and X rays can undergo interaction with a nucleus producing excitation and transmutation, but in this subsection we shall mainly concern ourselves only with the production of free electron-hole pairs by the incident radiation.

When X rays interact with matter there are three predominant mechanisms of interaction. They are the photoelectric, Compton, and pair production effects. The relative importance of each of these depends on the X-ray energy and the atomic number of the absorbing material.

For low energies ($\leq$ 100 kev) and large atomic numbers the photoelectric effect is the predominant process. The photoelectric effect is the process whereby the energy of the incident photon is totally absorbed in ejecting an electron from an atom and imparting kinetic energy to it.

For energies between 100 kev and 4 Mev the Compton process becomes important. It represents an interaction with an orbital electron of an atom to produce an energy-degraded photon and a recoil electron.

At higher energies, above 1.02 Mev, the pair production process becomes increasingly important with increase in photon energy. Pair production is an absorption process

for X rays in which the incident photon is annihilated in the vicinity of the nucleus of an atom, and an electron-hole pair is produced (reference 14).

When an X ray hits the semiconductor, electron-hole pairs are produced through direct ionization by photons or by the slowing down of electrons and positrons. In most materials an amount of energy equal to two to four times the ionization potential of the material would be expended for each ionization produced. The energy spectrum of secondary electrons due to X-ray interaction depends upon the type of processes involved in their generation (photoelectric, Compton, or pair production). The first generation of electrons will have predominantly high energies. The spectrum of the high energy secondary electrons is of the form of an inverse energy squared function. If this spectrum still has some high-energy components, these components are capable of producing further ionization. These electrons will then continue to lose their energy by further inelastic scattering until finally they are trapped or recombined (reference 14).

Ionization within a semiconductor therefore results in the production of electron-hole pairs. The hole-electron pairs may carry current either by diffusion, when there is a carrier concentration gradient, or by drift when there is an electric field. Since opposite charges attract, the free electron will be attracted towards the

positive terminal, and the hole moves towards the negative terminal in the presence of an applied electric field (reference 15). The total current flow is the sum of the hole- and electron-current components, and for a one-dimensional flow they may be expressed as

$$j_n = qu_n nE + qD_n \frac{\partial n}{\partial x} \tag{45}$$

$$j_p = qu_p pE - qD_p \frac{\partial p}{\partial x} \tag{46}$$

where

j_n = electron current density (ampere/cm^2)

j_p = hole current density (ampere/cm^2)

q = magnitude of electronic charge (1.6×10^{-19} coulomb)

u_n = electron mobility (cm^2/volt-sec)

u_p = hole mobility (cm^2/volt-sec)

n = electron concentration (cm^{-3})

p = hole concentration (cm^{-3})

E = electric field (volts/cm)

D_n = electron-diffusion constants (cm^2/sec)

D_p = hole-diffusion constant (cm^2/sec)

The first term in the above equation represents the drift-current component (proportional to the electric field), and the second term represents the diffusion-current component (proportional to the concentration gradient of carriers). Since the diffusion of carriers results from a

density gradient (i.e., the tendency of particles to move from a region of high concentration), one can see that the shorter the distance in which the electron density changes (i.e., the greater the gradient of density) the larger the diffusion current will be (reference 16).

If the air surrounding the semiconductor is ionized, the positive ions and electrons produced can move. But the positive ion has a much smaller mobility than the free electron of the air, and it does not add much to the flow of current. The electrons produced by ionization of gases around a semiconductor device often contribute significantly to the results of transient radiation measurements unless preventive steps are taken (references 17 and 18).

Sooner or later the excess electron-hole pairs produced by radiation are captured and can no longer contribute to the transient effects of the circuit. One method of immobilization would be by direct recombination of the electrons and positive ions. But this process happens very rarely as the probability of an electron coming within range of attraction of the positive ion is very small. Instead, more complicated multistep processes (trapping, attachment, and defect centers) are responsible for electron capture.

In semiconductors, where the freed electron occupies a state in the conduction band, the electron returns to a

valence band state in several sequential transitions by means of a recombination center. These recombination centers are discrete levels located near the center of the forbidden-energy gap, and are so called because they aid the recombination between electrons and holes. This process simply amounts to the center first capturing an electron and subsequently capturing a hole. A recombination center thus has a large capture cross section (probability that any localized level can capture an excess carrier) for both electrons and holes. In some cases, depending upon the atomic origin of the level, the level has a high-capture cross section for one of the mobile carriers, but an extremely small cross section for its mate. This level is called a trap because it tends to trap the carrier for which it has the larger capture cross section without capturing the other kind of carrier. Some trapping phenomena have been observed in which excess mobile carriers have been held for hours, or days, as in the formation of F centers in alkali halides (reference 13).

In a typical germanium or silicon transistor the recombination time is usually a few nanoseconds to a few microseconds. The recombination occurs indirectly by use of a recombination center and the rate of recombination is a function of the concentration of these recombination centers. The purer the material the longer is the lifetime

of excess carriers. The maximum experimental value for very pure single crystal silicon is about 500 microseconds.

a. Transient Effects on Diodes

Irradiation of a semiconductor p-n junction produces an excess carrier concentration. With constant voltage applied to the junction, the resulting current pulse depends on the radiation pulse width, the pulse shape, intensity, and the recombination time of the minority carriers. When the recombination time is long compared to the radiation pulse width, the concentration increases at a rate proportional to the radiation dose until the pulse is shut off. Then the semiconductor relaxes to its preirradiation steady state value within some characteristic time. But if the recombination time is short compared to radiation pulse width, then the excess-carrier concentration is proportional to the dose rate at any particular time and follows the shape of the radiation pulse.

A typical variation of majority and minority carriers in the vicinity of a one-dimensional germanium p-n junction is shown in figure 15. Solid lines indicate the equilibrium carrier concentration under bias before irradiation, and dotted lines indicate a typical carrier concentration immediately after irradiation (reference 18). In a reverse bias condition the minority carriers constitute the

leakage current (see figure 15a). Because the holes in the n-region are injected into the p-region and electrons are injected into the n-region, the direction of current flow is from the n-region to the p-region.

When the diode is irradiated by a pulse of ionizing radiation, electron-hole pairs are generated uniformly throughout the device. Since there is a built-in electric field, and perhaps an externally applied field across the junction transition region, the carriers generated in this region will be swept across the junction and collected in less than a few nanoseconds. If the radiation pulse is much wider than a few nanoseconds, these carriers constitute a current which has essentially no time delay relative to the radiation pulse. For this reason this current is referred to as the prompt photocurrent component.

In the regions outside of the junction transition region, there is a transient increase in the minority carrier densities as shown by the dotted lines in figure 15a. As indicated by the dotted lines, the minority carrier density gradients at the edges of the junction have increased. This would increase the minority carrier diffusion tendency (i.e., density gradient) in the vicinity of the junction and more carriers would diffuse towards the junction. Most of the excess minority carriers, which are within a diffusion length of the junction diffuse to the junction and contribute to a transient current. However, on the average, excess

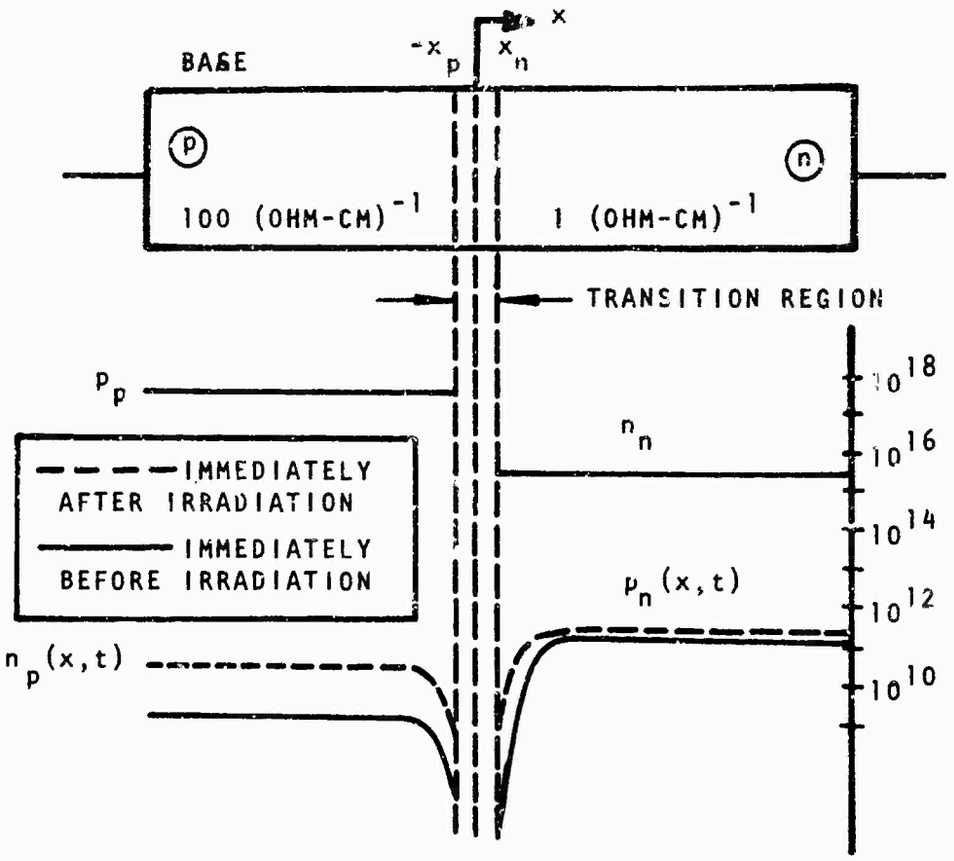

a) REVERSE BIASED

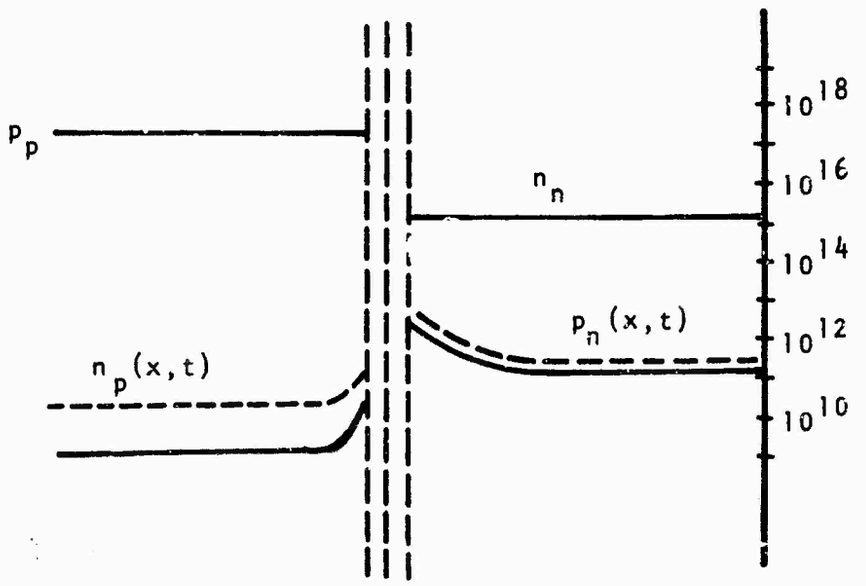

b) FORWARD BIASED

Figure 15. Approximate Minority and Majority Carrier Densities in a p-n Diode Before and Immediately After Irradiation

minority carriers generated in the p- and n-regions greater than one diffusion length from the p-n junction do not reach the junction before they recombine. Therefore, they do not contribute significantly to the transient current.

The diffusion component of current generally takes a time which is large compared to the duration of the radiation pulse to diffuse to the junction. It is therefore referred to as a delayed photocurrent component. The excess holes in the n-region diffuse towards the p-region, so that the radiation-induced delayed component of current is from the n- to the p-region. Since the depletion and diffusion photocurrent is in the same direction as conventional current flow in a reverse biased diode, the net result is a transient photocurrent superimposed on the steady state leakage current.

A forward biased junction can be regarded as a short circuit in most instances. The voltage drop due to applied voltage across the junction will be small and normally will not completely cancel out the built-in junction potential. Thus, an electric field will still exist in the same direction as in a reverse biased junction. Carriers which are generated in the junction transition region will, as before, be swept across the junction by this field and collected within a few nanoseconds. This current will be in opposition to the normal forward bias current. As indicated by the dotted lines in figure 15, the majority carrier

densities immediately after irradiation will not be altered appreciably (for radiation levels that do not generate majority carriers comparable to the normal equilibrium values), but the minority carrier density gradient will decrease. The net effect of pulsed X rays on a forward biased junction is a transient photocurrent opposite in direction to the normal steady state current.

The derivation of the junction transient current is given by Brown, van Lint, Caldwell, Keister, Wirth, et al (references 19, 20, 21, 22, and 23). The transient primary photocurrent response of a reverse biased diode (assuming that the contacts are greater than several diffusion lengths from the junction) to a burst of ionizing radiation has been shown to be given by

$$i_{pp}(t) = qAg[(W_t + \sqrt{D_n\tau_n}\ \text{erf}\ \sqrt{t/\tau_n} + \sqrt{D_p\tau_p}\ \text{erf}\ \sqrt{t/\tau_p})u(t)$$

$$- (W_t + \sqrt{D_n\tau_n}\ \text{erf}\ \sqrt{(t-t_o)/\tau_n} +$$

$$\sqrt{D_p\tau_p}\ \text{erf}\ \sqrt{(t-t_o)/\tau_p}\ )u\ (t-t_o)] \qquad (47)$$

where

$i_{pp}(t)$ = radiation induced primary photocurrent in amperes

q = the electron charge = 1.6×10^{-19} coulombs

A = junction area in cm^2

g = electron-hole pair generation rate = pairs/ $sec\text{-}cm^3$

W_t = depletion layer width in cm

D_n = diffusion constant for minority electron in the p-type material = cm^2/microseconds

D_p = diffusion constant for minority holes in the n-type material = cm^2/microseconds

τ_n = lifetime in microseconds for the minority carrier electrons in the p-material

τ_p = lifetime in microseconds for the minority carrier holes in the n-material

$u(t)$ and $u(t-t_o)$ = unit step function turned on at t=0 and $t=t_o$, respectively

$$\text{erf } x = \frac{2}{\sqrt{\pi}} \int_o^x e^{-x^2} dx$$

In Appendix II it is shown that the width of the depletion region is a function of the bias voltage (references 24 and 25). Thus, the primary photocurrent consists of the following two components: (1) a diffusion component that is contributed to by the p and n regions; and (2) a drift component that is contributed to by the depletion layer. The primary photocurrent prior to breakdown has been usually considered as a current generator connected across the junction as shown in figure 16. Figure 17 shows a typical response to be expected for various approximations of W_t, L_p, and L_n.

The behavior of i_{pp} as a function of voltage will depend on the relative size of the depletion to diffusion component.

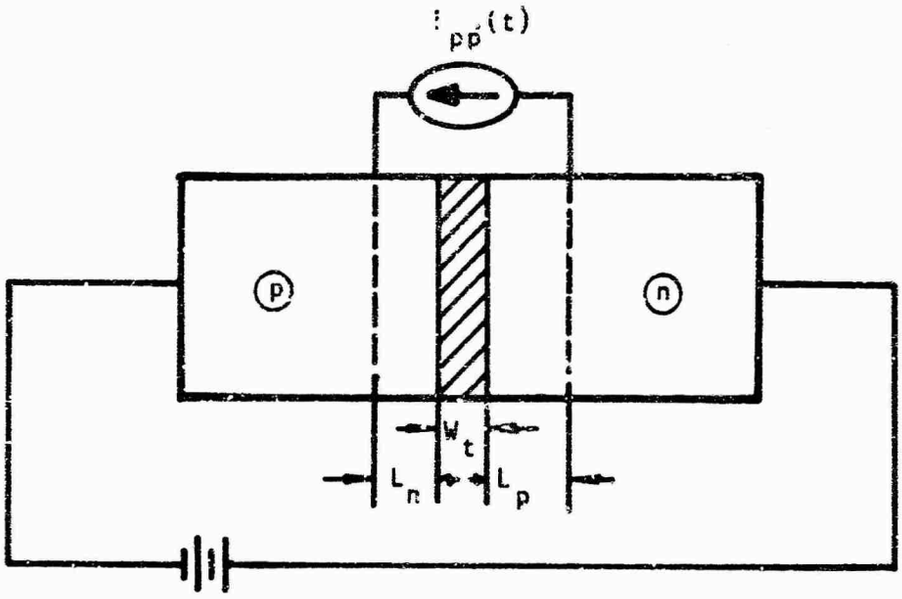

Figure 16. Simulation of Primary Photocurrent in a p-n Junction

Normally avalanche diodes are made from material in which the doping on one side of the junction is much higher than the doping on the other side. If a p+n diode is chosen, then most of the primary photocurrent that flows is due to the holes in the n-material diffusing to the junction and being swept across. This type of doping also ensures that the diffusion length in the n-material is much longer than that in the p+ material. Since the L_p is much greater than L_n, then equation (47) can be simplified to

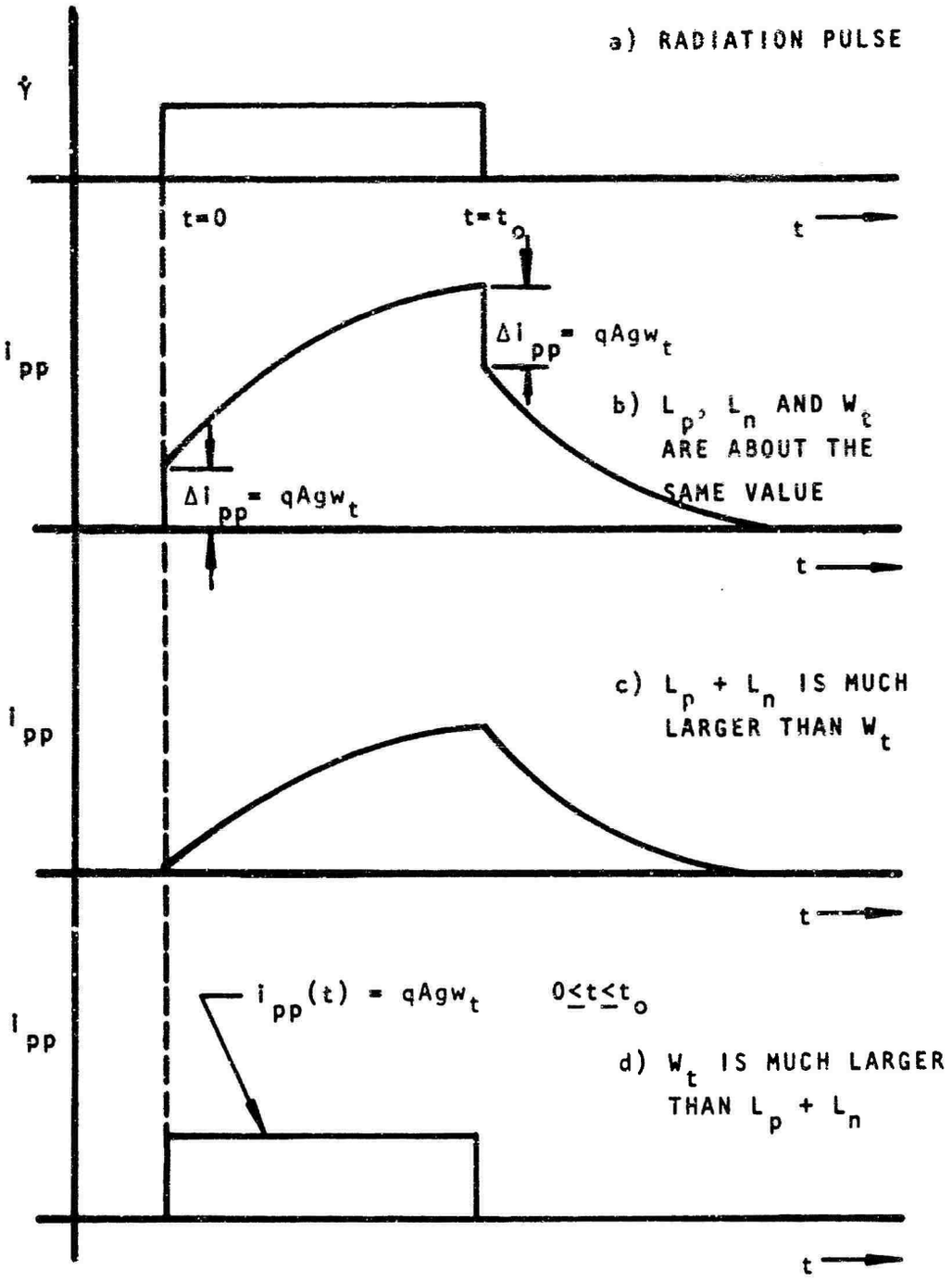

Figure 17. Typical Transient Radiation Response of a p-n Diode for Various Values of L_p, L_n and W_t

$$i_{pp}(t) = qAg[(W_t + L_p \text{ erf } \sqrt{t/\tau_p})\, u(t)$$

$$- (W_t + L_p \text{ erf } \sqrt{(t-t_o)/\tau_p})\, u(t-t_o)] \qquad (48)$$

where $L_p = \sqrt{D_p \tau_p}$ = minority carrier diffusion length in the n-material.

From the previous discussion on avalanche breakdown, it can be seen that the primary photocurrent should be in reality modified by the multiplication factor and be given by

$$i^*_{pp}(t) = Mi_{pp}(t) \qquad (49)$$

At low voltages, M is close to one, and any increase because of multiplication would be small. But as the reverse voltage across the diode approaches the breakdown voltage, the deviation starts increasing. Therefore, a response of peak multiplied photocurrent i^*_{pp} versus voltage up to about the breakdown voltage would be expected to behave somewhat as shown in figure 18.

M as a function of the reverse voltage can be obtained from figure 18. That is, the multiplication is given by

$$M = \frac{1}{1 - \left(\frac{V_j}{V_B}\right)^{n'}} \qquad (50)$$

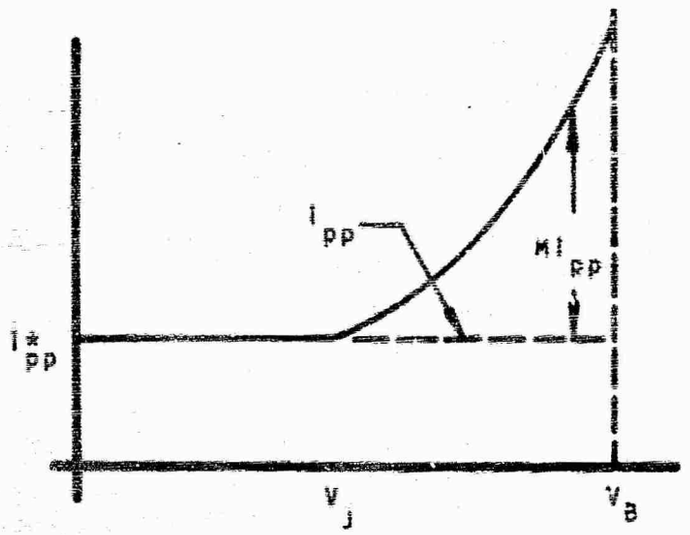

Figure 18. Peak Photomultiplied Current versus Reverse Voltage Across Depletion Region

or

$$1 - \frac{1}{M} = \left(\frac{V_j}{V_B}\right)^{n'} \tag{51}$$

Taking the logs of both sides, the equation can be put in the form

$$\log\left(1 - \frac{1}{M}\right) = n' \log V_j - n' \log V_B \tag{52}$$

This indicates that the M evaluated from figure 18 and plotted as $\log\left(1 - \frac{1}{M}\right)$ versus $\log V_j$ would result in a straight line. The slope of this line should be n'. At breakdown M goes to infinity, so that $1 - \frac{1}{M}$ equals 1, and V_j equals V_B. Thus, at the intercept of $\log\left(1 - \frac{1}{M}\right)$ equals log 1, V_B can be evaluated.

Once the device is operating in its avalanche region, the problem of analysis changes completely. From a standpoint of circuit analysis, it appears as a first approximation that the reverse biased diode could be represented under radiation as shown in figure 19. The diffusion capacitance, depletion capacitance, and the diode body resistance have been presently neglected. Assuming an ideal voltage supply, the input voltage supply and the breakdown voltage (transient will be super-imposed upon steady state value) can be neglected for a transient analysis. With this simplification, the equivalent circuit would look like figure 20. When the diode is slightly reverse biased, the shunt resistance is quite large (several hundred megohms) and the primary photocurrent acts like a constant current generator (i.e., the current flowing through R_S can be neglected as long as $R_S >> R_V$). But as the diode gets into avalanche, the resistance decreases quite rapidly. Therefore, i^*_{pp} will divide between R_V and R_S inversely proportional to their resistance. But if the current through R_S increases, R_S will decrease. This will again tend to increase the amount of current that is divided to R_S. In other words, the inherent characteristics of the device are providing a built-in feedback mechanism that is tending to keep the voltage across the device constant even though the current is changing. Thus, the device would seem to be radiation tolerant as a voltage regulator. Therefore, a

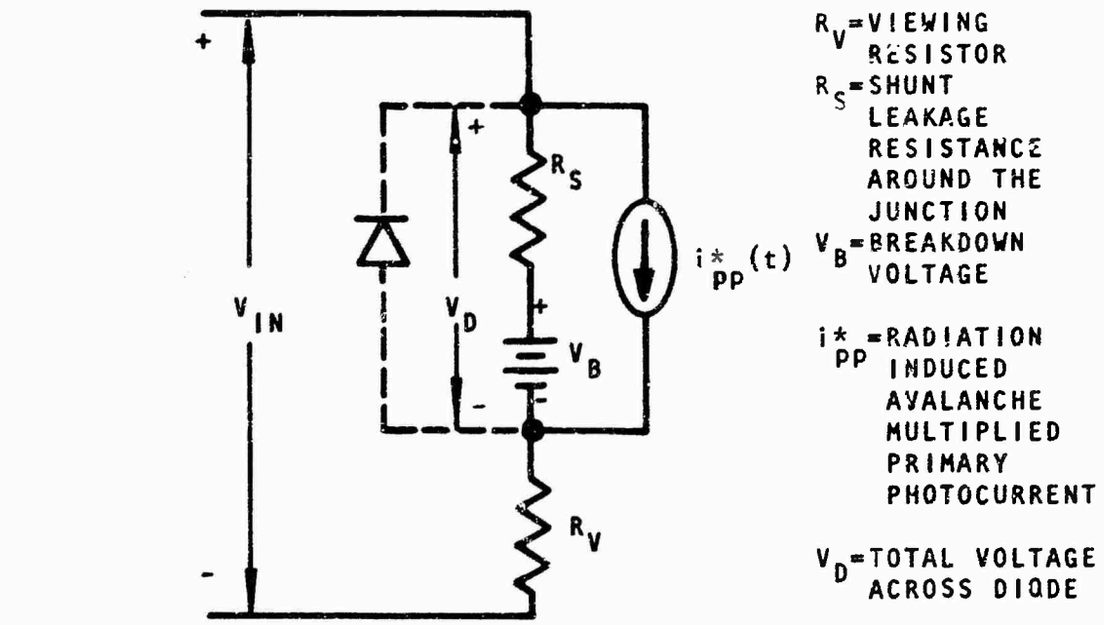

Figure 19. Radiation Equivalent Circuit for Diodes in Avalanche

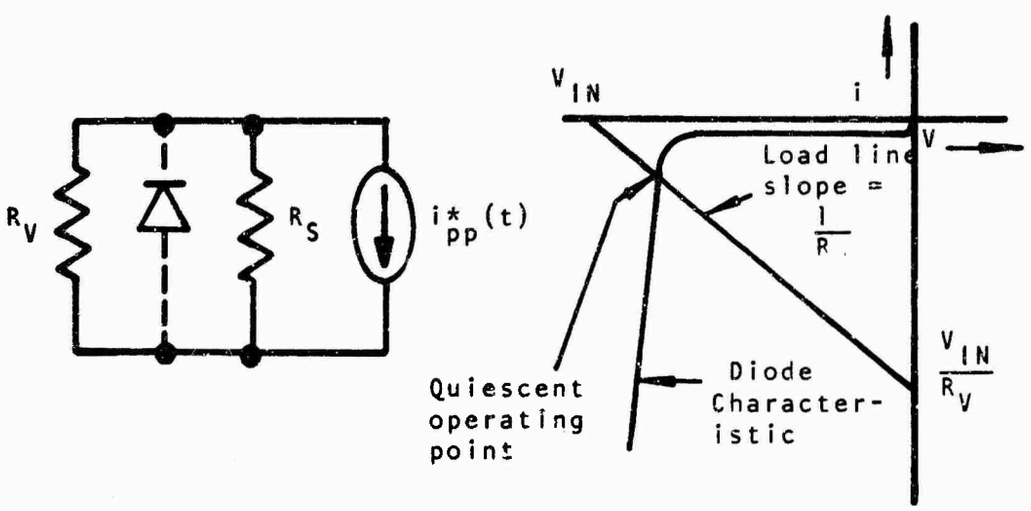

Figure 20. Transient Analysis of Radiated Diode

smaller response across R_V would be expected, once the device is in avalanche. This response would tend to decrease as the device is driven harder and harder into avalanche. The exact models under radiation will be discussed in a later section.

Transient effects have been observed that were not due to bulk effect, but due to surface effects. The ionizing radiation interacts with the encapsulated gas to produce gas ions. These ions apparently collect on the surface of the reverse-biased junction which tend to neutralize the electric field and at the same time produce an inversion layer. However, evacuation and passive coating on the device surface will help to decrease significantly the magnitude of this effect.

b. Effect of Ionizing Radiation on a Transistor

Consider an n-p-n transistor connected in the open base configuration and biased as shown in figure 21. When the transistor is irradiated by a short pulse of ionizing radiation, electron-hole pairs are created uniformly throughout the volume. Just as before in the case of the diode, the radiation generated electrons and holes will drift across the junction and diffuse to the junction. This will result again in a prompt photocurrent component from the transition region and a delayed component from the diffusion of minority carriers from one region to another. With an n-p-n transistor the electrons in the base will diffuse to the

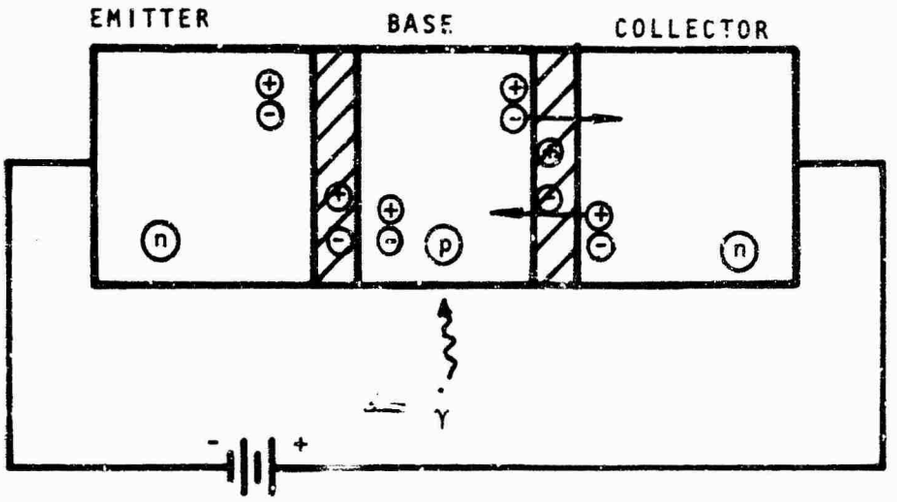

Figure 21. Open Base Transistor Under Irradiation

collector-base junction, and they will be collected as a component of the delayed photocurrent.

In the absence of these electrons, the holes left behind form an excess positive charge in the base. At the same time the electrons are diffusing from the base, the holes are diffusing from the collector to the collector-base junction, then they are swept into the base region. These holes will further increase the excess positive charge in the base. The excess majority carriers (holes) in the base will increase the forward bias of the emitter-base junction, which causes more electrons from the emitter to flow into the base. The electron current entering the base from the emitter is determined by the current gain of the device as well as the radiation-induced charge in the base. This results in a transient collector current (secondary photocurrent) in

addition to the collector component of the primary photocurrent. These injected minority carriers (electrons from the emitter into the base) will continue to diffuse to the collector-base junction and drift across the junction as long as an excess positive charge remains stored in the base region (references 19 and 22).

From the above it is seen that the photocurrent consists of the following contributions: (1) a depletion layer component contributed by the emitter-base and collector-base junction, and (2) a diffusion component contributed by the emitter, base, and collector regions.

In planar and mesa transistors most of the primary photocurrent usually originates in the collector region (reference 26). The collector diffusion length, L_c, is much greater than the base width and the depletion width. This means that the number of holes available from the diffusion of holes from the collector to base is much greater than the diffusion of electrons from the base to collector. Thus, after the termination of the radiation pulse, holes generated in the collector region within one diffusion length of the junction will diffuse into the base. The charge accumulated in the base due to diffusion of carriers from the collector will therefore not reach a maximum until approximately a time equal to one to two times the lifetime of minority carrier in the collector (τ_c).

3. Permanent Effects

When semiconductors are exposed to neutrons, they can undergo permanent damage to their electrical characteristics. Such damage is the result of neutrons having energies above several hundred electron volts causing lattice displacements or interstitial-vacancy pairs. The magnitude of the effect is dependent on the energy of the incident neutrons. These defects are created when an atom is knocked from its normal position in the semiconductor material and leaves a vacancy in the lattice. The atom usually comes to rest in a position out of the lattice structure a short distance from the vacated site and is known as an interstitial atom. A primary recoiling atom from a neutron collision may have sufficient energy to cause a large number of secondary displacements in traveling through the crystal. The energy transferred to a lattice atom has a wide range of values dependent on the neutron scattering angle. Therefore, the actual number of secondary displacements will have a varying range. However, in each displacement a pair is created: a vacancy site and an interstitial atom. This pair is referred to as a Frenkel Defect. Other effects such as thermal spikes and transmutation of the crystal atoms have a higher order effect on the semiconductor electrical characteristics and are negligible in this study (reference 13).

The vacancies and interstitials give rise to new energy levels in the forbidden energy gap of the crystal which act

as recombination centers to reduce the lifetime of minority carriers. The increase in recombination centers is proportional to the integrated neutron flux and inversely proportional to the minority carrier lifetime.

The defects introduced are located near the center of the energy gap, and the Fermi level is between the energy level introduced and the energy band which contains the majority carriers (conduction band in n-type and valence band in p-type semiconductor). These defects can also act as trapping center for the majority carrier. For example, in an n-type crystal, the trapping centers are below the Fermi level, and therefore would have a higher probability of occupancy by electrons rather than holes. The trapping of these electrons would tend to decrease the effective doping concentration and would result in a decrease in the crystal conductivity.

There are other effects (such as an increase in the scattering of free carriers which tends to decrease carrier mobility), but these effects have been found to have negligible influence on semiconductor's electrical characteristics compared to increase in recombination and trapping. In essence, neutrons mainly tend to degrade the electrical characteristics by two different mechanisms.

1. Introducing recombination centers reduces the lifetime τ of minority carriers according to the relationship

$$\frac{1}{\tau} = \frac{1}{\tau_o} + K_\tau \Phi \tag{53}$$

or

$$\tau = \frac{\tau_o}{1+\tau_o K_\tau \Phi} \tag{54}$$

where

φ = fast neutron fluence

τ_o = carrier lifetime before irradiation ($\Phi = 0$)

K_τ = lifetime damage constant, which is dependent on such things as device material, doping, temperature, energy spectrum of the incident fluxes, etc.

In essence, equations (53) or (54) say that recombination centers are added linearly with Φ (assuming the Fermi level is not altered appreciably by irradiation and the capture cross sections of the recombination centers do not change).

2. The defects act to decrease the crystal conductivity σ_i by introducing trapping centers for the majority carriers as described approximately by

$$\sigma_i = qu_i\left(N_i - \frac{\Delta N_i}{\Delta \Phi}\,\Phi\right) \tag{55}$$

where

q = electronic charge = 1.6×10^{-19} coulomb

u_i = carrier mobility

N_i = majority carrier concentration

$\frac{\Delta N_i}{\Delta \Phi}$ = carrier removal rate

i = n or p

Equation (55) implies that the crystal becomes intrinsic as the integrated neutron flux increases, and that the carrier removal varies with the number of carriers left to trap. Otherwise, the equation would suggest that the conductivity would reduce to zero and then become negative. Previous experimental evidence has indicated that as the number of majority carriers approaches the intrinsic concentration, the carrier removal rate approaches zero.

It must again be emphasized that even though many things are known about the defect mechanism, accurate prediction of the effects of neutron degradation is still difficult. This is mainly because such factors as device material, device structure, device operating condition, doping levels of the semiconductor, device encapsulation, oxygen concentration of the device, defect density of the device, environmental temperature, uncertainties in dosimetry, and energy spectrum of the incident particles may

cause differences large enough to cause large variation in the test results.

a. Degradation of Diodes

Experimentally it has been found that with a constant current applied, the forward voltage of a diode will generally increase with neutron fluence. This result can be explained by assuming that the universal diode equation is a good approximation for the current-voltage relation and examining its behavior under neutron radiation. The general expression for the forward current I in a diode in which minority carrier injection is much less than the density of majority carriers is given by

$$I = qA\left[\frac{n_p D_n}{L_n} + \frac{p_n D_p}{L_p}\right]\left[e^{qV_j/kT} - 1\right] \simeq qAp_n\left(\frac{D_p}{\tau_p}\right)^{1/2}\left(e^{qV_j/kT} - 1\right) \quad (56)$$

for a p+n diode where V_j is the junction voltage. The junction voltage V_j is equal to the externally applied voltage V_e minus the potential drop across the light doped n-region, V_ℓ, where

$$V_\ell = IR_\ell = \frac{IL}{\sigma_n A} \simeq \frac{IL}{qu_n A}\left(\frac{1}{N_D}\right) = V_e - V_j \quad (57)$$

where

R_ℓ = resistance of lightly doped region

L = length of lightly doped region (n-region in this case)

σ_n = conductivity of n-region $\simeq qu_n N_D$

Equation (56) indicates that if the lifetime decreases, the junction voltage must decrease for constant current. However, equation (57) indicates that if the majority carriers are removed by trapping (conductivity decreased), then V_ℓ will increase. If the current is to remain constant as V_ℓ increases, this means that V_e will have to increase. However, the change due to the minority carrier lifetime effects will predominate at low flux level where we do not see any conductivity modulation. At a higher exposure level where we see a conductivity change, the conductivity modulation will usually rapidly suppress the effect because of the lifetime changes. This fact can be seen by observing that the diode current varies as the inverse of the square root of the minority carrier lifetime and exponentially with V_ℓ. The exact extent to which the forward voltage of a diode for a constant current will change with neutron exposure depends mainly on the initial impurity concentrations, device structure, fabrication techniques, the level of current injection, the widths of the p and n region, lifetime damage constant, carrier removal rate, etc. Then, the dominant effect in most rectifiers is the increase in series resistance due to the removal of majority carriers from the conduction process in the lightly doped material.

In a reverse biased condition, the reverse leakage shows an increase with device exposure. Equation (56) only gives the reverse-diffusion-saturation current

$\left(qAp_n\left(\frac{D_p}{\tau_p}\right)^{1/2}\right)$, which would tend to increase as τ decreased. However, in reality, the reverse leakage current deviates from the universal diode equation by a carrier generation current and surface leakage current components. The carrier generation component can be approximated by

$$I_{rg} = qA\left(\frac{W_t n_i}{2\tau}\right) \propto \frac{(V_j)^{1/2} n_i}{\tau} \qquad (58)$$

for a p+n alloy diode where W_t is width of the transition region and n_i is intrinsic carrier density concentration. In silicon this current is larger than the diffusion current, but in germanium the carrier generation current is less than the diffusion current. The surface leakage current component is dependent on such things as surface condition, the presence of surface charge, surface area, and surface recombination; therefore, it is not easy to calculate. In many silicon diodes, this component will dominate over the other two components; but if the diode surfaces have been passivated, the bulk current will dominate over the surface leakage.

The reverse breakdown voltage shows a tendency to increase with increasing neutron exposure. The amount of increase depends on the doping concentration of the material, but for a p+n avalanche junction the breakdown voltage is mainly dependent on the conductivity or doping concentration of the n-region. The effect of conductivity

modulation will depend mainly on the initial doping concentration, the carrier removal rate, and the integrated neutron flux.

One normally does not worry about the breakdown voltage when using a diode as a rectifier in a neutron environment because the breakdown voltage will tend to increase with radiation due to carrier removal. In this study we will observe its behavior, as it is one of the main factors that influence the operation of avalanche devices. By using breakdown voltage versus impurity concentration and carrier removal data published in the literature, we can make a rough prediction of the neutron exposure required to show any degradation in the breakdown voltage. Figure 22 shows the avalanche breakdown voltage versus impurity concentration in a p+n silicon junction. Assuming that two to four carriers are removed per neutron/cm^2 (removal rates depend on dopant types, doping levels, fabrication processes, temperature of measurement, etc.), it can be shown that neutron exposure in excess of about 1×10^{15} neutron/cm^2 is required to show a change of ten percent in the breakdown voltage for 100-volt Zener diodes or less. Experimental results have been obtained which show that the breakdown voltage may change slightly in directions opposite to those indicated above.

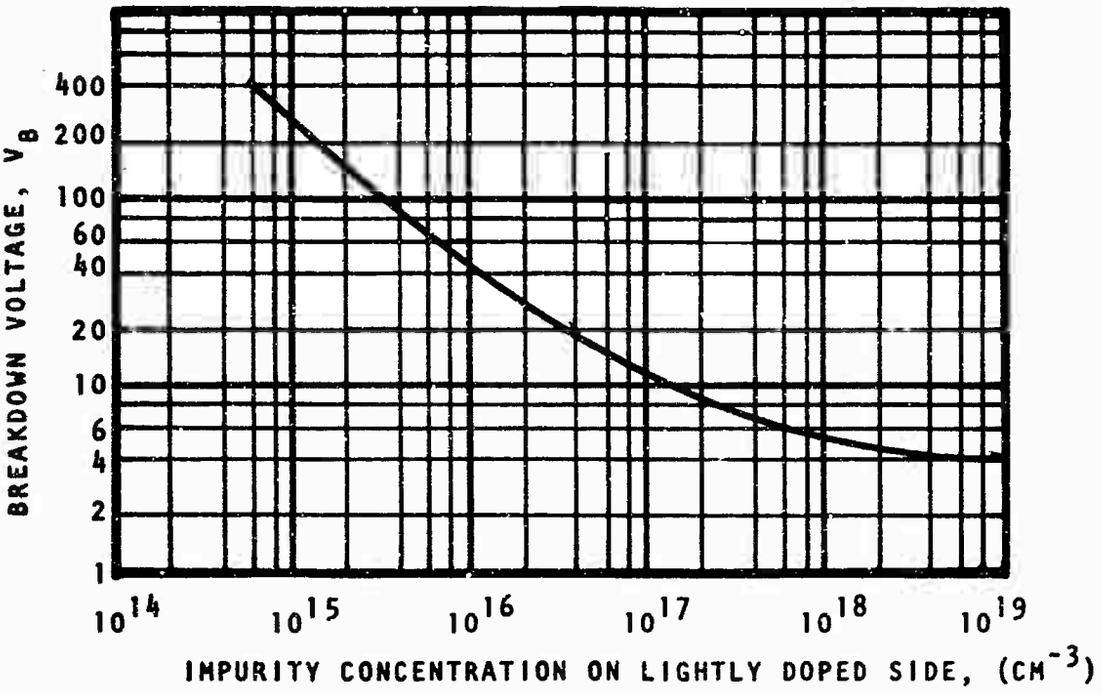

Figure 22. Breakdown Voltage Versus Impurity Concentration on the Lightly Doped Side of a Silicon Step Junction (References 3, 6 and 8)

Since the depletion capacitance of a p+n alloy junction is proportional to the square root of the donor concentration in the n-region, N_D, for a fixed voltage, it would be generally expected for the depletion capacitance to decrease as N_D decreases because of exposure. However, no conclusive evidence is available to indicate the frequency response of the trapping defects (i.e., if defect sites can contribute to capacitance at different frequencies), and no general trends in depletion capacitance have been indicated. The switching time is directly dependent on minority-carrier lifetime, and it will be expected to decrease with radiation.

b. Degradation of Transistors

Degradation observations in transistors have been related to bulk and surface effects. The bulk effect is the predominant effect and is caused mainly by a decrease in current gain (i.e., current-gain reduction limits usefulness of device usually long before majority carrier degradation effects are seen). Some of the other bulk effects that have been observed are changes in junction depletion capacitance, breakdown voltages, saturation voltage, punch-through voltage, base-spreading resistance, collector-body resistance, leakage current, switching time, storage time, turn-off time, and turn-on time. The degree to which the above changes affect the device depends on the device structure or fabrication and application. Generally, a device that has a thin base, high cutoff frequency, and small junction area will be more radiation resistant.

A general expression used to estimate the degradation in the common-emitter-current gain is given by (reference 13)

$$\beta_\Phi = \frac{\beta_o}{1 + \frac{1.00}{2\pi}\left(\frac{\Phi\beta_o K_\tau}{f_t}\right)} = \frac{\beta_o}{1 + a\Phi} \qquad (59)$$

where

β_Φ = gain at some fast-neutron fluence

β_o = initial gain

Φ = fast-neutron fluence

K_τ = lifetime damage constant

f_t = gain-bandwidth product frequency or the frequency at which the magnitude of β is unity $\propto f_{\alpha t}$ (base transport cutoff frequency)

$$a = \frac{1.00\ \beta_o K_I}{2\pi f_t}$$

The above expression shows that $1/\beta_\Phi$ is a linear function of Φ. However, the extent to which the above approximation holds depends on base width, base conductivity and type, uniformity of base resistivity, certainty of K_τ (experimental data for K_τ vary from about 4×10^{-8} to 2×10^{-6} n/cm^2-sec for silicon and 1×10^{-8} to 6×10^{-8} n/cm^2-sec for germanium, depending on base type), whether the device was biased while radiated or not, surface effects, emitter efficiency, surface recombination velocity, conductivity modulation, recombination in the base region, etc. Frank and Larin have experimentally confirmed that in the current range where carrier recombinations in the base region are the major cause of gain degradation that (reference 13)

$$1/\beta_\Phi \cong 1/\beta_o + \bar{t}\ K_\tau\ \Phi \qquad (60)$$

where $\bar{t}$ is the mean base transit time. Therefore, the change in reciprocal gain because of neutron radiation is

$$\Delta(1/\beta) \cong \bar{t}\ K_\tau\ \Delta\Phi \qquad (61)$$

Easley did some of the initial work on degradation of α, and a meaningful expression derived from his work for the common-base current gain (reference 13) is

$$\alpha_\Phi = \alpha_o - \frac{0.61K_\tau}{\pi f_\alpha} \Phi \tag{62}$$

where f_α is the alpha cutoff frequency of the transistor. The above linear dependence of α_Φ on Φ has been shown to be a good approximation for silicon transistors, but it is not as good for germanium transistors. Equation (62) indicates that devices with high alpha cutoff frequency are more radiation resistant. Such devices are usually the type of transistors used in avalanche design.

Two of the important parameters in avalanche circuitry are the collector-base-breakdown voltage BV_{CBO} and the collector-emitter-breakdown voltage BV_{CEO}. The breakdown voltage of any junction was discussed in subsection 3.a. The BV_{CEO} or sustaining voltage was discussed in Section II and it was approximately related to gain β of the transistor by

$$BV_{CEO} = BV_{CBO} \, (\beta+1)^{-1/n'} \tag{63}$$

The above empirical equations suggest that one should be able to predict the behavior of BV_{CEO} by doing pre- and post-testing. Pre-testing means electrical testing of the device prior to any irradiation, and post-testing means

electrical testing of the device after exposure to nuclear radiation. Assuming that n' stays constant, equation (63) indicates that BV_{CEO} should increase with neutron fluence, provided irradiation is sufficient to cause significant changes in doping concentrations and β degradation.

SECTION IV

EXPERIMENTAL AND THEORETICAL EFFECTS OF AVALANCHE DIODES DURING IONIZING IRRADIATION

1. Instrumentation and Equipment

An important parameter for the avalanche diode, which has to be experimentally measured, is the radiation induced transient photocurrents $Mi_{pp}(t)$. These resulting currents, which vary as a function of time, have peak magnitudes which depend on the radiation level and the value of the diode voltage, V_D.

Experimentally, tests were made on the different avalanche diodes with the dose and dose rate held constant for each transient pulse of radiation, while V_D was varied over a range of reverse bias voltages. From the resulting current pulses, the peak values of $Mi_{pp}(t)$ were obtained as a function of the diode reverse voltage, V_D.

All the irradiation tests were made using the KAFB 2-Mev flash X-ray machine. The instrumentation setup used was that shown in figure 23. As preliminary tests indicated that the test circuit time constants had to be kept small compared to the diode response risetime, the value for the resistor R_L, was made 51 Ω. A Keithley 110, zero decibel gain amplifier was used to drive the coaxial cable going to the oscilloscope. If additional amplification was required, a Keithley 109, 10X amplifier was inserted after the cable driver amplifier. Everything,

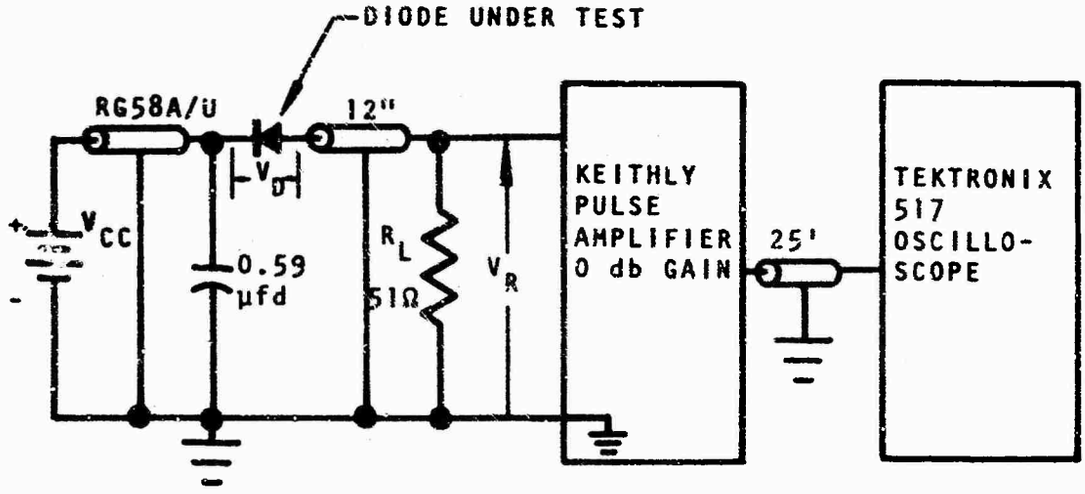

Figure 23. Avalanche Diode Photocurrent Test Circuit

with the exception of the diode under test, was shielded from the incident radiation by at least four inches of lead. The Tektronix 517 oscilloscope input was matched for a 51 Ω cable input, and a calibrated variable attenuator was added to the vertical input. The test equipment and test sample were enclosed in a double-walled rf shield room. Inside this screen room the rf noise is reduced by 120 db.

2. Experimental Results on Avalanche Diodes

The diodes used in these tests were Continental Device Corporation high performance 400-milliwatt silicon voltage regulators. The devices exhibit a very low leakage current which assures the "hardness" of the reverse characteristics

and a minumum of surface effects. Only diodes that exhibited essentially an avalanche characteristic were used in these tests. This required using diodes with breakdown voltages greater than 7 volts.

The diodes were of alloy construction made from an n-silicon wafer that was phosphorous doped to provide correct doping for a specified breakdown. The p-material was obtained by alloying an aluminum button into the n-wafer. This provided a p+n step junction. The devices were not gold doped.

Using the circuit shown in figure 23, the V_{CC} voltage was varied in steps from 0 to some value above V_B, and the primary photocurrent was measured at each voltage step. The voltage above V_B was limited to a value such that the power rating of the device was not exceeded.

Typical plots of the resulting transient induced photocurrent are shown in figure 24 for the 1N3516 diode at various values of V_{CC}. These data were taken at a dose rate of about 2×10^9 R/sec. At low voltages, the device decay response behaved close to the theoretical prediction presented in Section III. However, for diode voltages above the avalanche breakdown, the device radiation response decay increased. This behavior was shown (see appendix I) to be related to the electric field developed by the voltage drop across the lightly doped n-region as the diode currents became large after avalanche breakdown. From

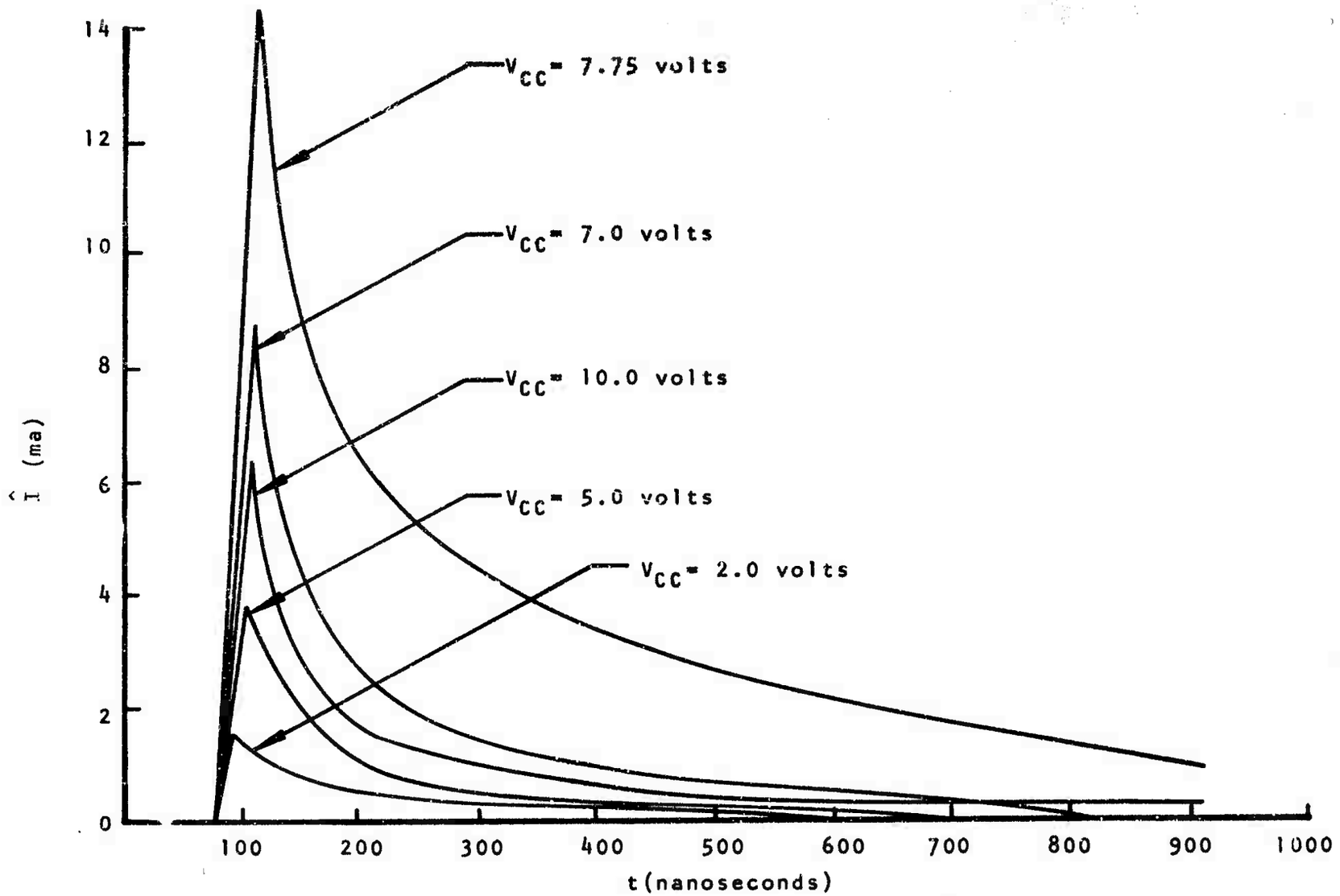

Figure 24. 1N3516 Photocurrent at 2 x 10^9 R/sec

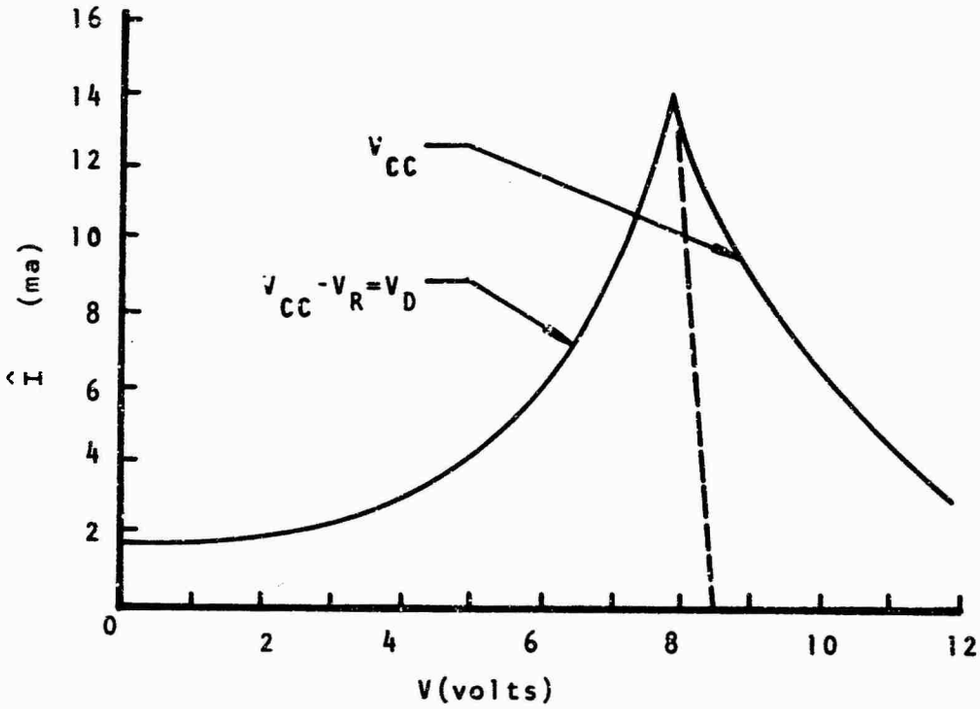

Figure 25. Peak Photocurrent versus V_{CC} and V_D for the IN3516

figure 24, the peak value of the photocurrent as a function of the diode voltage V_D was obtained. The resulting plot of peak I(t) (current observed in the circuit) versus the diode voltage, V_D (see figure 23) and the battery voltage, V_{CC}, is shown in figure 25.

As discussed earlier, the primary photocurrent under avalanche multiplication, $i^*_{pp}(t)$, can be expressed as

$$i^*_{pp}(t) = Mi_{pp}(t) \tag{64}$$

where $i_{pp}(t)$ is the normal primary photocurrent without multiplication. Since at low voltages M is one, $i_{pp}(t)$ behavior as a function of voltage can be determined. The

change in $i_{pp}(t)$ as a function of voltage V_D is attributed to both depletion and diffusion components. For low breakdown diodes, the change in photocurrent with voltage may be so small as to be indiscernible. By calculating from figure 25 the ratios of the peaks of i^*_{pp} to i_{pp}, one can determine M at various voltages up to about V_B. The multiplication factor M has previously been given as

$$M = \frac{1}{1 - \left(\frac{V}{V_B}\right)^{n'}} \tag{65}$$

which can also be expressed as

$$1 - \frac{1}{M} = \left(\frac{V}{V_B}\right)^{n'} \tag{66}$$

If one now plots log $(1 - \frac{1}{M})$ versus log (V), one can approximately obtain a straight line plot up to V_B with a slope equal to n'. The fact that this plot results in a straight line tends to verify the fact that avalanche multiplication is occurring. From the point at which $1 - \frac{1}{M} = 1$ (i.e., $M = \infty$) one can obtain the value of V_B needed to satisfy equation (66). It should be noted that due to possible experimental errors, not all the points lay on this straight line. The value of V_B obtained by this method is usually larger than the value obtained by the dc method in Appendix II.

TABLE I

BREAKDOWN VOLTAGE DATA

Device No.	n'	V_B(radiation) Volts	V_B(dc) Volts
1N3516-1	1.43	8.6	7.75
1N3516-2	1.36	8.4	7.89
1N3518-6	2.59	9.75	9.78
1N3518-7	2.24	9.6	10.39
1N3526-11	2.52	22.4	21.78
1N3526-12	2.0	21.5	21.01
1N3534-16	2.83	49.5	47.76
CD3171-21	4.31	59.0	57.3
CD3174-22	3.25	85.5	82.2

The values obtained from the experimental radiation results are tabulated in table I. It will be noted that the tabulated values of V_B do not agree closely with those obtained by dc measurements. It was also observed that, in the plot of log $(1 - \frac{1}{M})$ versus log V_D, the resulting points fell below the theoretically predicted straight line values as V_D approached V_B. This accounts for the discrepancy between the graphically obtained value for V_B and the dc value of V_B. The reason that the plotted points fell below the straight line relationships is that as V_D approaches V_B, the multiplication factor behaves as $\frac{1}{M} = m(1 - \frac{V_D}{V_B})$ where m is an empirical constant (reference 27). Plotting the experimental data using this new expression for M results in linear plots as V_D approaches V_B as shown in figure 26.

When V_D exceeded V_B, the peak values of the photocurrent began to decrease. This phenomenon is due to the inherent reduction of the internal shunting resistance of the diode

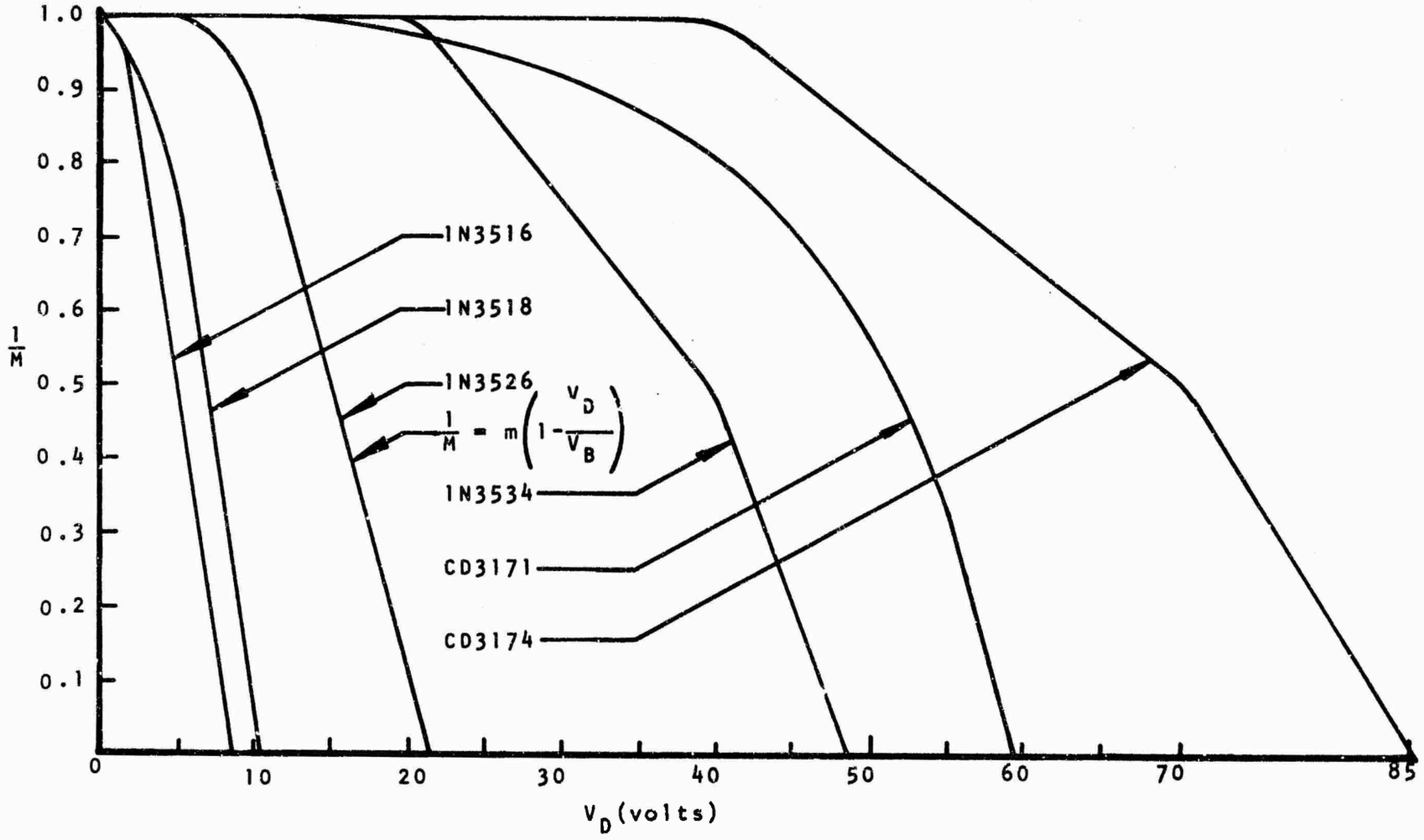

Figure 26. Plot of $\frac{1}{M}$ versus V_D

operating in the avalanche region. This result is analogous to the usual behavior of a diode voltage regulator.

As previously discussed (see equation 27), we defined the leakage current as

$$I = MI_{CO} = \frac{I_{CO}}{1 - \left(\frac{V_D}{V_B}\right)^{n'}} \tag{67}$$

where I_{CO} is the dc diode leakage current at low voltage levels. As V_D approaches V_B, M can be redefined as

$$\frac{1}{M} = m\left(1 - \frac{V_D}{V_B}\right) \tag{68}$$

where m is an empirical constant. With this new definition of M, equation (67) becomes with the use of figure 23

$$I = \frac{I'_{CO}}{1 - \frac{V_D}{V_B}} = \frac{I'_{CO}}{1 - \left(\frac{V_{CC}-IR}{V_B}\right)} \tag{69}$$

where $I'_{CO} = \frac{I_{CO}}{m}$, R is the total series circuit resistance (this includes R_L and the diode bulk and ohmic resistance, r_b) and V_{CC} is the external source voltage. Equation (69) can then be put in the form

$$I^2 + \left(\frac{V_B - V_{CC}}{R}\right) I - \frac{I'_{CO} V_B}{R} = 0 \tag{70}$$

The physically correct solution to this quadratic equation is

$$I = \frac{V_{CC}-V_B}{2R} + \sqrt{\left(\frac{V_{CC}-V_B}{2R}\right)^2 + \frac{I'_{CO}V_B}{R}} \qquad (71)$$

Similarly, we can define I' as the peak value of total current obtained when we subject the device to ionizing radiation. I' would then be the sum of the normal dc current multiplied by avalanche and the peak value of the avalanche multiplied photocurrent i^*_{pp}. I' can then be expressed as

$$I' = \frac{I'_{C1}}{1 - \frac{V_D}{V_B}} = \frac{I'_{C1}}{1 - \left(\frac{V_{CC}-IR}{V_B}\right)} \qquad (72)$$

where $I'_{C1} = \frac{I_{CO} + \text{Peak of } i^*_{pp}}{m}$. The physically correct solution to this equation is

$$I' = \frac{V_{CC}-V_B}{2R} + \sqrt{\left(\frac{V_{CC}-V_B}{2R}\right)^2 + \frac{I_{C1}V_B}{R}} \qquad (73)$$

Subtracting I from I', the peak value of the avalanche multiplied photocurrent observed in the external circuit is given by

$$\hat{I}^*_{pp} = \sqrt{\left(\frac{V_{CC}-V_B}{2R}\right)^2 + \frac{I'_{C1}V_B}{R}} - \sqrt{\left(\frac{V_{CC}-V_B}{2R}\right)^2 + \frac{I_{CO}V_B}{R}} \qquad (74)$$

Using typical circuit and device parameters, a plot of $\hat{I}^*_{pp}$ as a function of V_{CC} is shown in figure 27. Note that the resulting shape of this curve is extremely close

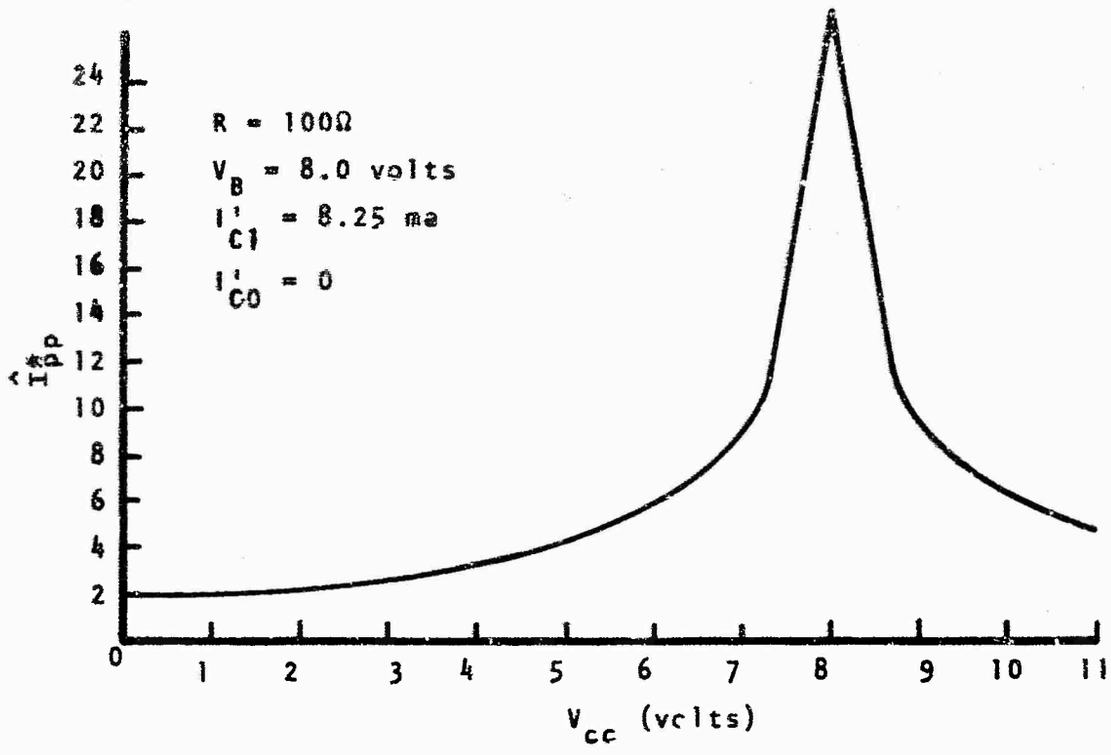

Figure 27. Theoretical Plot of $\hat{I}^*_{pp}$

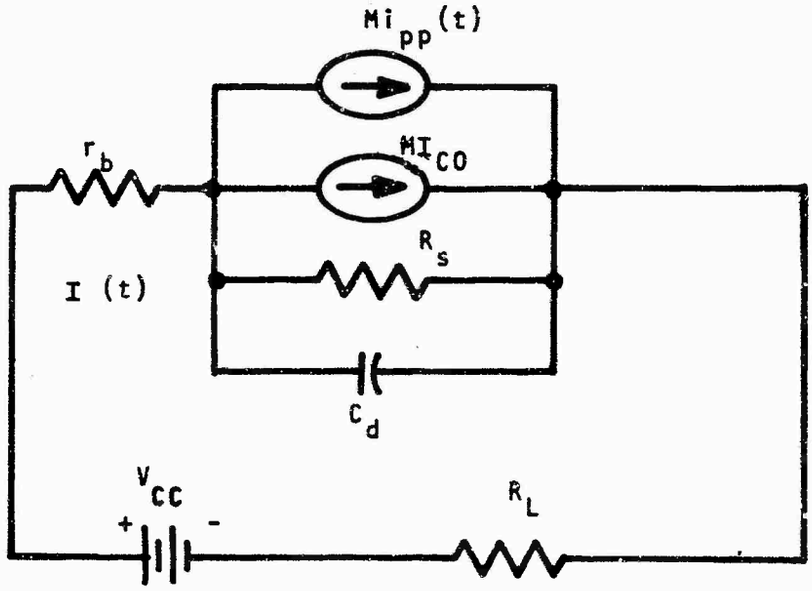

Figure 28. Equivalent Circuit of a Reverse Bias Avalanche Diode Prior to Breakdown

to that of figure 27 which was obtained experimentally. This indicates that the theoretical models used and the assumptions made are reasonably accurate.

3. Equivalent Models of Avalanche Diodes

Using the experimental and theoretical results, the following simplified models were developed to explain the behavior of avalanche p+n alloy diodes under transient ionising radiation and reverse bias dc conditions. Figure 28 shows the equivalent circuit prior to breakdown where r_b is the total diode bulk and spreading resistance, R_s is the diode shunt leakage resistance, and C_d is the junction depletion capacitance. Neglecting the depletion capacitance, it can be shown that the external transient current observed in the load resistor R_L, is given by

$$I(t) = \frac{Mi_{pp}(t)R_s}{R_s+R_L+r_b} = \frac{Mi_{pp}(t)}{1 + R_L/R_s+r_b/R_s} \qquad (75)$$

Usually before breakdown, R_s is much greater than r_b or R_L, and the equation (75) can be reduced to

$$I(t) \approx Mi_{pp}(t) \quad . \qquad (76)$$

This equivalent circuit implies that $Mi_{pp}(t)$ is acting like a constant current generator. However, as the diode approaches and enters the avalanche region of operation, the relation that $R_s >> R_L$ and $R_s >> r_b$ will no

longer hold due to the breakdown mechanism of the device. An equivalent circuit in the avalanche region is shown in figure 29, where R_s has been replaced by the avalanche

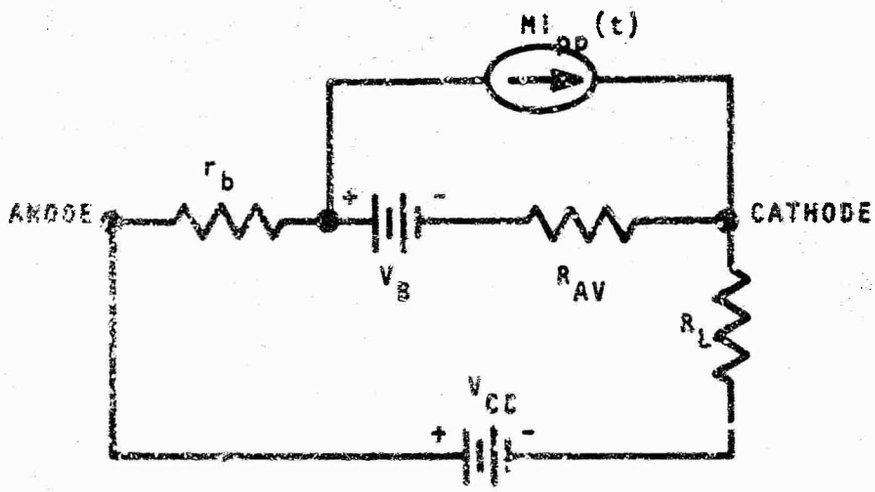

Figure 29. Equivalent Circuit of Avalanche Diode in the Breakdown Region

resistor, R_{AV}. This resistance is current sensitive and tends to decrease as the diode voltage increases. Again using a Thevenin equivalent, I(t) can be shown to equal

$$I(t) = \frac{Mi_{pp}(t)}{1 + R_L/R_{AV} + r_b/R_{AV}} \qquad (77)$$

which decreases as R_{AV} decreases. As the diode is driven further into avalanche by increasing V_{CC}, R_{AV} tends to decrease which decreases I(t). In essence, once the device is in the avalanche region, $Mi_{pp}(t)\ R_{AV}$ behaves like a voltage generator.

SECTION V

EXPERIMENTAL RESULTS AND HARDENING OF AVALANCHE TRANSISTOR TO IONIZING RADIATION

1. Introduction to Avalanche Hardening

The avalanche transistor without special design considerations is sensitive to irradiation by transient pulses of X rays. The predominat radiation effect is the switching of the transistor from the off state to the on state because of the induced transient primary photocurrents. However, by using proper biasing and/or junction compensation, one can harden the avalanche transistor so it will not switch at various levels of radiation. This section will present the experimental and theoretical results of the effect of X rays on avalanche circuits and hardening ciriteria.

2. Avalanche Transistor Pulse Generator

Figure 30 shows the diagram of an avalanche transistor pulse generator. This circuit will trigger whenever the internal base to emitter voltage becomes large enough that the base emitter junction becomes forward biased causing the emitter to inject carriers. In Addition, as discussed in Section II, the pulse generator will also fire under certain conditions because of an increase in the collector to emitter voltage, V_{CE}.

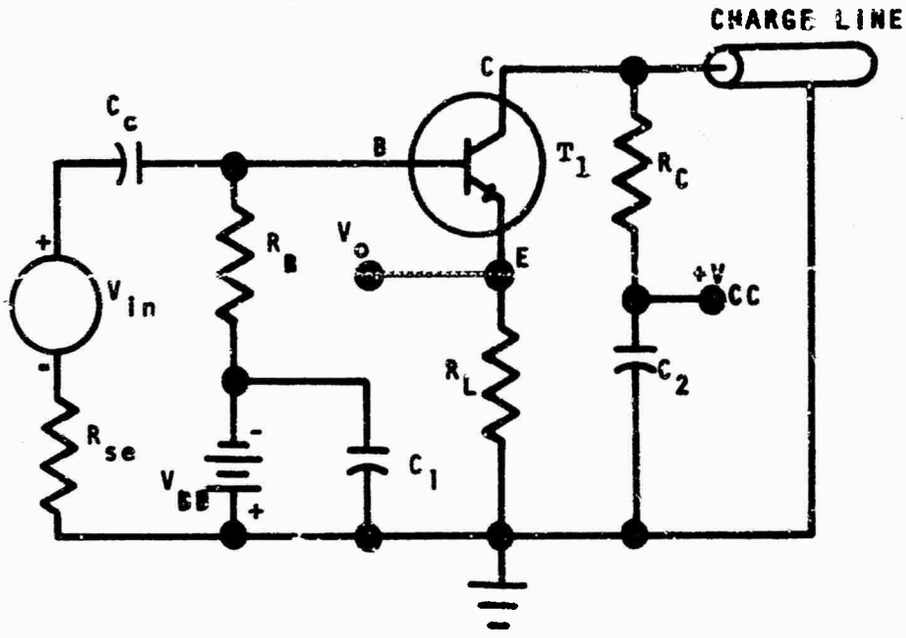

Figure 30. Avalanche Transistor Pulse Generator

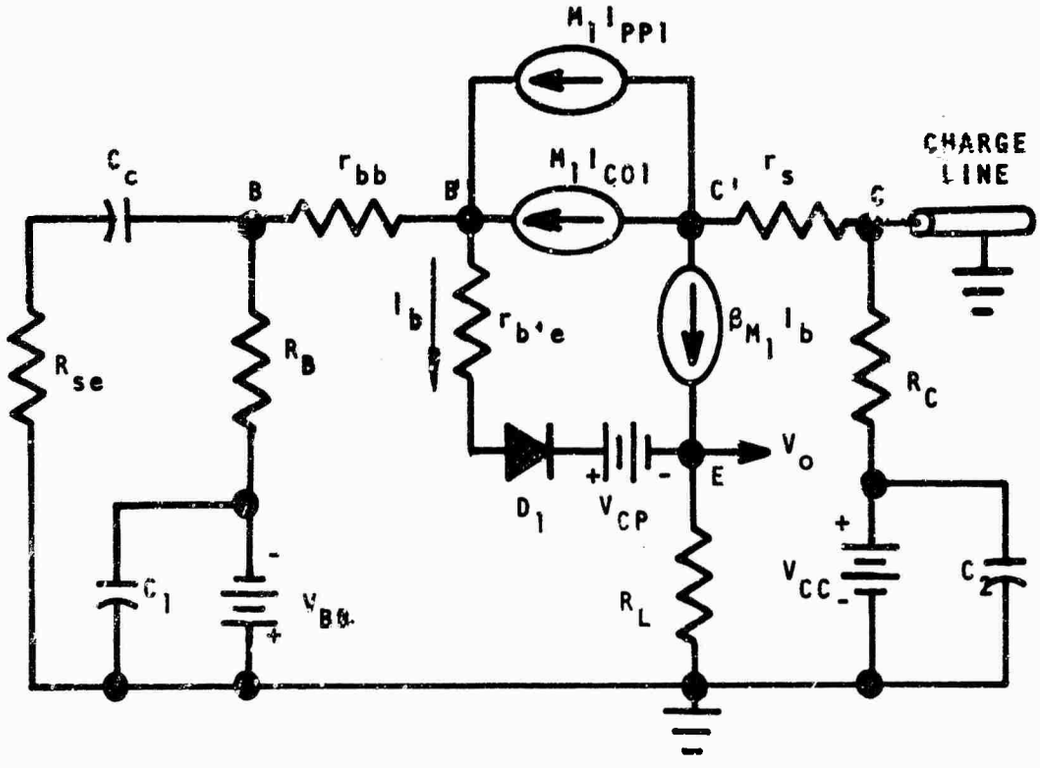

Figure 31. Cutoff Mode Equivalent Circuit

Figure 31 shows an approximate equivalent circuit of the pulse generator for the cutoff mode. This equivalent circuit, which includes the radiation effects, may be used for a steady state or quasi-steady state type of analysis when the junction capacitances and stray capacitances are ignored.

The circuit's equivalent components shown in figure 31 are defined as follows:

R_{se} = the input signal source equivalent output resistance

r_{bb} = the transistor base spreading and bulk resistance

r_s = the transistor collector bulk series resistance

$r_{b'e}$ = the transistor base-emitter junction equivalent internal resistance

I_{CO1} = transistor T_1 collector to base leakage current when the emitter to base junction is reverse biased

D_1 = the base emitter idealized diode

V_{CP} = the base emitter contact potential $\cong$ 0.6 volt

I_{pp1} = the X-ray induced transient primary photocurrent produced in T_1

M_1 = the avalanche multiplication factor for transistor T_1, or

$$M_1 = \frac{1}{1 - \left(\frac{V_{CE}}{BV_{CBO}}\right)^{n'}}$$

V_{CE} = the collector to emitter voltage before firing

BV_{CBO} = the collector to base breakdown voltage with the emitter open

n' = an empirical constant

$$\beta_{M_1} = \frac{M_1\alpha_o}{1 - M_1\alpha_o} = \frac{\alpha^*}{1-\alpha^*} \quad \text{(reference equation 28)}$$

α_o = h_{fb} = the low frequency collector-emitter forward current ratio

The effect of transient gamma irradiation is accounted for by the $M_1 I_{ppl}$ idealized current generator. This transient current during irradiation tends to switch the pulse generator because of the resulting increase in the internal base to emitter voltage $V_{B'E}$. When $V_{B'E}$ becomes greater than approximately V_{CP}, the junction becomes forward biased and I_b (see figure 31) is no longer zero. This causes the avalanche switching of T_1 to occur. Therefore, in order that the avalanche circuit does not switch during exposure to transient X rays, it is necessary that V_{CE} does not increase significantly and that $V_{B'E}$ is less than approximately the contact potential.

3. Hardening Considerations for Pulse Generator Without Use of Junction Compensation Techniques

When the pulse generator is subjected to a pulse of ionizing radiation, the V_{CE} and $V_{B'E}$ magnitudes change. The resulting maximum peak change in the collector voltage (ΔV_C) is negative and is given by

$$\Delta V_C \doteq - R_C M_1 I_{pp1} \tag{78}$$

assuming that the transistor does not switch. For the transistor in the cutoff mode, V_O is essentially zero, therefore, ΔV_C is the resulting maximum peak change in V_{CE} due to irradiation. This value will never be achieved unless the radiation pulse is much longer than the time required to reach this steady state value. That is, as long as the transistor is off, the charge line behaves as a capacitor and steady state will be reached in four time constants, $4R_C C_{CL}$ (where C_{CL} is the charge line effective capacitance). The main point to be made here is to notice the direction of change of V_C. Since ΔV_C is negative, the unit will not fire because of the change in V_{CE} during irradiation. In fact, since

$$M_1 = \frac{1}{1 - \left(\frac{V_{CE}}{BV_{CBO}}\right)^{n'}} \tag{79}$$

the value of M_1 should decrease during irradiation, and thus, slightly reduce the problem of possible switching of the transistor due to the increase of $V_{B'E}$.

The next consideration is the effect of the radiation-induced photocurrent on $V_{B'E}$ as it is changing at the same time V_{CE} is. Referring to figure 31, the peak value of $V_{B'E}$ during irradiation is

$$V_{B'E} = - V_{BB} + M_1(I_{ppl} + I_{COl})r_{bb} + M_1 I_{COl} R_B + M_1 I_{ppl} R_{se} \| R_B \tag{80}$$

where we have neglected the effect of the input coupling capacitor, as far as the transient pulse is concerned.

Using the criterion for nonswitching that $V_{B'E} < V_{CP}$ at all times yields the result that for radiation hardening one requires

$$V_{BB} > M_1 I_{COl}(r_{bb} + R_B) + M_1 I_{ppl}(r_{bb} + R_{se} \| R_B) - V_{CP} \tag{81}$$

Inspection of equation (81) shows that to make the avalanche transistor radiation hardened one should do the following:

a. Make R_B and R_{se} as small as possible consistent with other design requirements,

b. Select a transistor which has minimum I_{ppl}, I_{COl} and $r_{bb'}$,

c. Minimize the value of M_1 to the extent possible by transistor selection and the establishment of the quiescent value of V_{CE}, but yet have the required output amplitude,

d. Make V_{BB} large enough to ensure that $V_{B'E} < V_{CP}$ up to the maximum level of radiation for which hardening is desired. This value of V_{BB} may be determined experimentally during irradiation or approximately calculated from equation (81). However, practical limits on how large V_{BB} can be made are imposed by the base to emitter junction breakdown voltage, the input trigger source voltage available, and the amount of power gain required.

Application of the above criteria will result in considerable radiation hardening of avalanche transistor circuits in general. However, reducing R_B and increasing V_{BB} tends to cause an increase in the minimum allowable input trigger pulse voltage for proper switching.

The experimental results of testing this circuit during irradiation were completely consistent with the theoretical hardening criteria developed in this section. Increasing V_{BB} and decreasing R_B and R_{se} resulted in increased radiation hardening of the avalanche pulse generator. It was found that finally the transient voltage developed across r_{bb} and R_B was the limiting factor for preventing hardening by increasing V_{BB}. That is, the

transient voltage developed across r_{bb} and R_B overcame the reverse biased effects of V_{BB} and V_{CP}, which caused the transistor to switch. However, increasing V_{BB} to achieve increased radiation hardening is limited by the breakdown voltage of the emitter base junction and the amount of power gain required.

The experimental results using the Motorola 2N2219 in the test circuit as shown in figure 32 were that the circuit switched when V_{BB} was -3 volts or above, but did not switch when V_{BB} was lowered to -4 volts or lower. This was at a radiation level of about 2×10^9 R/sec, as obtained at the KAFB Field Emission 2-Mev flash X-ray system. Similar results were obtained using the TI 2N3035 in place of the 2N2219.

For certain severe practical applications, the requirement $V_{BB} >> M_1 I_{ppl} (r_{bb} + R_{se} \| R_B) - V_{CP}$ (neglecting leakage effects) may be impractical or impossible to achieve. Therefore, some other type of hardening that places very few or no limitations on V_{BB} must be pursued to make the circuits' use more feasible. The next two subsections provide several means of doing this.

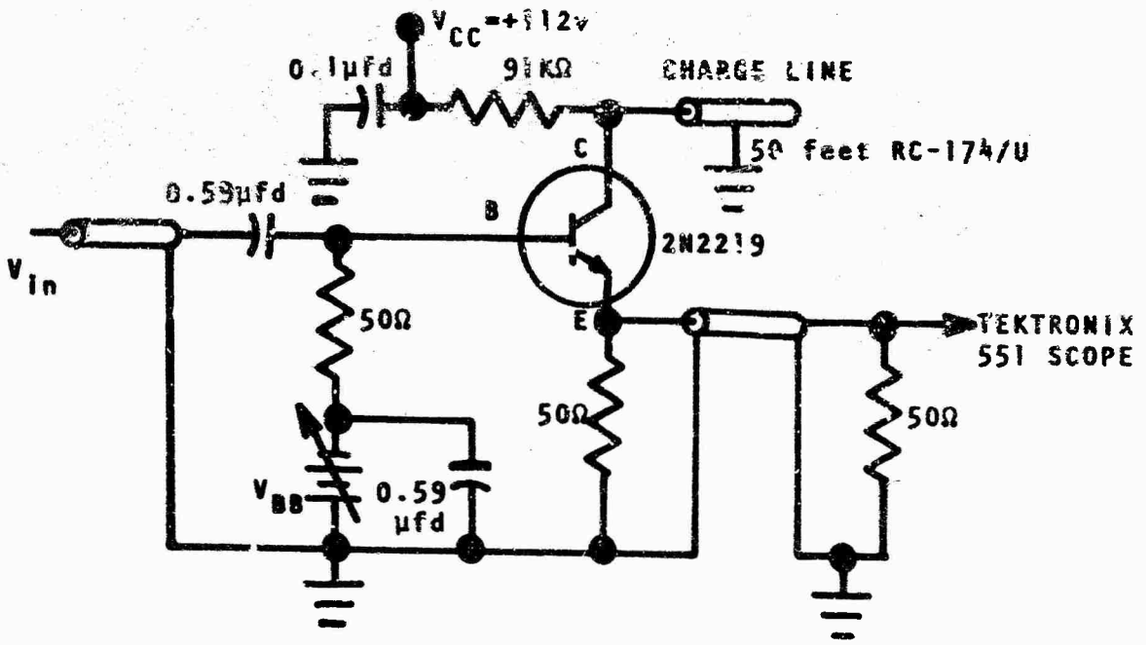

Figure 32. Experimental Circuit used in Radiation Testing of the 2N2219

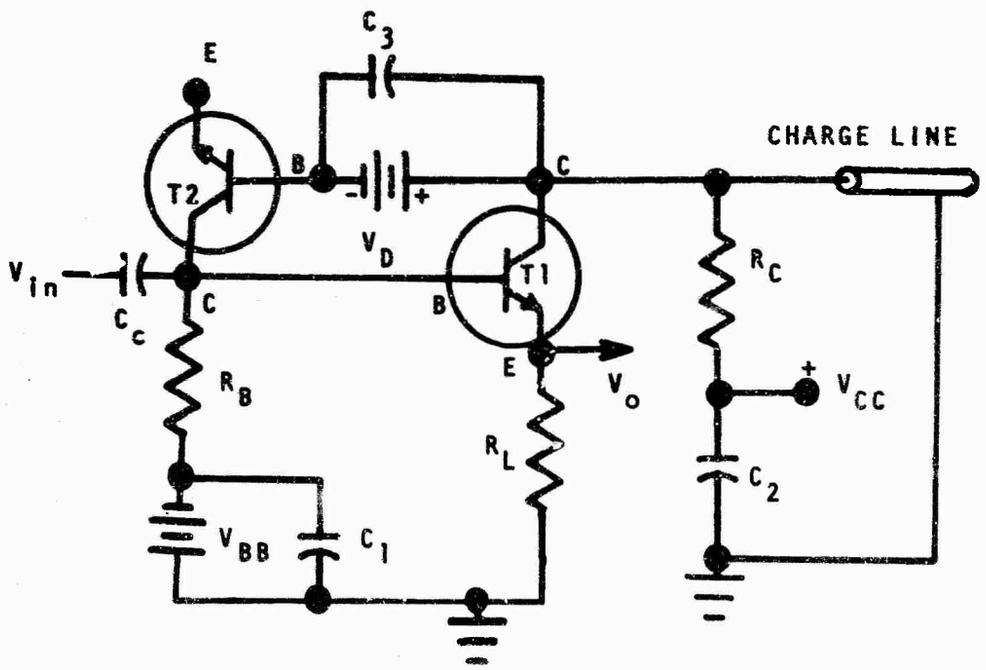

Figure 33. Collector to Base Diode Compensation Hardened Circuit

4. Collector to Base Diode Compensation Hardened Circuit

The $M_1 I_{pp1}$ radiation induced current tends to forward bias the base emitter junction, and thus, switch the transistor at high radiation exposures. $M_1 I_{pp1}$ flowing through $r_{bb} + R_{se} R_B$ causes a positive increase in $V_{B'E}$ which is of sufficient magnitude to trigger the transistor. If this increase of $V_{B'E}$ due to $M_1 I_{pp1}$ could be decreased or cancelled in some fashion without affecting general operation of the unit, increased radiation hardening of the avalanche circuit would be achieved.

One method of partially cancelling the effect of $M_1 I_{pp1}$ is to add a back biased diode junction between the base and collector of transistor T_1 as shown in figure 33. This diode, T_2, can be a diode per se or the collector to base junction of another avalanche transistor with the emitter connection open (or shorted to the collector to obtain increased primary photocurrent). The main requirement on T_2 is that its transient radiation induced photocurrent, $M_2 I_{pp2}$, be of the correct magnitude and shape for optimum hardening. An approximate relationship between $M_2 I_{pp2}$ and other circuit parameters needed for hardening will be developed in this section.

If it is assumed that T_2 is an avalanche transistor or diode, then M_2 is defined the same as M_1, where the

appropriate voltages and constants for T_2 are used. It should be noted that it will be required that T_2 have a sufficiently large breakdown voltage so that it does not also go into avalanche breakdown when T_1 switches. If T_1 and T_2 were simultaneously to be in avalanche breakdown, there is a possibility that the resulting current flow would destroy both transistors. Also, to ensure that the T_2 diode is never forward biased, it is necessary that V_D always be greater than V_{CB} of T_1.

Figure 34 shows an approximate equivalent circuit which includes the collector base junction compensation. The resistor r_d is the total series spreading and bulk resistance for diode T_2 and $M_2 I_{CO2}$ is its associated reverse leakage current. It is assumed that the transistor T_1 is sufficiently cut off to neglect any emitter current leakage while in the off state.

When the circuit is subjected to ionizing radiation, the approximate maximum peak pulse change in V_{CE} (assuming T_1 does not switch) is

$$\Delta V_C \doteq \Delta V_{CE} \doteq (M_2 I_{pp2} - M_1 I_{pp1}) R_C \qquad (82)$$

Thus, to ensure that T_1 does not switch because of an increase in V_{CE}, it is required that

$$M_1 I_{pp1} \geq M_2 I_{pp2} \qquad (83)$$

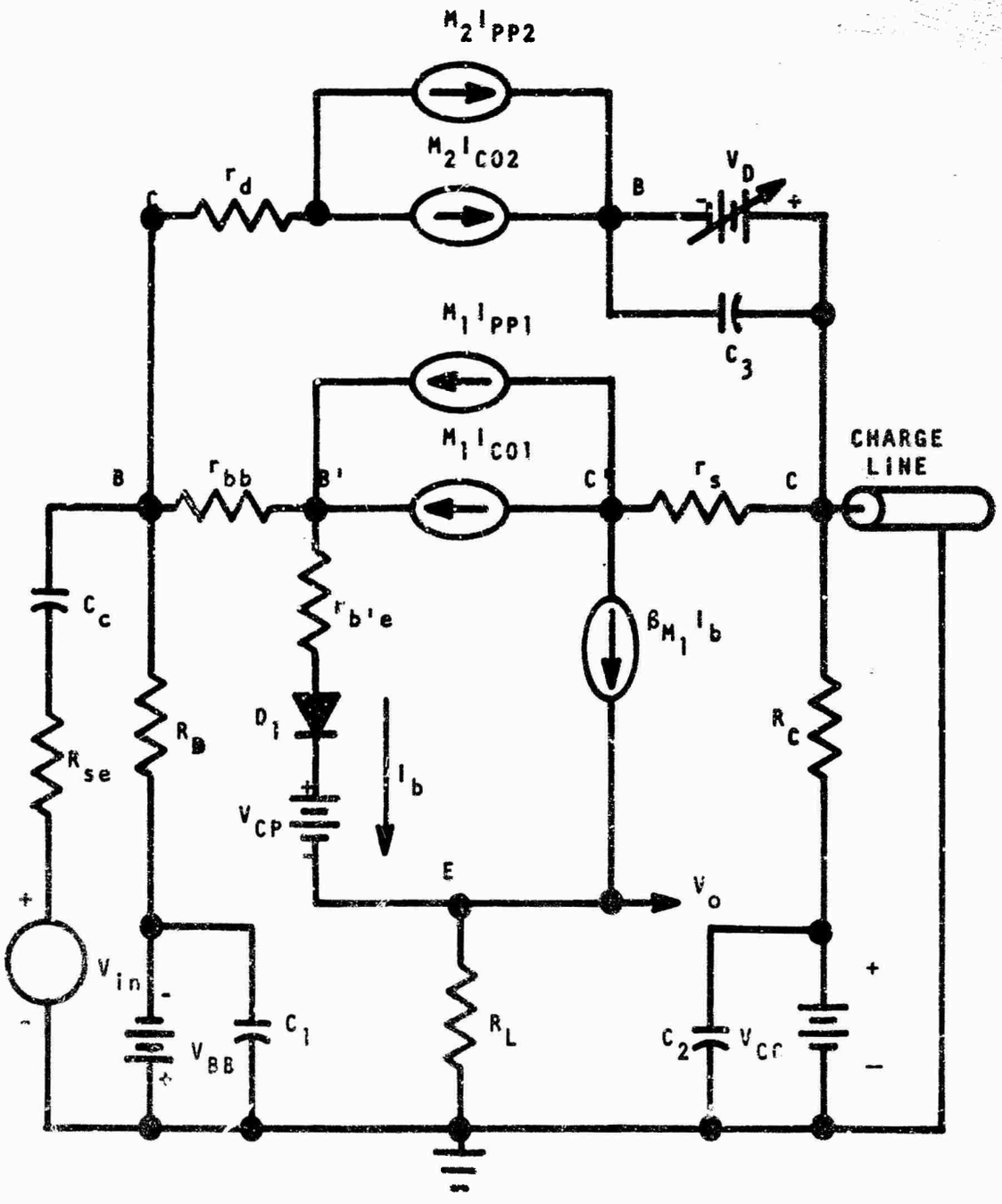

Figure 34. Cutoff Mode Equivalent Circuit for Collector to Base Compensation

The requirement that $V_{B'E}$ be less than V_{CP} for the hardening of T_1 yields the approximate design hardening criteria

$$V_{BB} > M_1 I_{CO1}(r_{bb} + R_B) + M_1 I_{pp1}(r_{bb} + R_{se} \| R_B) - M_2 I_{CO2} R_B - M_2 I_{pp2} R_{se} \| R_B - V_{CP} \quad (84)$$

Thus the general criteria for radiation hardening using collector to base junction compensation technique are given by equations (83) and (84). For many applications, a logical and adequate design approach would be to select T_1, T_2 and the quiescent operating levels such that

$$M_1 I_{pp1} = M_2 I_{pp2} \quad (85)$$

Using this relation as an assumed design criterion, further simplification of equation (84) is possible. The result is

$$V_{BB} > M_1 I_{pp1} r_{bb} + M_1 I_{CO1}(r_{bb} + R_B) - M_2 I_{CO2} R_B - V_{CP} \quad (86)$$

Typical values for r_{bb} are 10 to 100 ohms, and $MI_{CO} \doteq 50$ μa. A typical value for $M_1 I_{pp1}$ is 20 ma. Thus, the dominant factor in equation (86) is $M_1 I_{pp1} r_{bb} - V_{CP}$. The leakage current terms may be neglected for reasonably small values

of R_B. Using the above assumptions, the final approximate criteria for radiation hardening become

$$V_{BB} > M_1 I_{pp1} r_{bb} - V_{CP} \text{ and } M_1 I_{pp1} = M_2 I_{pp2} \qquad (87)$$

How much has been gained by the addition of the cancellation diode can be seen by comparing equation (81) and equation (86). These equations show that the requirements on V_{BB} for hardening have been essentially reduced by approximately $M_1 I_{pp1} R_{se} \| R_B$ volts by the addition of the cancellation diode. For many applications, this reduction will be significant and adequate.

One disadvantage to the above described method of hardening of avalanche transistor circuits is the requirement that $M_1 I_{pp1} \doteq M_2 I_{pp2}$ and, additionally, that $M_2 I_{pp2}$ must never be significantly greater than $M_1 I_{pp1}$ so that T_1 does not fire because of a significant increase of V_{CF}. Again for certain severe applications the requirement [illegible] $I_{pp1} r_{bb} - V_{CP}$, may be impractical or impossible to [illegible] For these applications, the addition (at the collector of T_1) of a forward biased clamping diode D_C with a voltage source ($+V_C'$) in series with it to ground might be worthwhile. This arrangement would essentially clamp the collector of T_1 at the $+V_C'$ voltage source level. Thus, the desired T_1 collector quiescent operating value is determined by V_C'. The supply voltage V_{CC} is made some value greater than V_C'. If V_{CC} is made much greater than

V_C', this arrangement will increase the recovery time of the pulse generator, as the charge line will be charging from a higher V_{CC} voltage source.

From the standpoint of radiation hardening, the possibility exists that considerable improvement can be made by the addition of the clamping diode circuit. The diode clamp will prevent V_{CE} from increasing during irradiation and the requirement $M_1 I_{pp1} \geq M_2 I_{pp2}$ will no longer be needed. If $M_2 I_{pp2}$ is greater than $M_1 I_{pp1}$, the excess current is shorted to ground through the clamp diode, and therefore V_{CE} cannot increase. Thus, the tricky problem of always ensuring $M_1 I_{pp1} \geq M_2 I_{pp2}$ is avoided. In addition, deliberately making $M_2 I_{pp2}$ greater than $M_1 I_{pp1}$ can be employed to assure that $V_{B'E}$ is less than V_{CP}.

Recall that for hardening we required that

$$V_{BB} > M_1 I_{CO1}(r_{bb} + R_B) + M_1 I_{pp1}(r_{bb} + r_{se} \| R_B) - M_2 I_{CO2} R_B - M_2 I_{pp2} R_{se} \| R_B - V_{CP} \qquad (88)$$

A conservative criterion for hardening would be to have

$$V_{BB} + V_{CP} > M_1 I_{CO1}(r_{bb} + R_B) + M_1 I_{pp1}(r_{bb} + r_{se} \| R_B) - M_2 I_{CO2} R_B - M_2 I_{pp2} R_{se} \| R_B \leq 0 \qquad (89)$$

$$\frac{M_2 I_{pp2}}{M_1 I_{pp1}} \geq 1 + \frac{r_{bb}}{R_{se} \| R_B} \quad \text{and} \tag{90}$$

$$\frac{M_2 I_{co2}}{M_1 I_{co1}} \geq 1 + \frac{r_{bb}}{R_B} \tag{91}$$

Under these conditions, the hardening criteria have reduced to $V_{BB} + V_{CP} > 0$. As V_{CP} is nominally about 0.6 volt, it should be possible to safely eliminate the source voltage V_{BB} entirely ($V_{BB} = 0$) while still achieving high intensity transient gamma radiation hardening. By proper selection of T_1, T_2, and the quiescent operating conditions it would appear possible to satisfy the conditions imposed by equations (90) and (91).

It is felt that the use of a collector to base cancellation diode combined with a clamping diode offers one of the better possibilities for avalanche circuits hardened to extremely high transient radiation levels.

Experimentally it was shown that significant radiation hardening is achieved by the use of the base to collector diode compensation technique. Additionally, these circuits tested should not be considered as the ultimate in hardened design, but rather as an indication of the feasibility of the design approach. The Motorola 2N2219 transistor was used for the active avalanche transistor in the test circuit as shown in figure 35, and a TI 1N499 was used for the compensation junction diode.

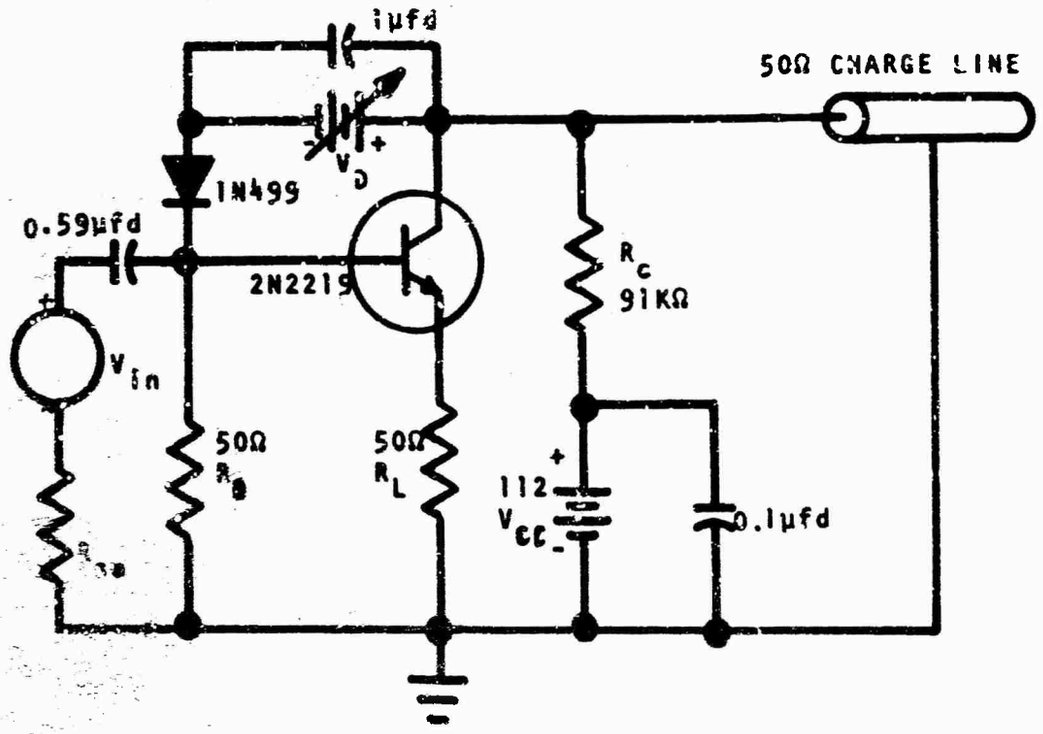

Figure 35. Collector to Base Compensation Circuit Used Experimentally to Harden Basic Avalanche Circuit

The circuit as shown required about a 700-mv external pulse (from a 50 Ω source) for triggering without exposure to X rays. As the radiation induced compensation current ($M_2 I_{pp2}$) from the IN499 is diode-voltage sensitive (due to depletion widening and avalanche multiplication), the radiation sensitivity level was a function of V_D. At a fixed radiation level, the circuit would fire due to radiation if V_D was too small and would not fire if V_D was large enough to produce sufficient avalanche photocurrent (within the limitation of the IN499 reverse breakdown voltage). However, if $M_2 I_{pp2}$ was made significantly greater than

$M_1 I_{pp1}$ by increasing V_D, the unit would fire because of the transient increase of V_{CE}. This is as predicted by the theoretical models.

Typical results when irradiated at about 7×10^9 R/sec were

a. Unit switched for $V_D \leq 150$ volts.

b. No switching for $V_D = 180$ volts.

In these tests (when the units did not fire) the base to ground voltage was negative, indicating that $M_2 I_{pp2}$ was greater than $M_1 I_{pp1}$. Increased hardening would have been achieved by the inclusion of a V_{BB} source, but this would have increased the required amplitude of the input trigger voltage.

Tests similar to the above were also performed on the 2N3035 at the 7×10^9 R/sec level. Satisfactory hardening was not achieved because of the apparently larger r_{bb} of this unit. This increased base resistance required a prohibitively large $M_2 I_{pp2}$ to cancel out the $M_1 I_{pp1} r_{bb}$ voltage drop. Hence there was no $M_2 I_{pp2}$ level at which $V_{B'E}$ could be made less than V_{CE} without increasing V_{CE} sufficiently to trigger the unit. At a reduced radiation level, $\sim 10^9$ R/sec, the circuit using the 2N3035 could be hardened employing this technique. Tests were also made on this circuit utilizing a clamping diode from the collector to ground. The results did not indicate

significant improvement, but it is felt that with careful adjustment of device and circuit parameters, hardening gains should be achievable.

5. Base to Ground Diode Compensation Hardened Circuit

One additional method of using compensating back biased junctions to achieve transient radiation hardening of avalanche transistor circuits is of special interest. Consider the circuit in figure 36. A back biased diode, T_2, has been added from the base of T_1 to ground. The action of this diode is quite similar to that for the cancellation diode from the collector to base of T_1.

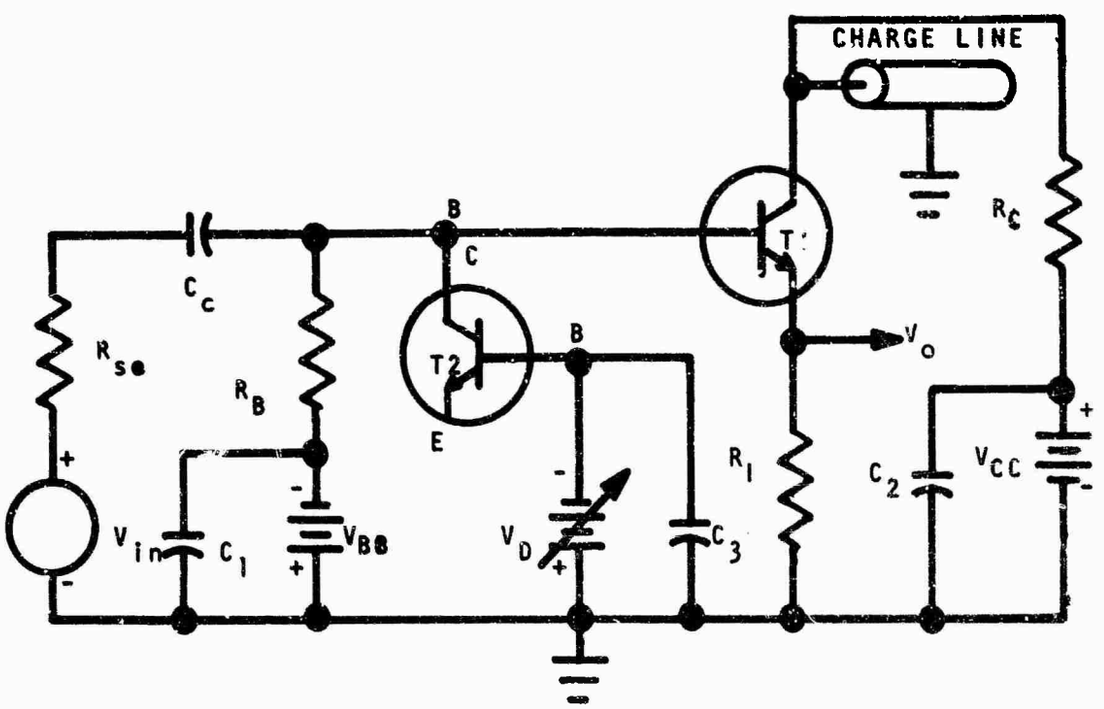

Figure 36. Base to Ground Diode Compensation Hardened Circuit

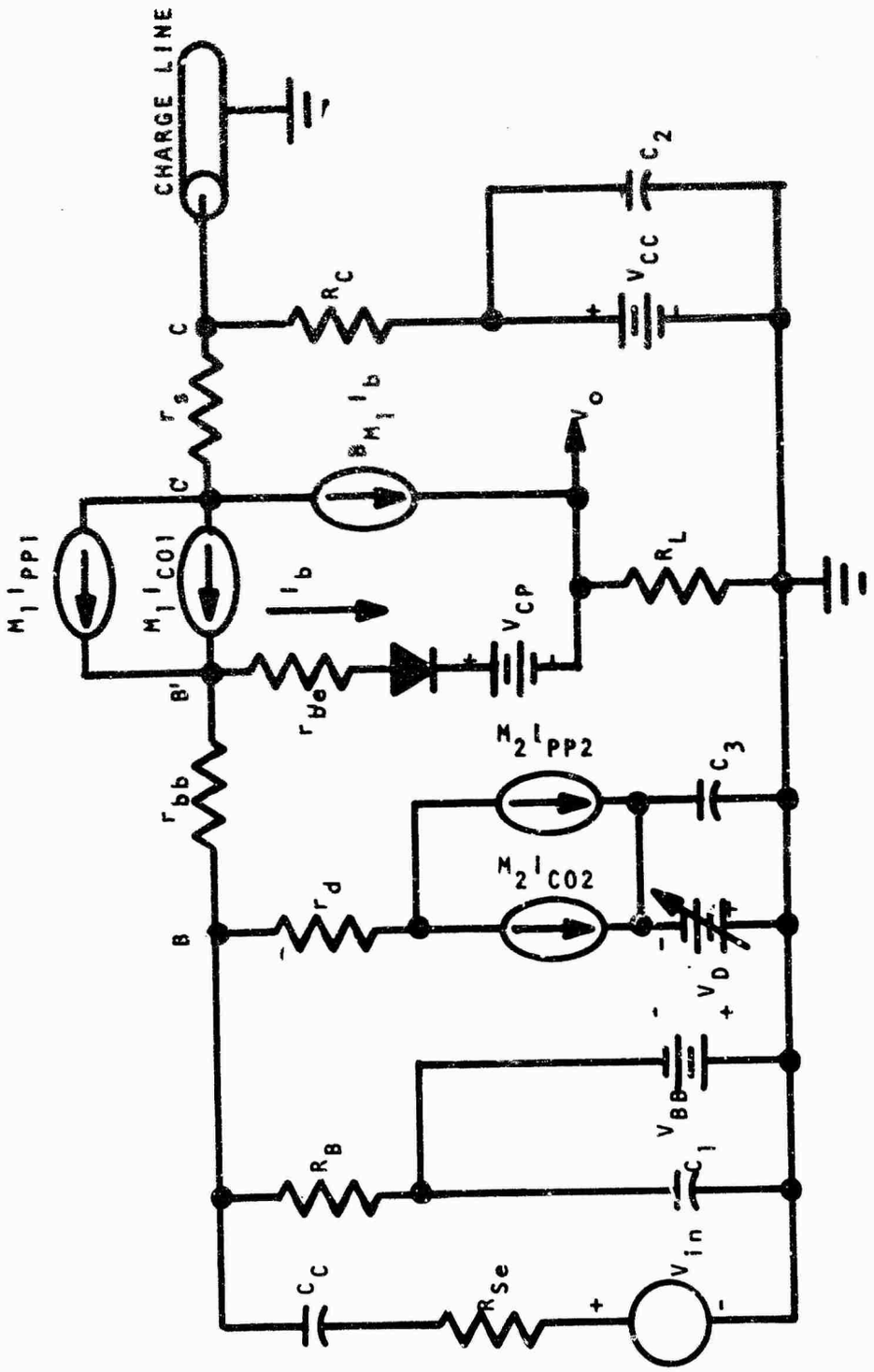

Figure 37. Equivalent Circuit for Base to Ground Compensation

A simplified equivalent circuit is shown in figure 37. Note that the transient maximum peak change of the collector voltage given by

$$\Delta V_C \cong \Delta V_{CE} \cong - M_1 I_{pp1} R_{\;} \tag{92}$$

is negative. Thus, there is no problem of possible firing of T_1 because of the increase of V_{CE}, or any associated restriction on the ratio of I_{pp1} to I_{pp2}. So, no clamping diode is needed in this circuit unless it is desired to increase the avalanche circuit recovery time.

As far as the requirement that $V_{B'E}$ has to remain less than V_{CP}, this circuit is the mathematical equivalent of that for the collector to base compensation technique without the requirement that $M_2 I_{pp2}$ never be greater than $M_1 I_{pp1}$. The criteria established for nonfiring of T_1 are

$$V_{BB} > M_1 I_{co1}(r_{bb} + R_B) + M_1 I_{pp1}(r_{bb} + R_{se} \| R_B) - M_2 I_{co2} R_B - M_2 I_{pp2} R_{se} \| R_B - V_{CP} \tag{93}$$

Once again, if we make

$$\frac{M_2 I_{pp2}}{M_1 I_{pp1}} \geq 1 + \frac{r_{bb}}{R_{se} \| R_B} \qquad \text{and} \tag{94}$$

$$\frac{M_2 I_{co2}}{M_2 I_{co1}} \geq 1 + \frac{r_{bb}}{R_B} \tag{95}$$

the hardening criteria has reduced to $V_{BB} + V_{CP} > 0$. Thus, it should be possible to eliminate the source voltage V_{BB} entirely, while still achieving high intensity, transient gamma radiation hardening. It is felt that, of the hardening techniques discussed, the use of a base to ground compensation junction offers the best possibility for avalanche circuits hardened to extremely high transient radiation levels. As the above theoretical results indicated, even with $V_{BB} = 0$, it appears feasible to design an avalanche transistor circuit for very high transient radiation environments. The experimental results confirmed this conclusion.

The test circuit for the base to ground cancellation technique is shown in figure 38. A 2N3035 was the active

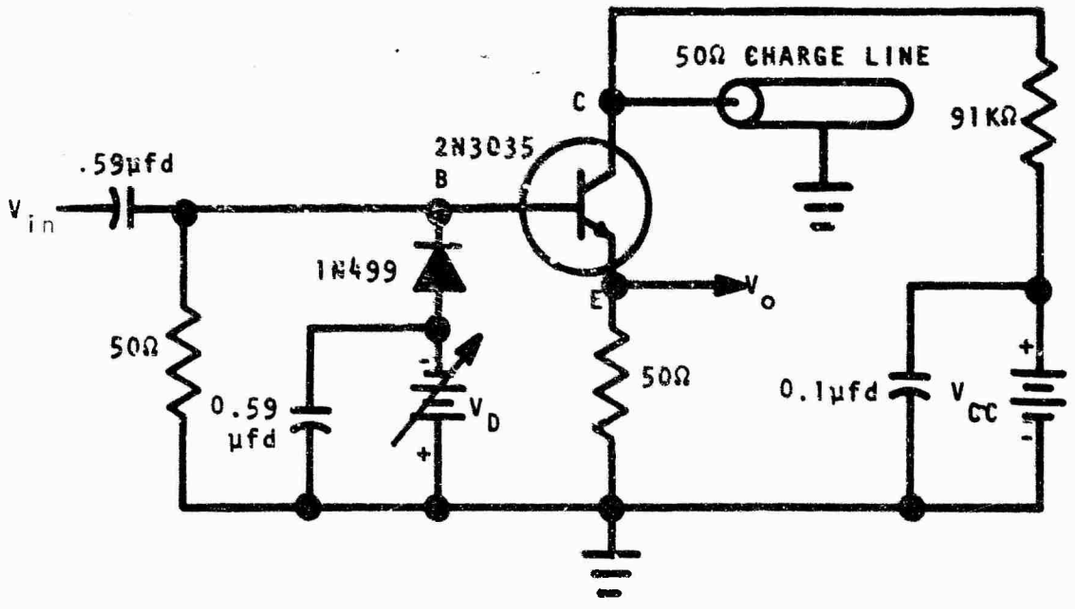

Figure 38. Base to Ground Compensation

device and a 1N499 was the compensating diode. Once again the compensation junction photocurrent was adjusted by varying V_D. Tests were first run at the 7×10^9 R/sec level and no problems were encountered in preventing firing using this compensation technique. As a side comment, it should be noted that previously, using the 2N3035 in the collector-base compensation technique, satisfactory radiation hardening was not achievable above 10^9/R sec.

In all of the tests of circuits under irradiation previously discussed, only the active transistor and compensation device were exposed to the radiation. The passive components were all shielded. However, in the next test the complete circuit was irradiated at approximately 4×10^{10} R/sec, which is the highest radiation dose level available. The circuit did not fire at this extremely high radiation level. Actually, the requirements on V_D were relaxed as compared to the lower radiation level. Apparently other unknown circuit phenomena were contributing to the hardening of the unit, but upon removing the compensating junction the device did switch during irradiation, as expected.

It should be stated, once again, that these circuits tested under radiation were not the ultimate in hardening design. It should be possible, with additional design efforts, to achieve radiation-hardened avalanche circuits at even higher levels. Evaluating both the theoretical derivations and the experimental results, it is concluded that the order of decreasing hardness is as follows.

1. Base to ground compensation
2. Base to collector with clamping diode
3. Base to collector without clamping diode
4. Just using V_{BB}.

6. Methods of Obtaining Bias Voltages

In the circuits analyzed in this section, numerous bias supply sources have been indicated as batteries. Also in some cases, up to four different "battery" or voltage sources were symbolically indicated as being necessary. In most situations, to have this many power sources is either impractical designwise or prohibitive in cost.

Methods will now be shown whereby only one voltage source is required for biasing the circuits which have been discussed.

For a circuit design which requires a V_{BB} source, a V_D bias source for collector to base diode compensation, a V'_C source for a clamping diode, and the usual V_{CC} source refer to figure 39. Only one source voltage, V_{PS}, is required. The ground point is positive with respect to the negative of the supply. If it is desired to have the power supply negative at ground, merely change the bypass capacitors to the negative of the supply and shift the ground point. R_X should be reasonably large in comparison to the other circuit resistance so that part of I_{pp2} is not shunted to ground through the power supply.

Similarly for the base to ground compensation diode circuit, a one voltage source system is shown in figure 40.

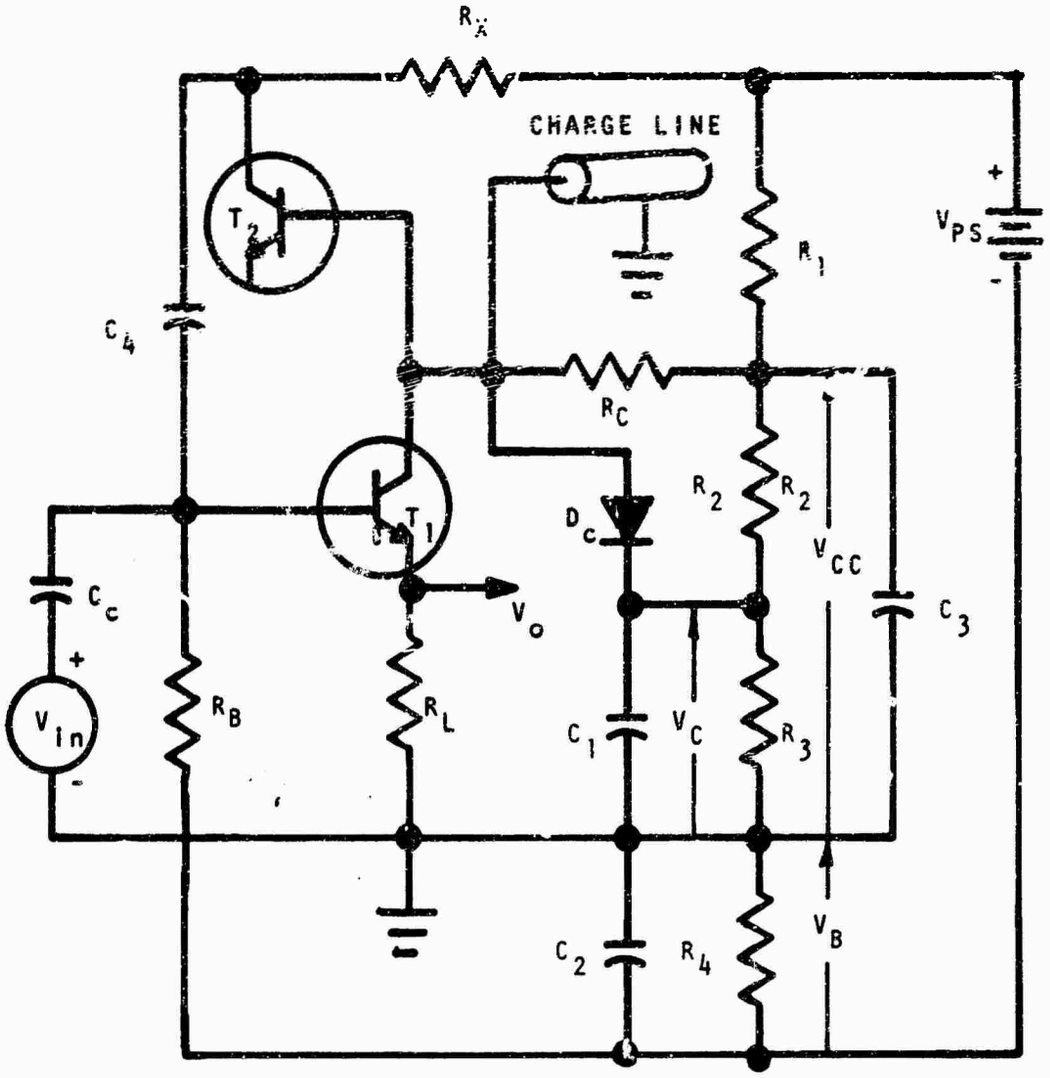

Figure 39. Circuit Employing Single Power Supply for Base to Collector Compensation Circuit with Collector Clamping Diode

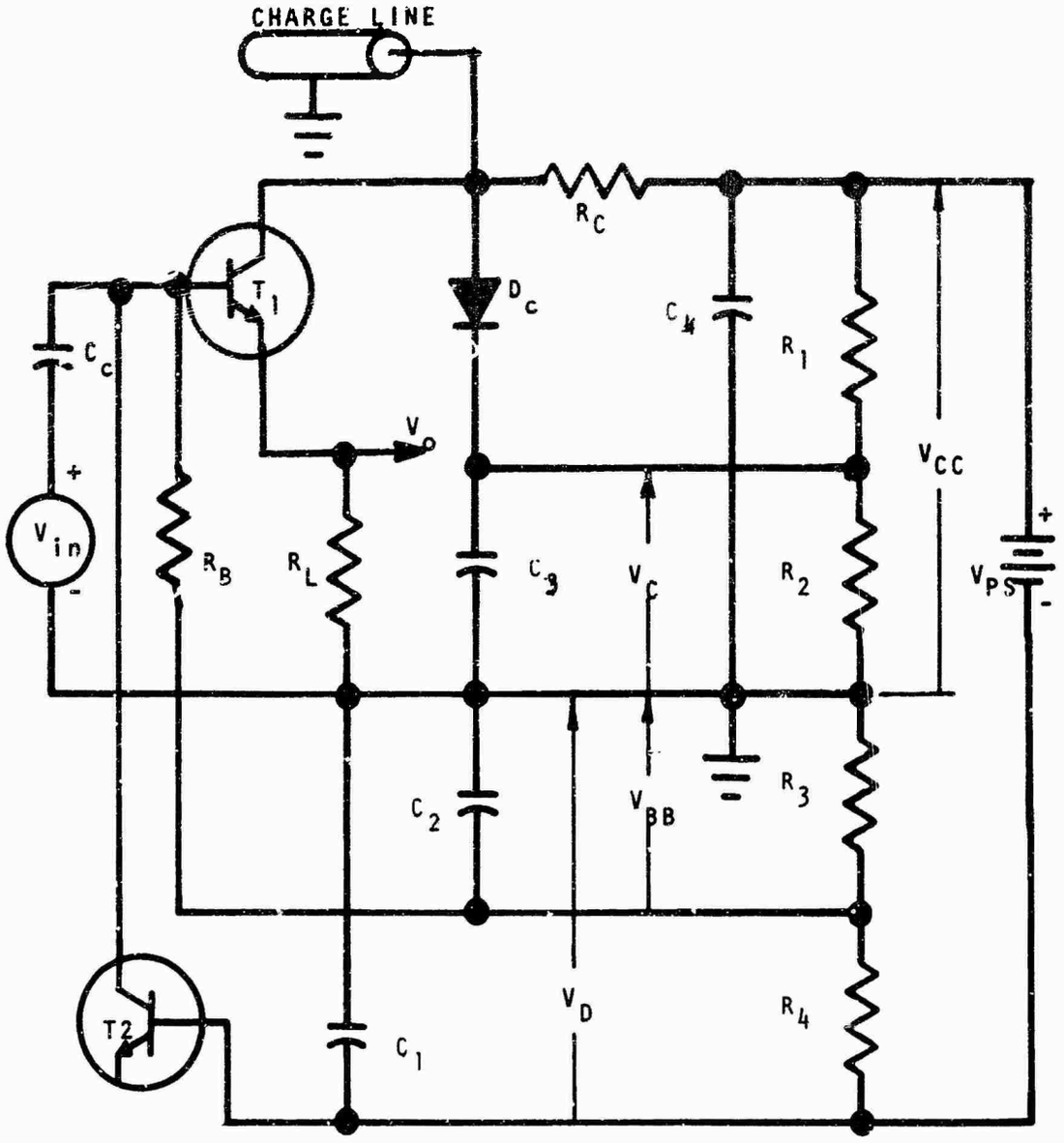

Figure 40. Circuit Employing Single Power Supply for Base to Ground Compensation Circuit with Collector Clamping Diode

SECTION VI

EXPERIMENTAL RESULTS OF NEUTRON DEGRADATION ON AVALANCHE TRANSISTORS AND DIODES

1. Degradation of Avalanche Diodes

Six different Continental Device Corporation high performance 400-milliwatt silicon voltage regulators were exposed at the Sandia Corporation Engineering Reactor (hole 8-S) from about 10^{13} neutron/cm^2 to 10^{16} neutron/cm^2 (E >0.01 mev). Sulfur and nickel detectors (effective threshold E > 3 mev) were used to measure the integrated neutron flux incident on the samples. The measurements were converted to the plutonium threshold (E >0.01 mev) by using the conversion factor $\varphi_{pu} = \frac{\varphi \text{ sulfur}}{0.132}$.

The impurity concentration on the high resistivity side of the diodes can be obtained by using figure 22 and dc measurements of V_B. Once the impurity concentration is known, the resistivity can be determined from previous experimental graphical data (reference 3). The results of this method are shown in table II; the accuracy is expected to be within ± 20 percent.

The data taken were in the form of pre- and post-neutron irradiation testing using a Fairchild 500 to obtain the desired test results on the diodes. The parameters of interest for this series of tests were diode reverse voltage (V_R) versus reverse or leakage current (I_R), and forward voltage (V_F) versus forward current (I_F).

TABLE II

IMPURITY AND RESISTIVITY DATA

Device No.	V_B(volts)	$N_D(cm^{-3})$	(ρ-cm)	$\sigma(\Omega\text{-cm})^{-1}$
1N3516	8.2	2.40×10^{17}	0.055	18.20
1N3518	10.0	1.45×10^{17}	0.073	13.70
1N3526	22.0	4.00×10^{16}	0.200	5.00
1N3534	47.0	1.3×10^{16}	0.500	2.00
CD3171	62.0	8.7×10^{15}	0.630	1.59
CD3174	82.0	5.7×10^{15}	0.900	1.11

From the above generated data as a function of neutron induced damage, we were able to observe carrier removal rates and minority carrier-lifetime effects in order to be able to predict the expected amount of degradation in the electrical characteristics of these diodes. The dominant effects were the decrease in minority carrier lifetime in the lightly doped region, the increase in series resistance because of removal of majority carriers from the conduction process in the lightly doped region, and an increase in V_B. The measurements were made before irradiation at each of seven levels between approximately 10^{13} nvt and 10^{16} nvt. Typical results of these measurements are summarized in figures 41 to 63. The abbreviation PT stands for post-test made using the Fairchild 500 after neutron exposure. The levels of total accumulated neutron flux for PT-1, PT-2, PT-3, PT-4, PT-5, PT-6, and PT-7 are, respectively, 0.9860×10^{13}, 4.7560×10^{13}, 0.9316×10^{14}, 4.008×10^{14}, 0.8408×10^{15}, 4.1378×10^{15}, and 0.8612×10^{16} nvt using sulfur detectors.

The following general trends in the data are observed:

1. In diodes 1N3516, 1N3518, and 1N3526, in which the doping level in the lightly doped material is greater than

4×10^{16} cm^{-3} (see table II), the minority-carrier-lifetime changes predominated (i.e., using discussion of Section III, equation (56) and the universal diode equation to indicate that if lifetime decreases, the junction voltage must decrease for constant current) up to highest exposure encountered in the forward biased condition.

2. In diodes 1N3534, CC3171, and CD3174 ($N_D \leq 1.3 \times 10^{16}$ cm^{-3}) the minority-carrier-lifetime changes predominated at low flux level where no conductivity modulation was prevalent. At a higher exposure where we see a conductivity change, the conductivity modulation rapidly suppressed the effect due to the lifetime change. This is because the diode current varies inversely with the square root of the minority-carrier-lifetime and exponentially with carrier modulation. After a certain level of exposure, the diodes start to become intrinsic due to carrier removal with the resultant loss of their rectification property.

3. The diode can be approximately represented in the forward biased direction by a battery V_d(V_d is intersection of extrapolation of straight line portion of I_F versus V_F curve on voltage axis with current equal to zero) and a series resistance r_p equal to the inverse slope of the current-voltage curve (see figure 41). As indicated on these figures, V_d tends to decrease with exposure. All of the curves for a particular device appear to be fairly parallel over some or all of the exposure levels. This would seem to indicate that r_p is staying fairly constant at a particular operating current.

TABLE III

TOTAL ACCUMULATED NEUTRON FLUX FOR EACH TEST

Test Number	nvt = neutron/cm^2
PT-1	0.9860×10^{13}
PT-2	4.7560×10^{13}
PT-3	0.9316×10^{14}
PT-4	4.008×10^{14}
PT-5	0.8406×10^{15}
PT-6	4.1373×10^{15}
PT-7	0.8612×10^{16}

4. The reverse breakdown, V_B, generally showed a tendency to increase with neutron exposure. The amount of increase depended on the doping of the lightly doped n-region. A very rough maximum estimate of the change in breakdown voltage can be obtained by using carrier removal data and breakdown voltage versus impurity concentration data from published literature. Before irradiation one can measure V_B electrically and then obtain doping concentration on the lightly doped side from figure 22. The doping concentration after irradiation can then be computed by using published carrier removal rates, which vary between about 2 and 4 carriers removed per neutron/cm^3. Using this post-calculated doping concentration and figure 22, one can predict the V_B after exposure.

5. The reverse leakage current (contributed mainly by the carrier-generation component in silicon) generally showed an increase with device exposure due to the decrease in minority carrier lifetime and an increase in the depletion width.

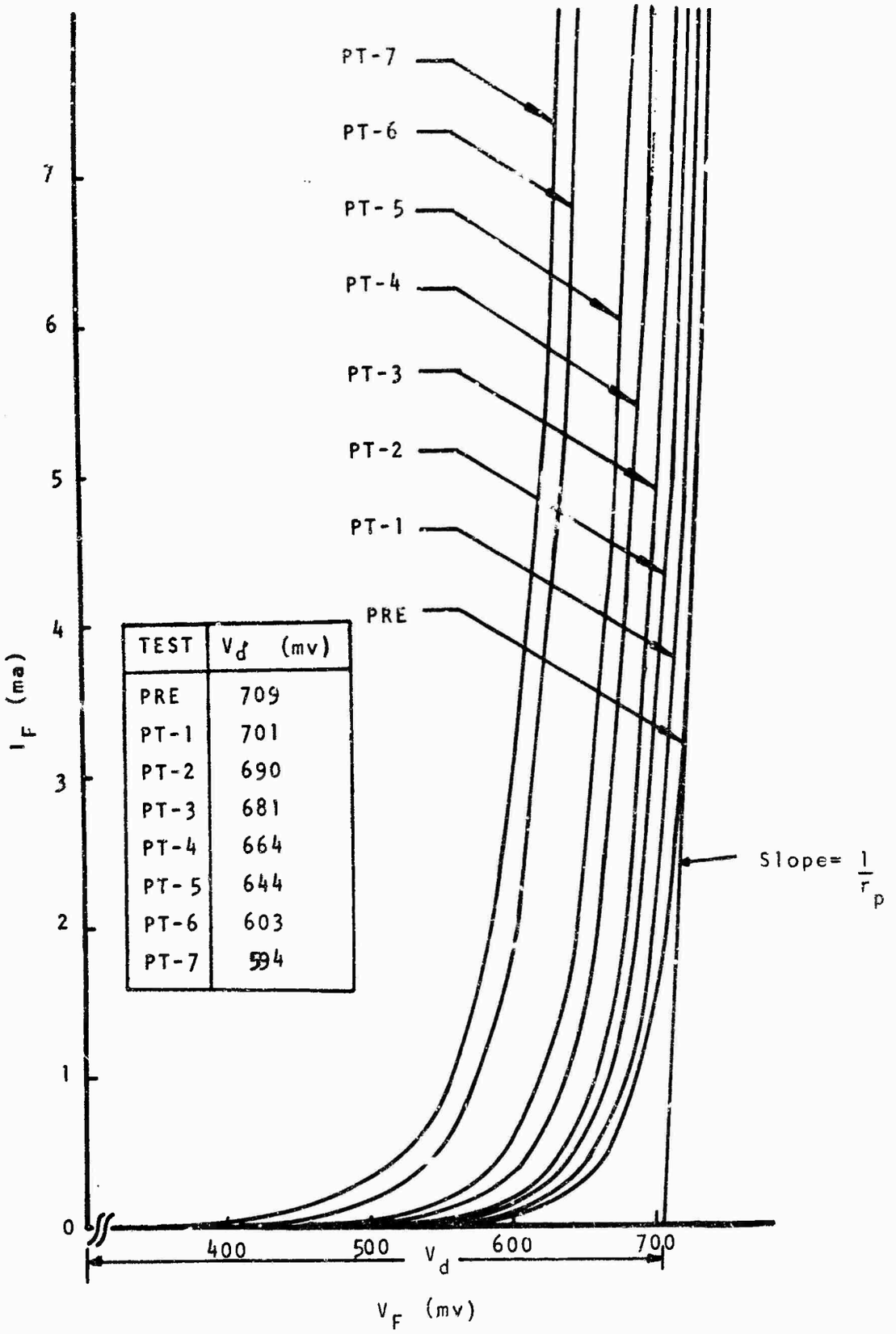

Figure 41. I_F versus V_F for IN3516-1 at Different NVT Exposures

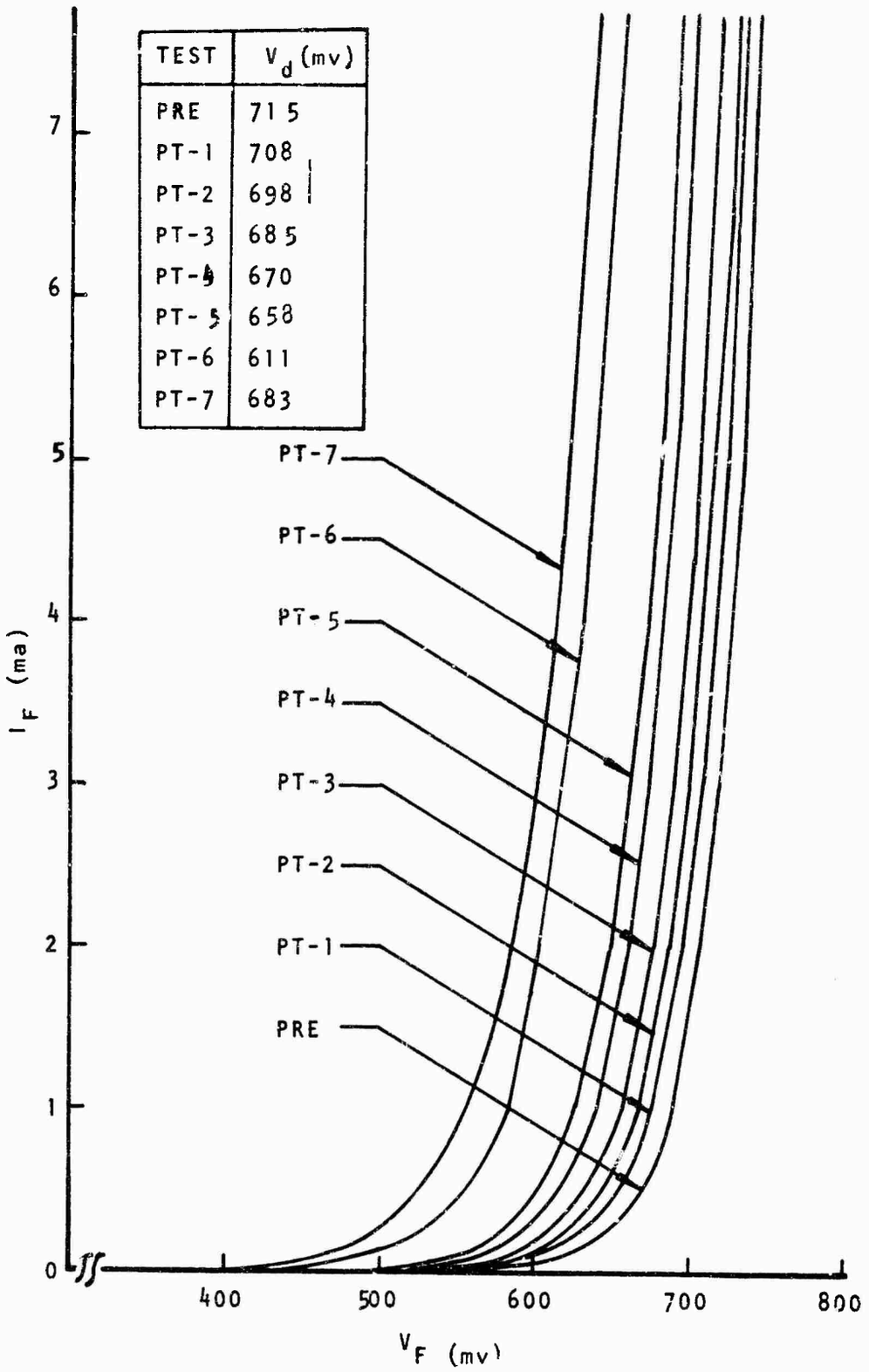

Figure 42. I_F versus V_F for 1N3516-2 at Different NVT Exposures

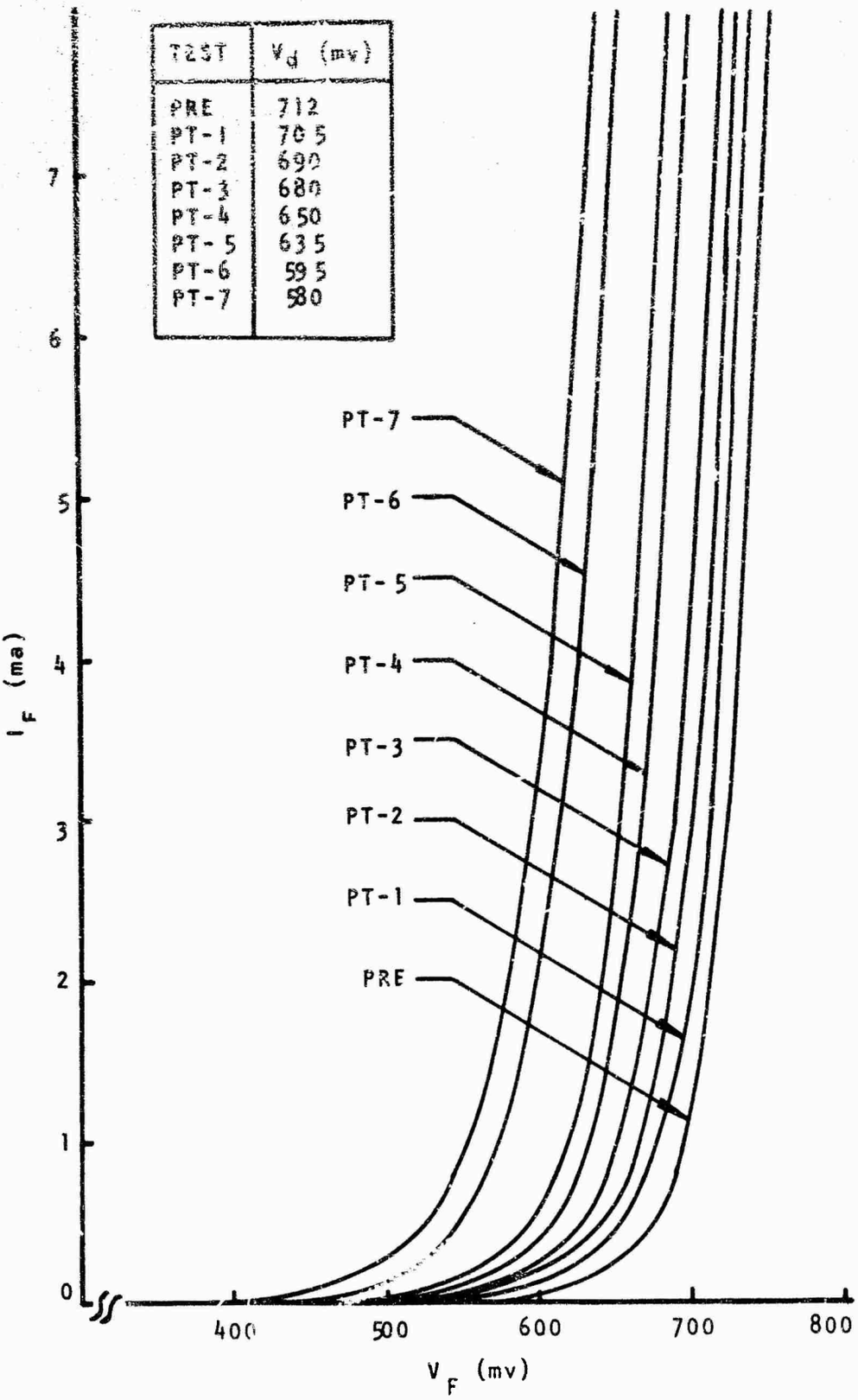

Figure 43. I_F versus V_F for IN3518-6 at Different NVT Exposures

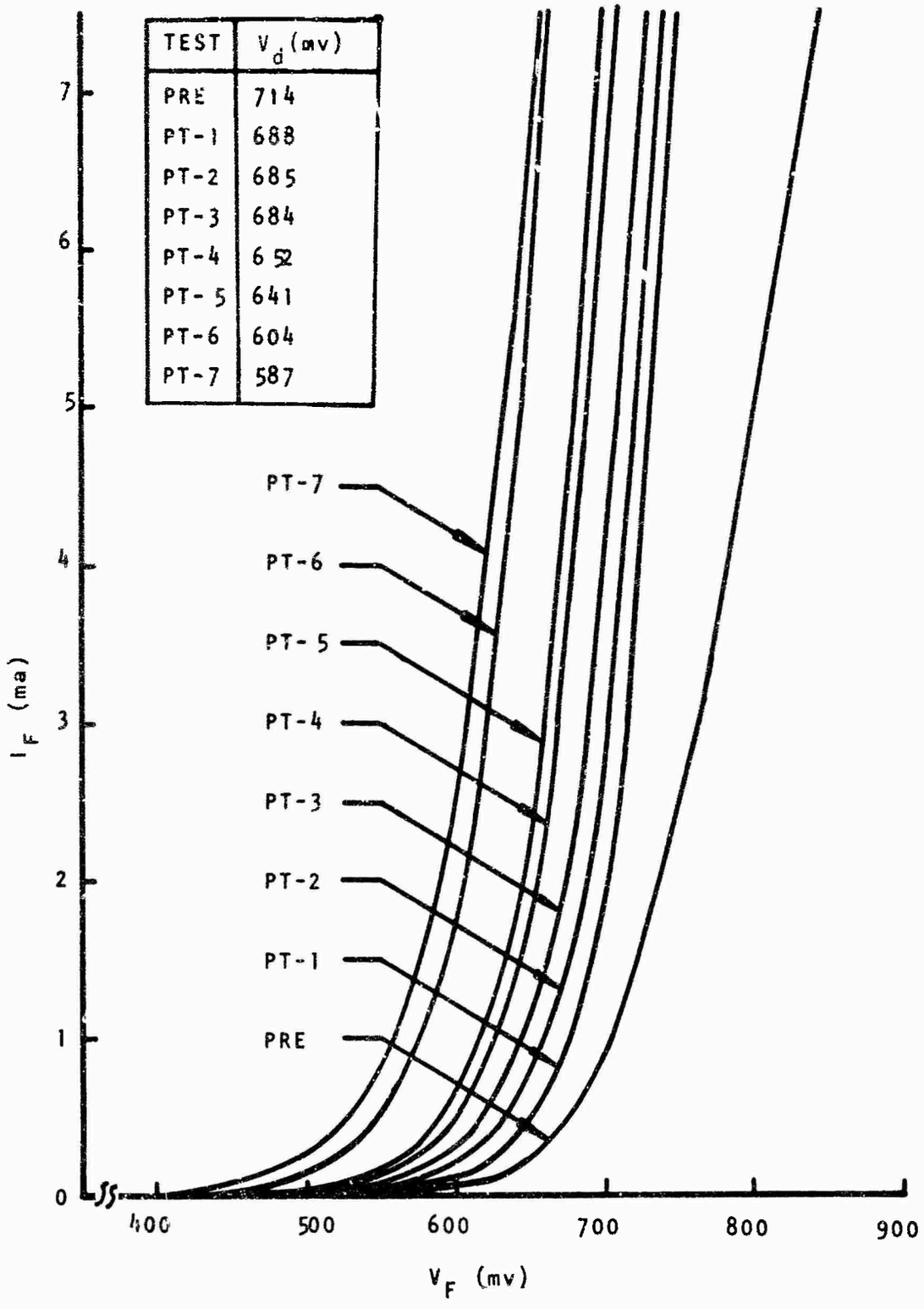

Figure 44. I_F versus V_F for IN3518-7 at Different NVT Exposures

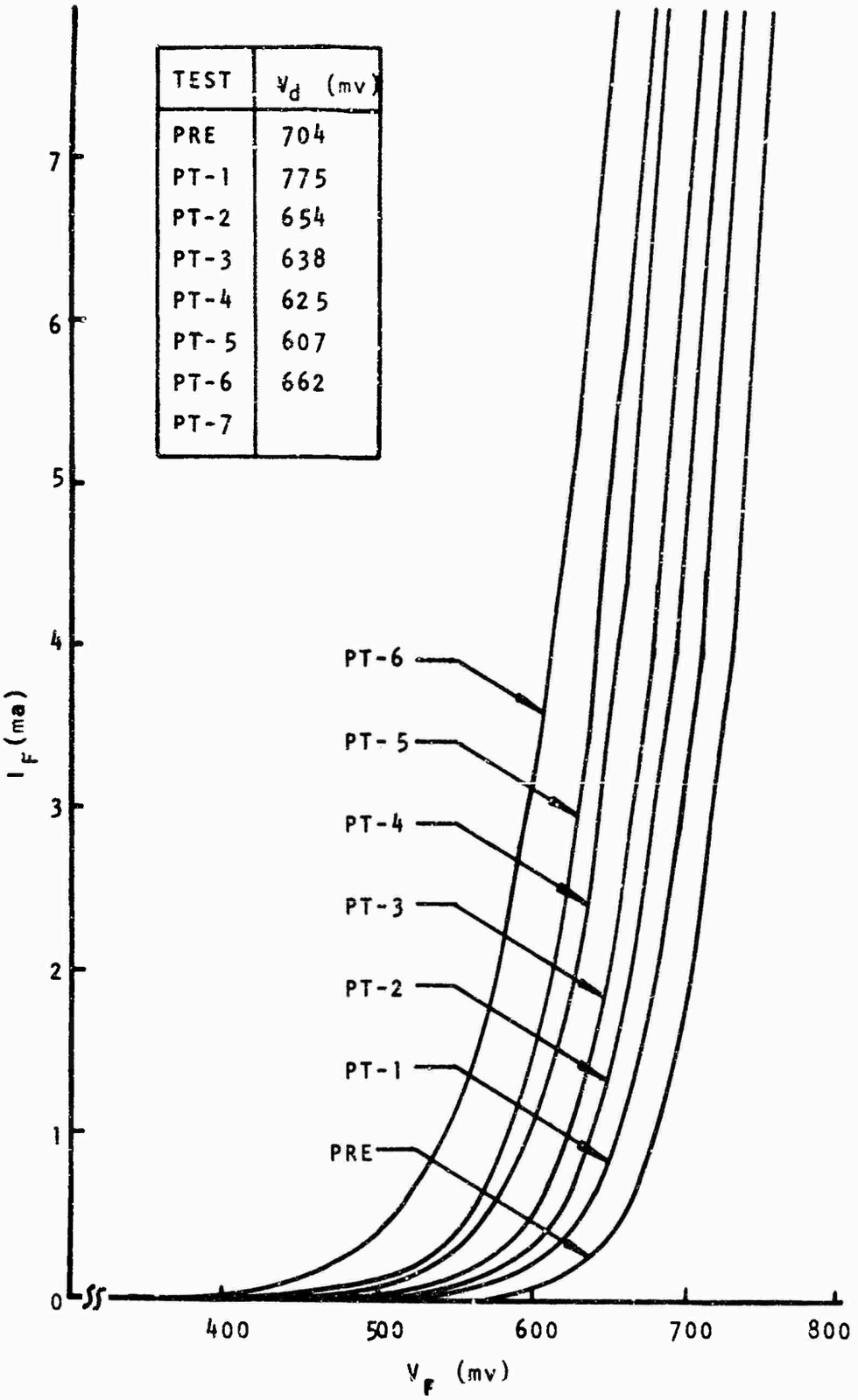

Figure 45. I_F versus V_F for IN3526-11 at Different NVT Exposures

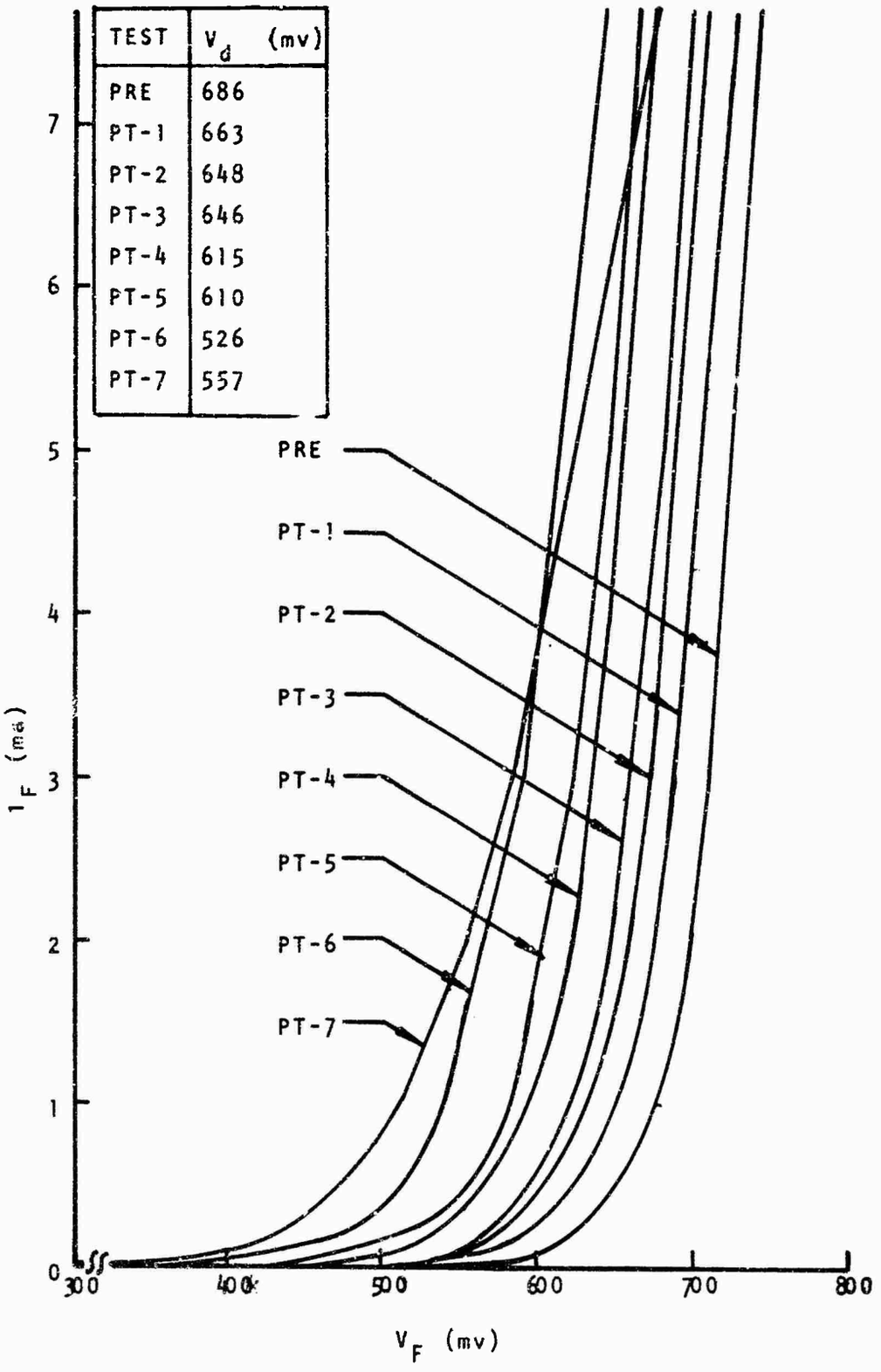

Figure 46. I_F versus V_F for IN3526-12 at Different NVT Exposures

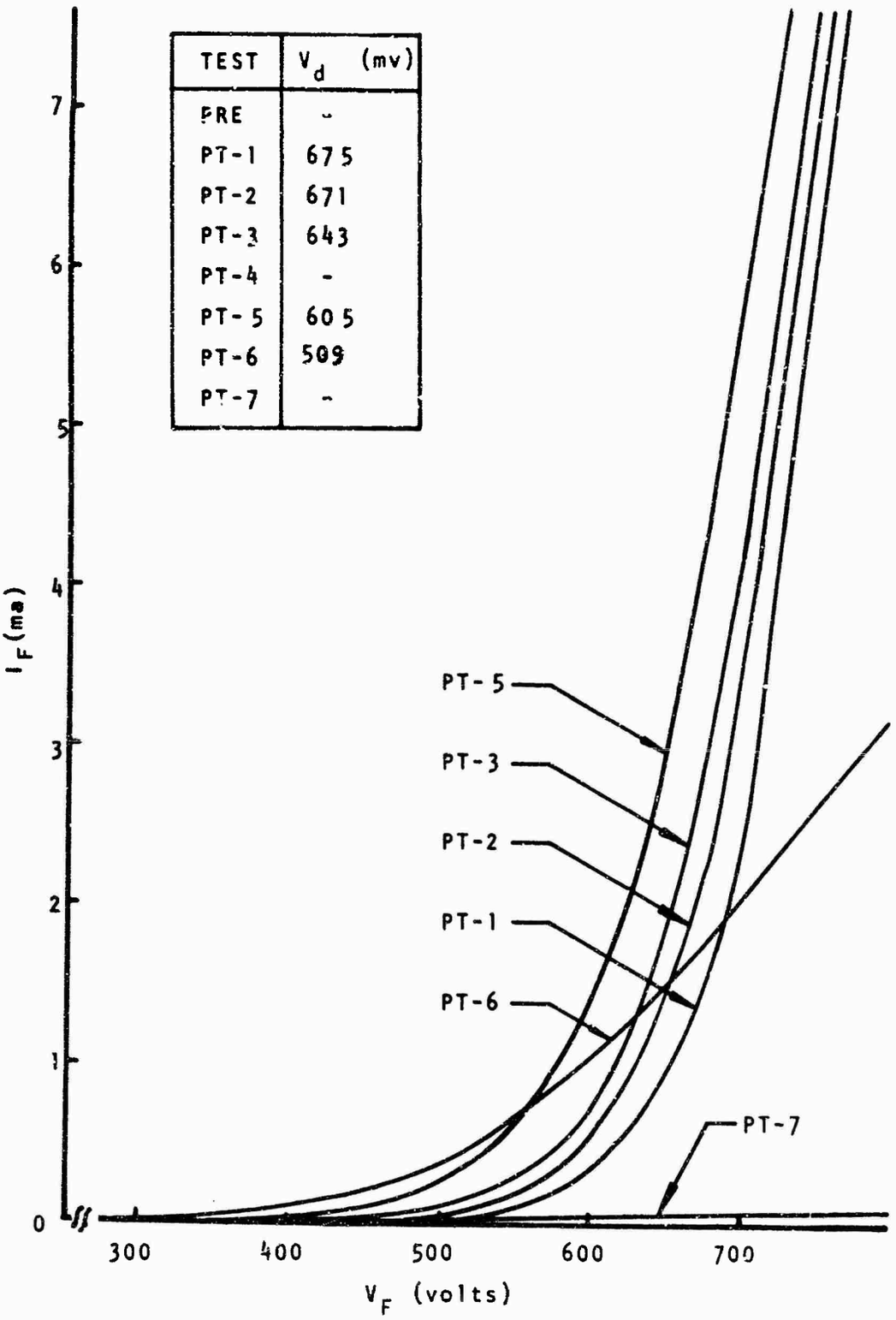

Figure 47. I_F versus V_F for IN3534-16 at Different NVT Exposures

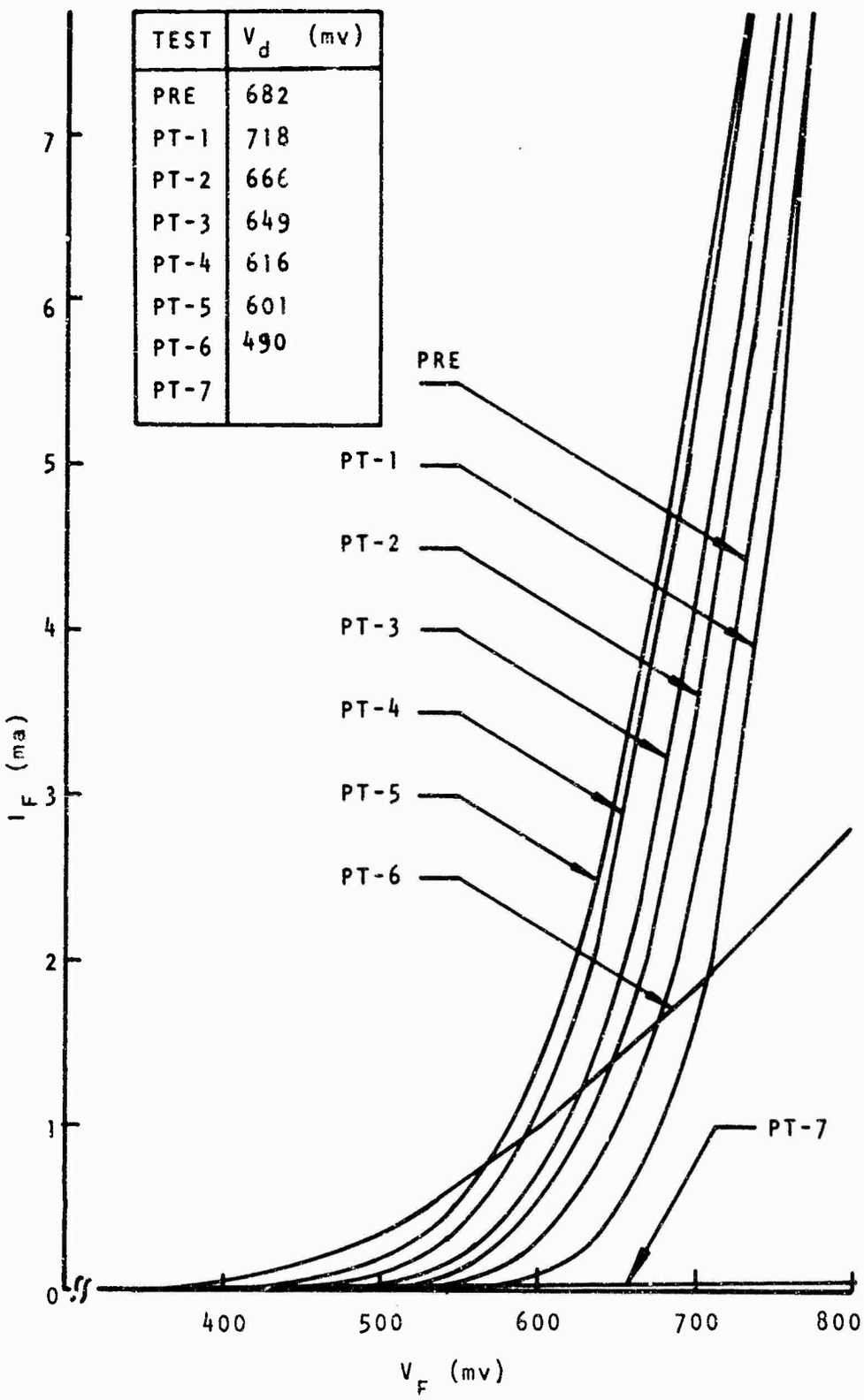

Figure 48. I_F versus V_F for IN3534-17 at Different NVT Exposures

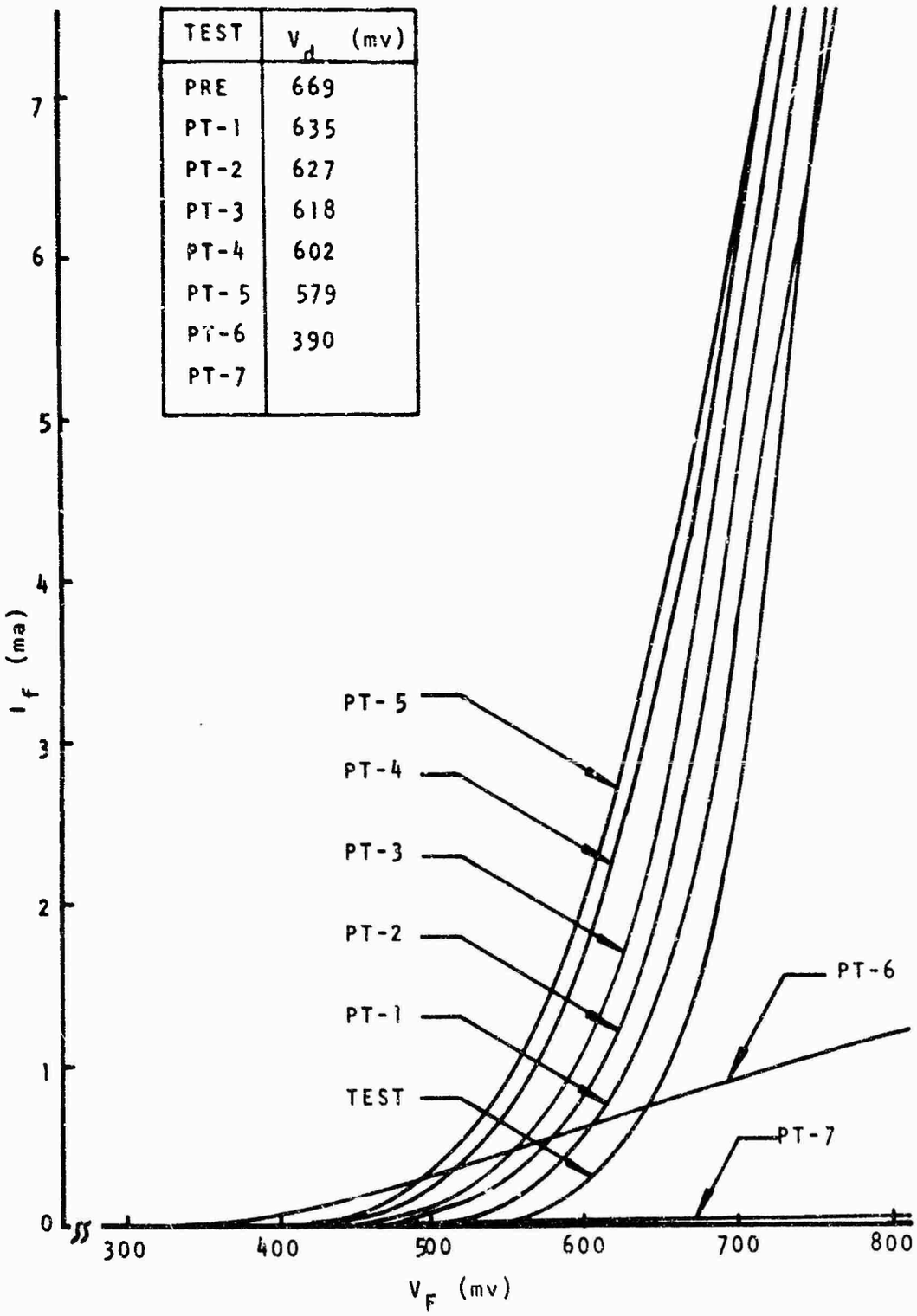

Figure 49. I_F versus V_F for CD5171-21 at Different NVT Exposures

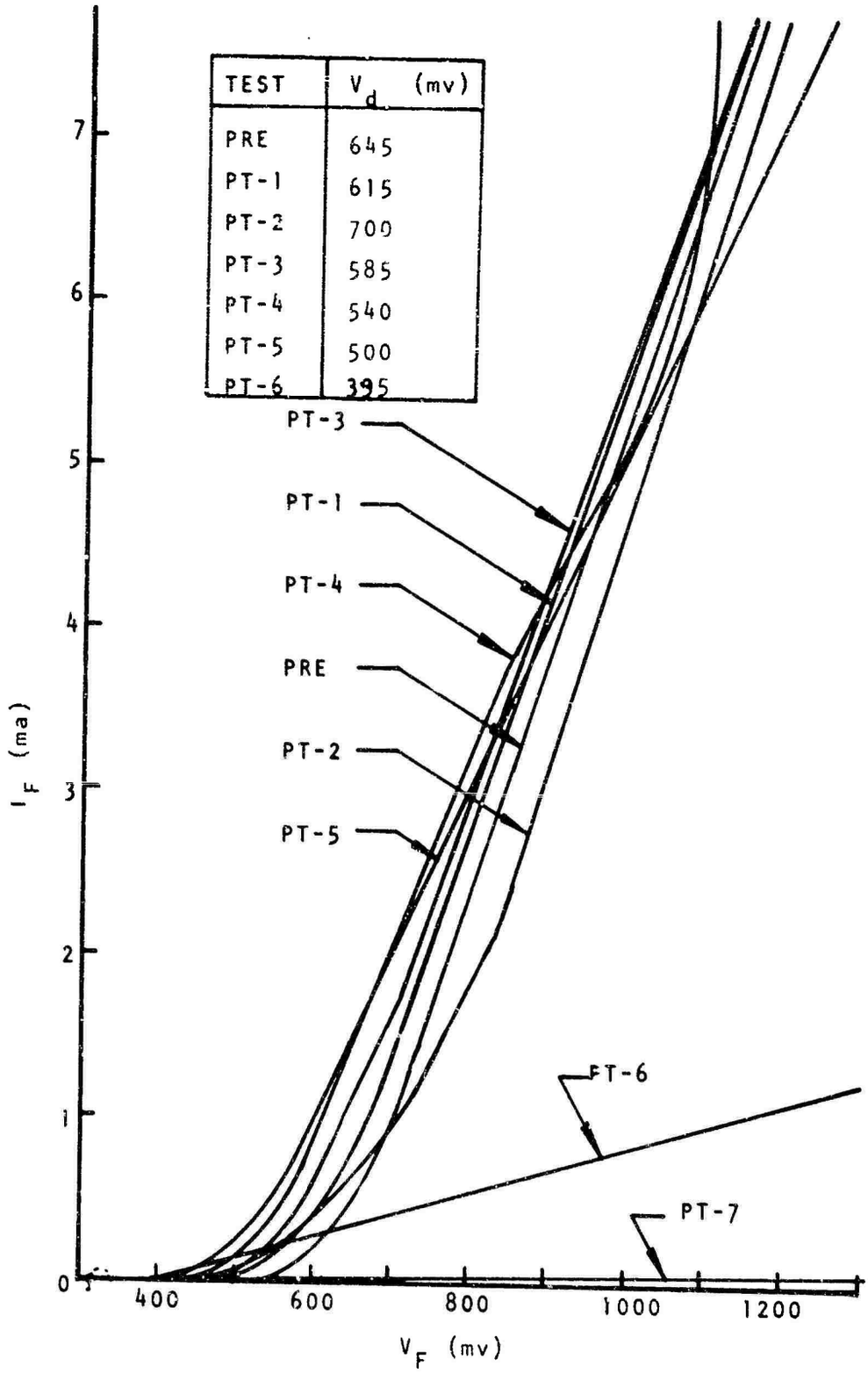

Figure 50. I_F versus V_F for CD5171-22 at Different NVT Exposures

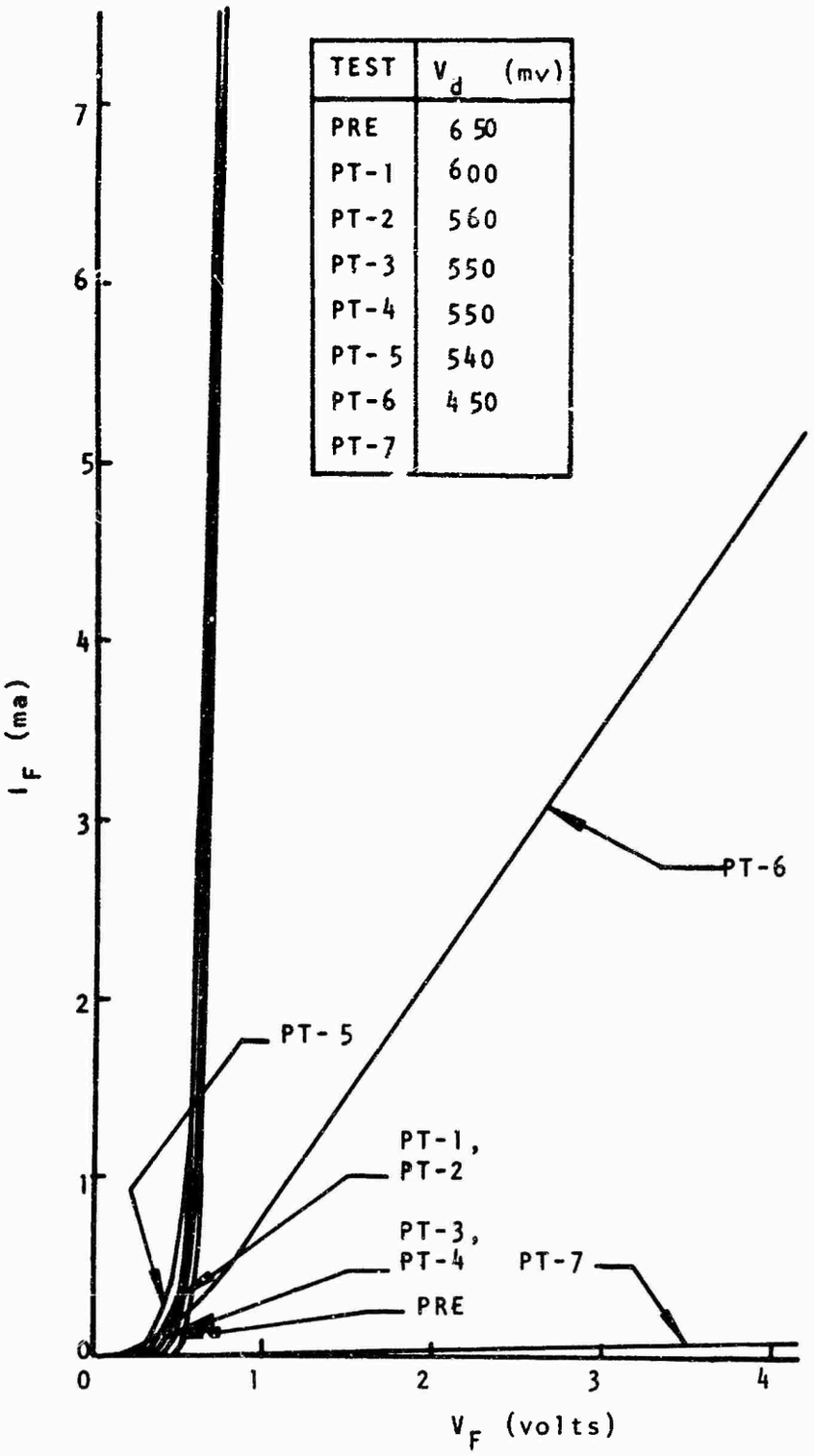

Figure 51. I_F versus V_F for CD3174-26 at Different NVT Exposures

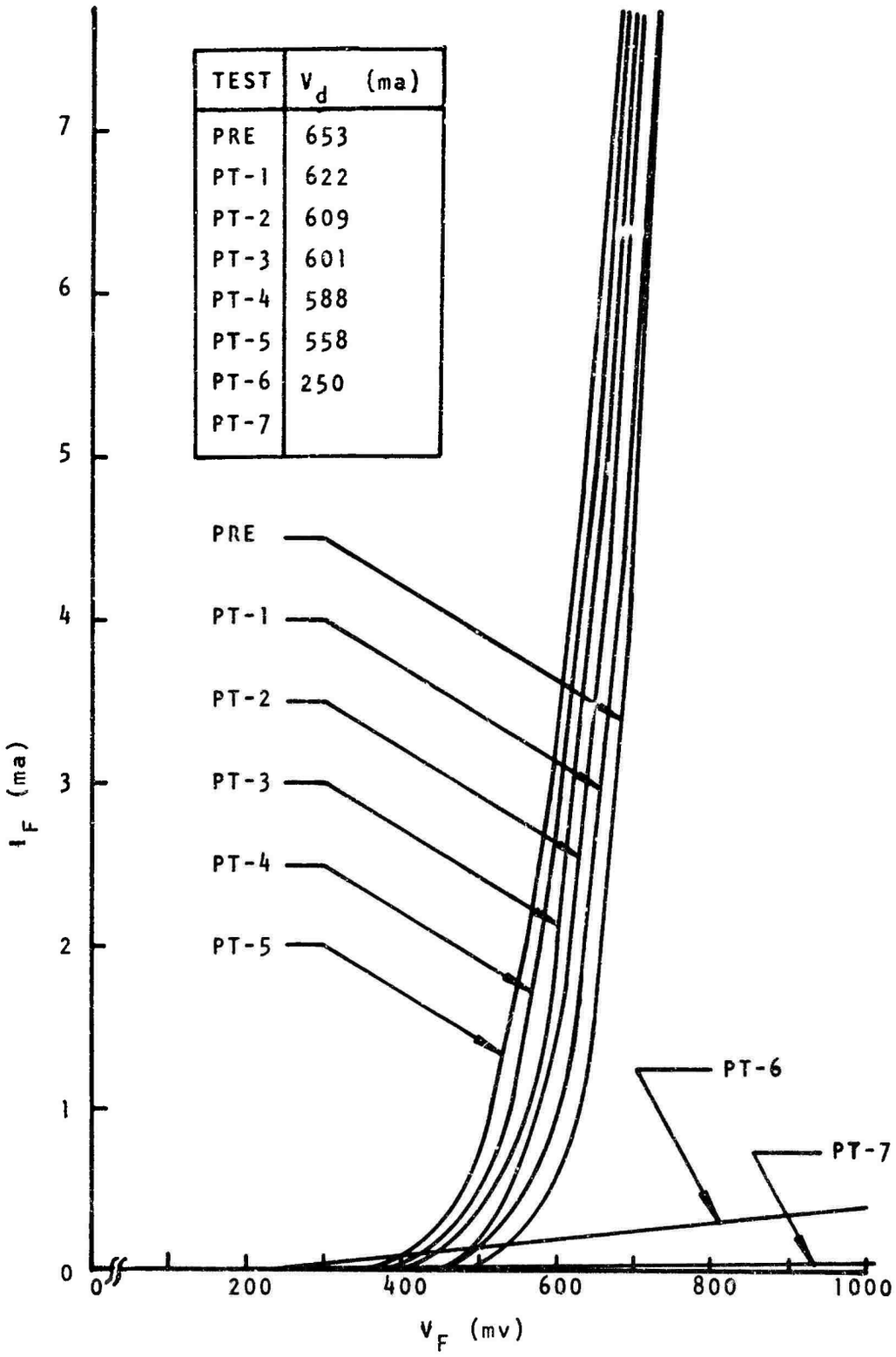

Figure 52. I_F versus V_F for CD3174-27 at Different NVT Exposures

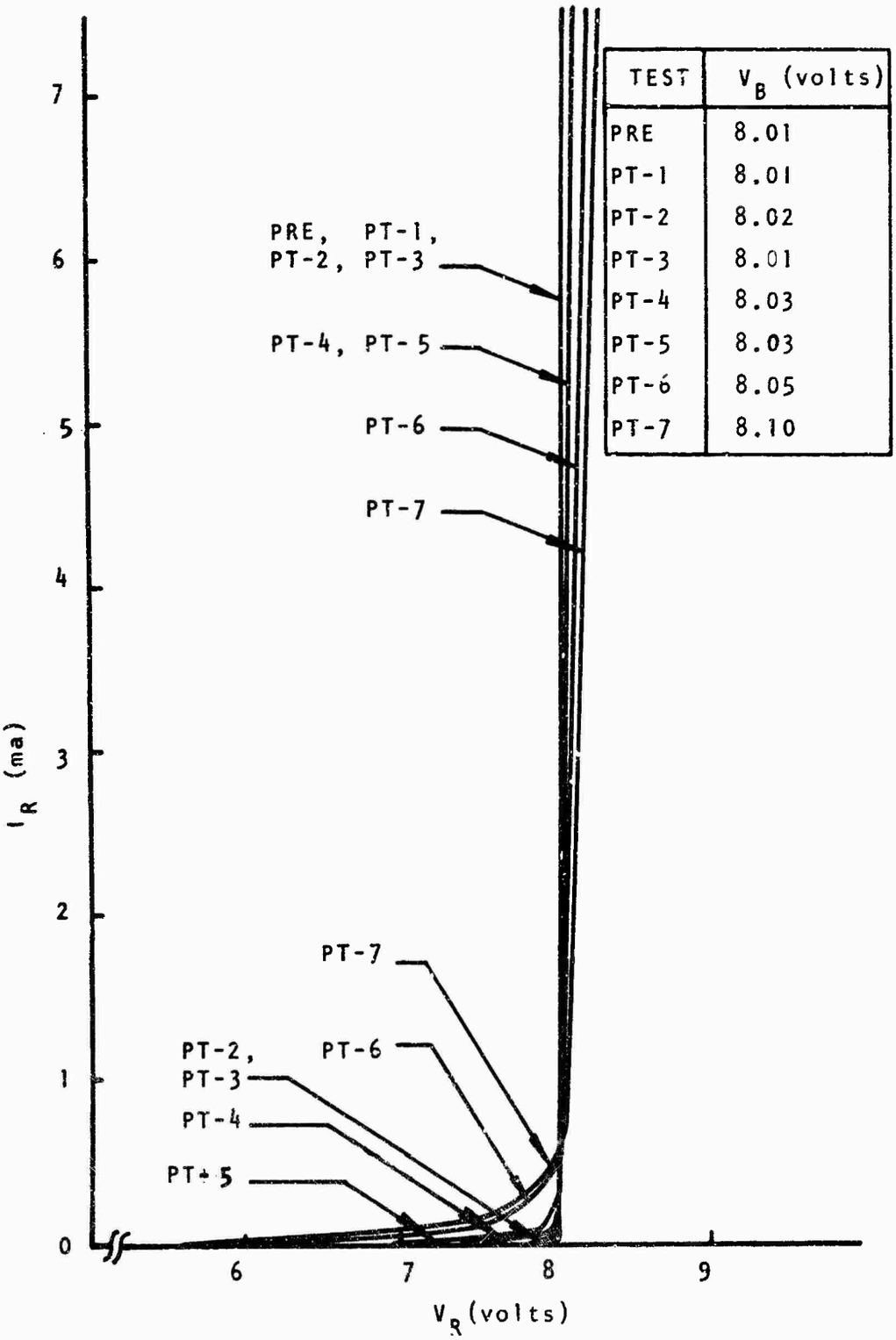

Figure 53. I_R versus V_R for IN3516-1 at Different NVT Exposures

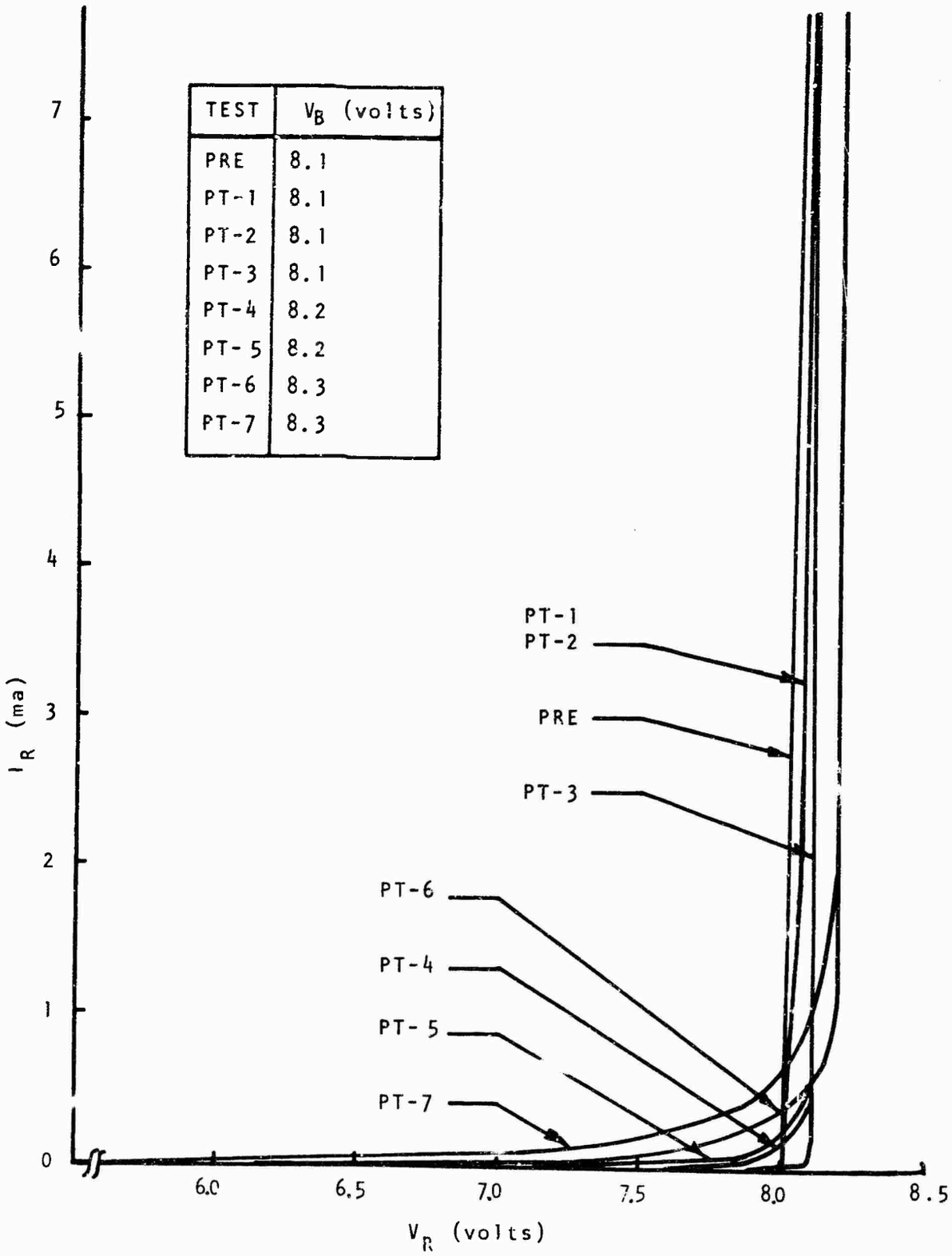

Figure 54. I_R versus V_R for IN3516-2 at Different NVT Exposures

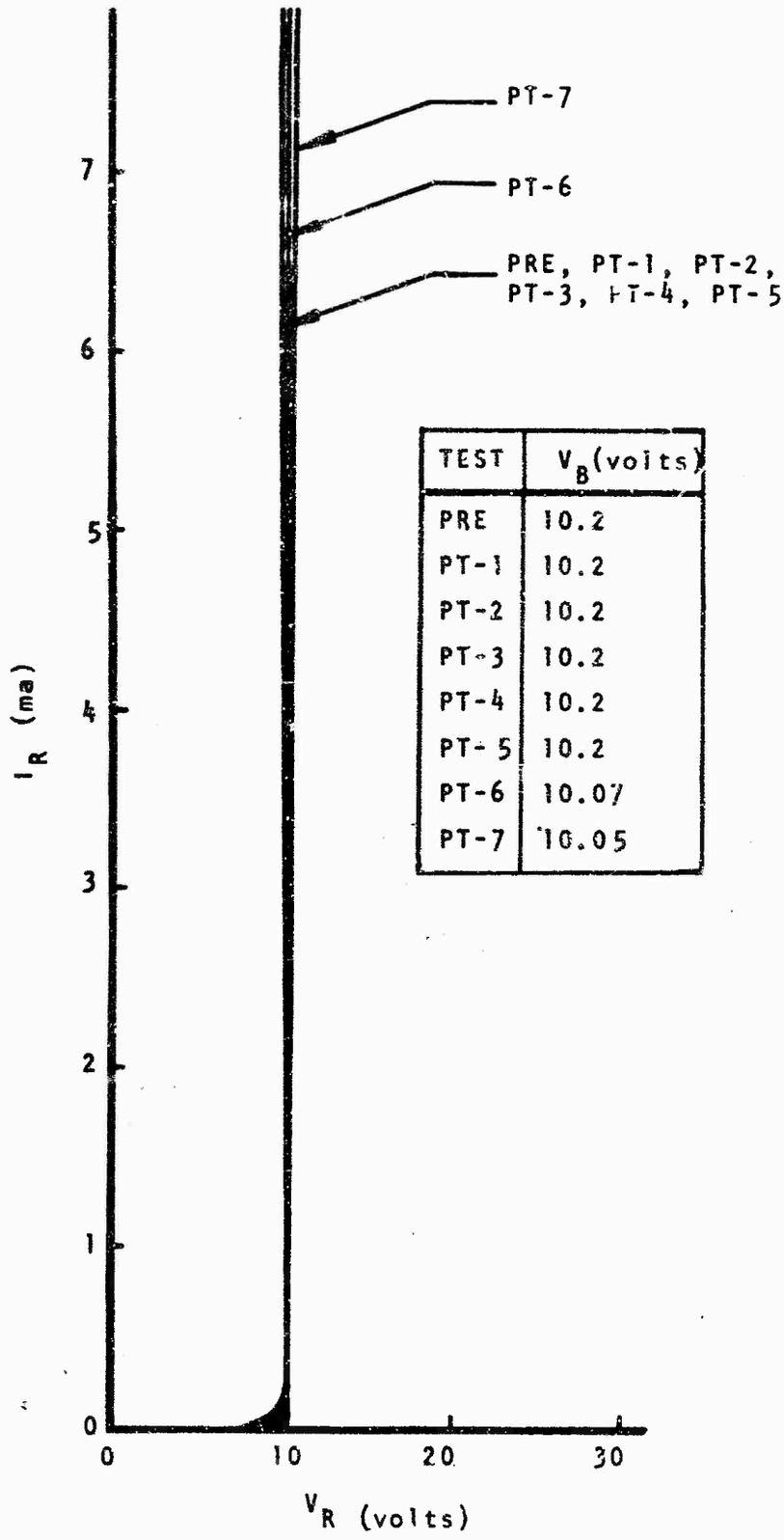

Figure 55. I_R versus V_R for IN3518-6 at Different NVT Exposures

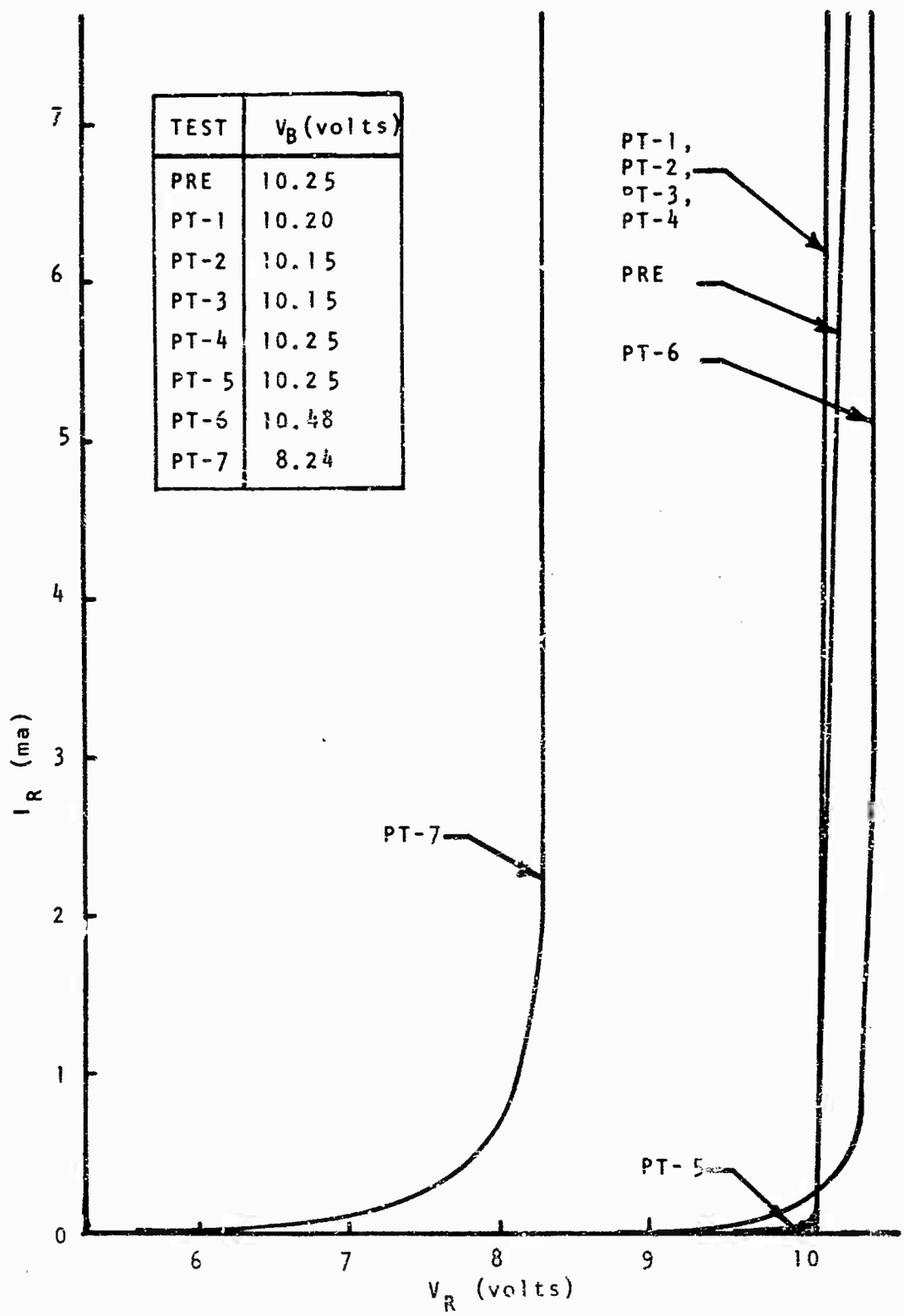

Figure 56. I_R versus V_R for IN3518-7 at Different NVT Exposures

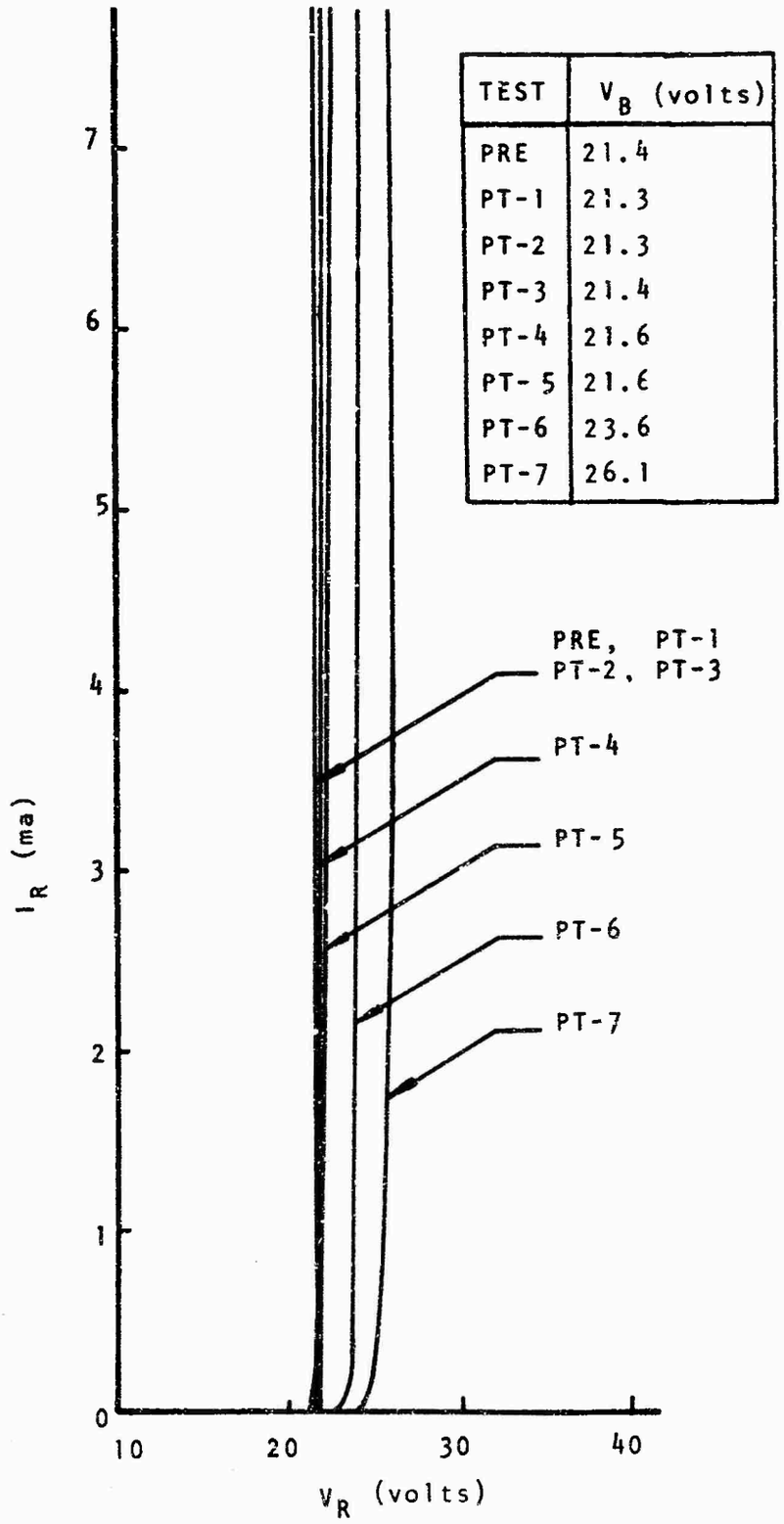

Figure 57. I_R versus V_R for IN3526-11 at Different NVT Exposures

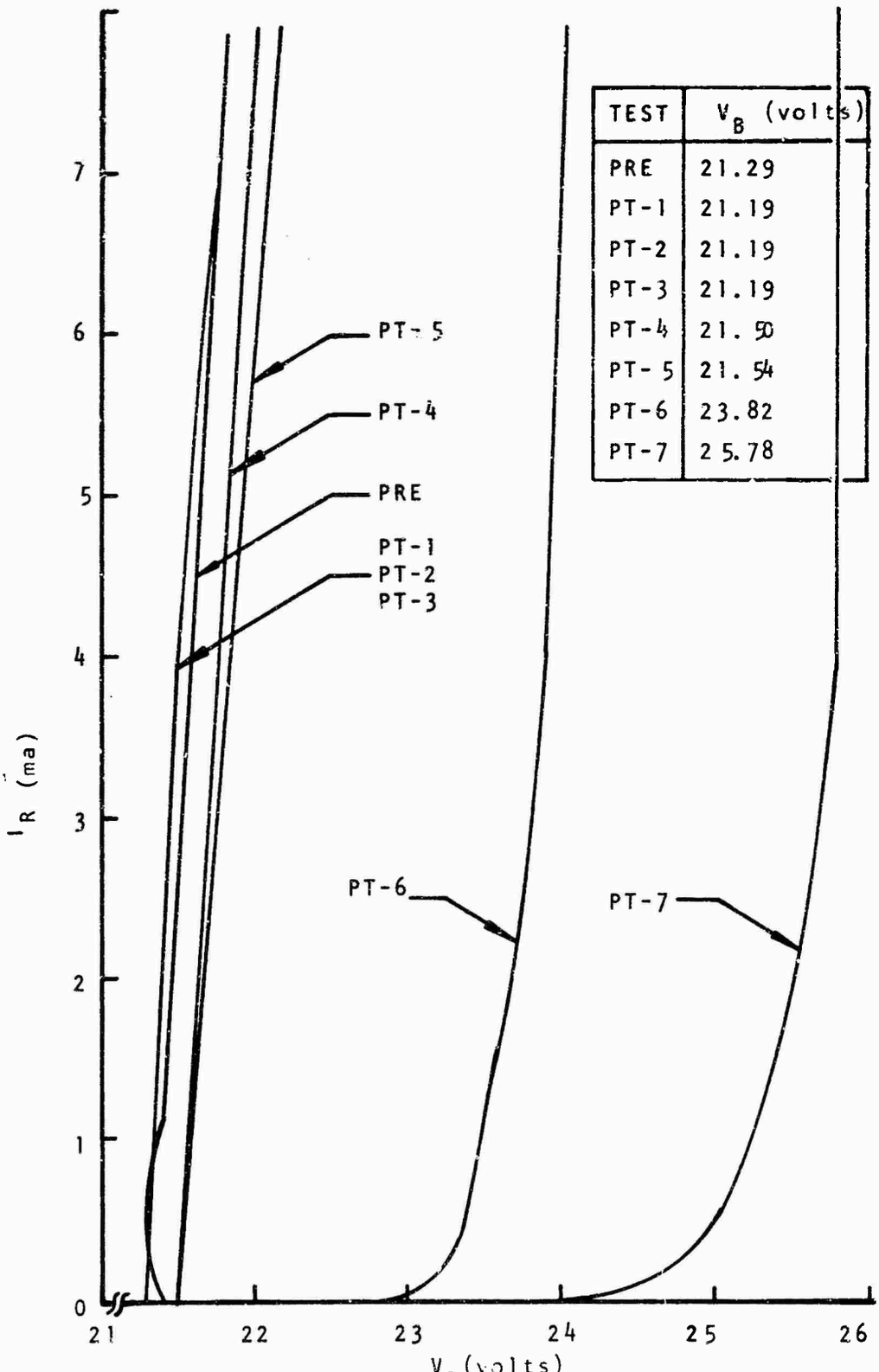

Figure 58. I_R versus V_R for IN3526-12 at Different NVT Exposures

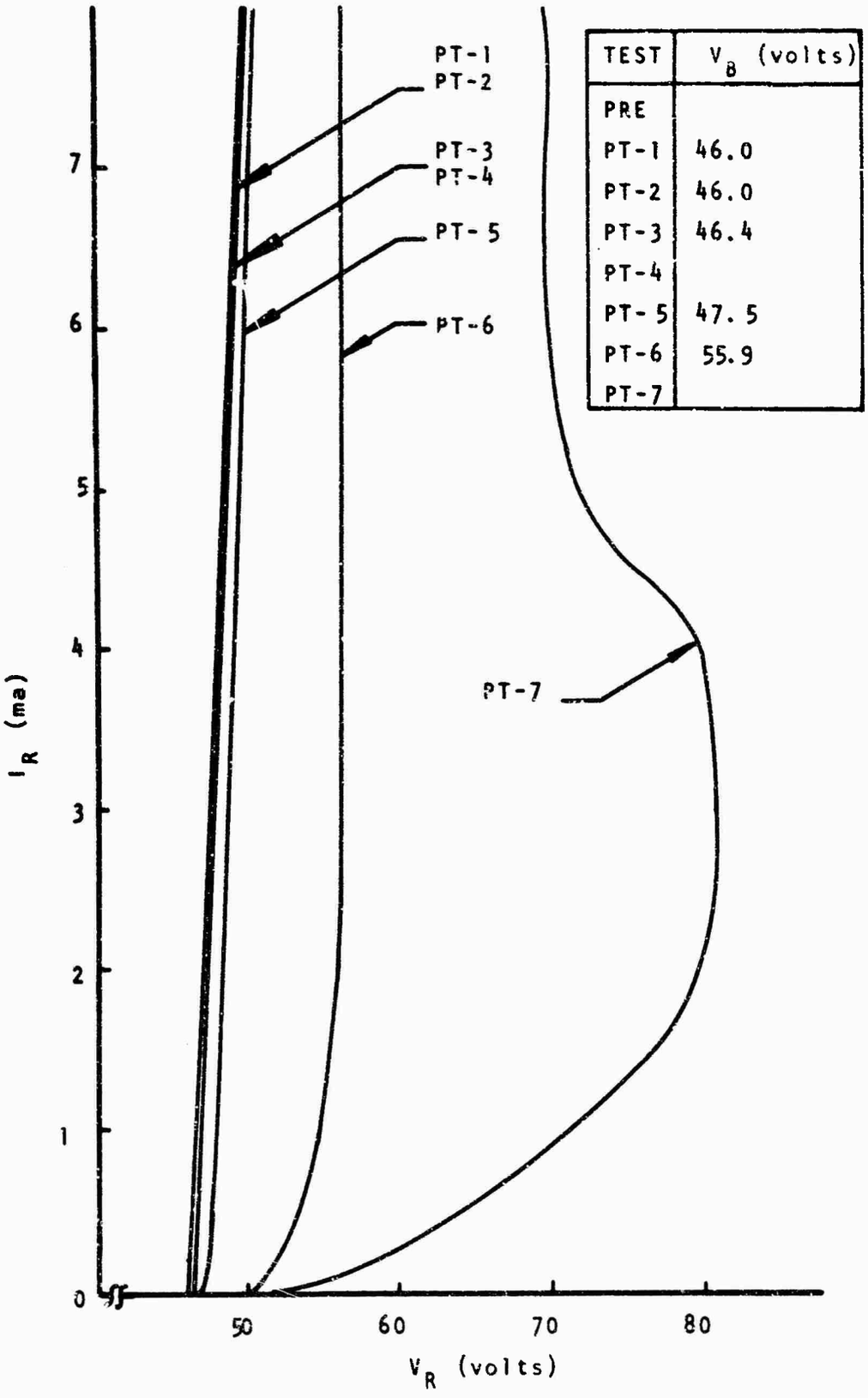

Figure 59. I_R versus V_R for IN3534-16 at Different NVT Exposures

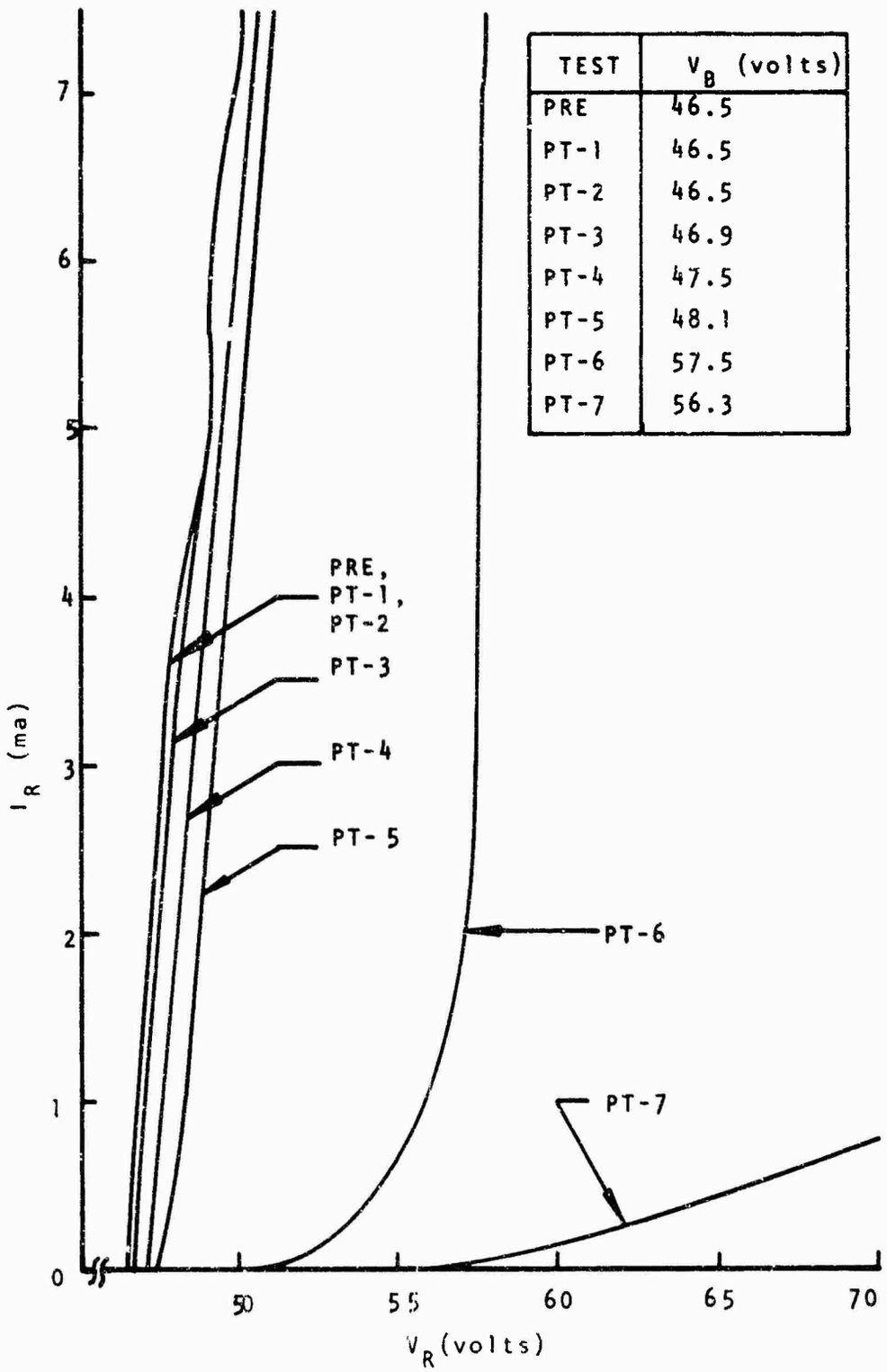

Figure 60. I_R versus V_R for IN3534-17 at Different NVT Exposures

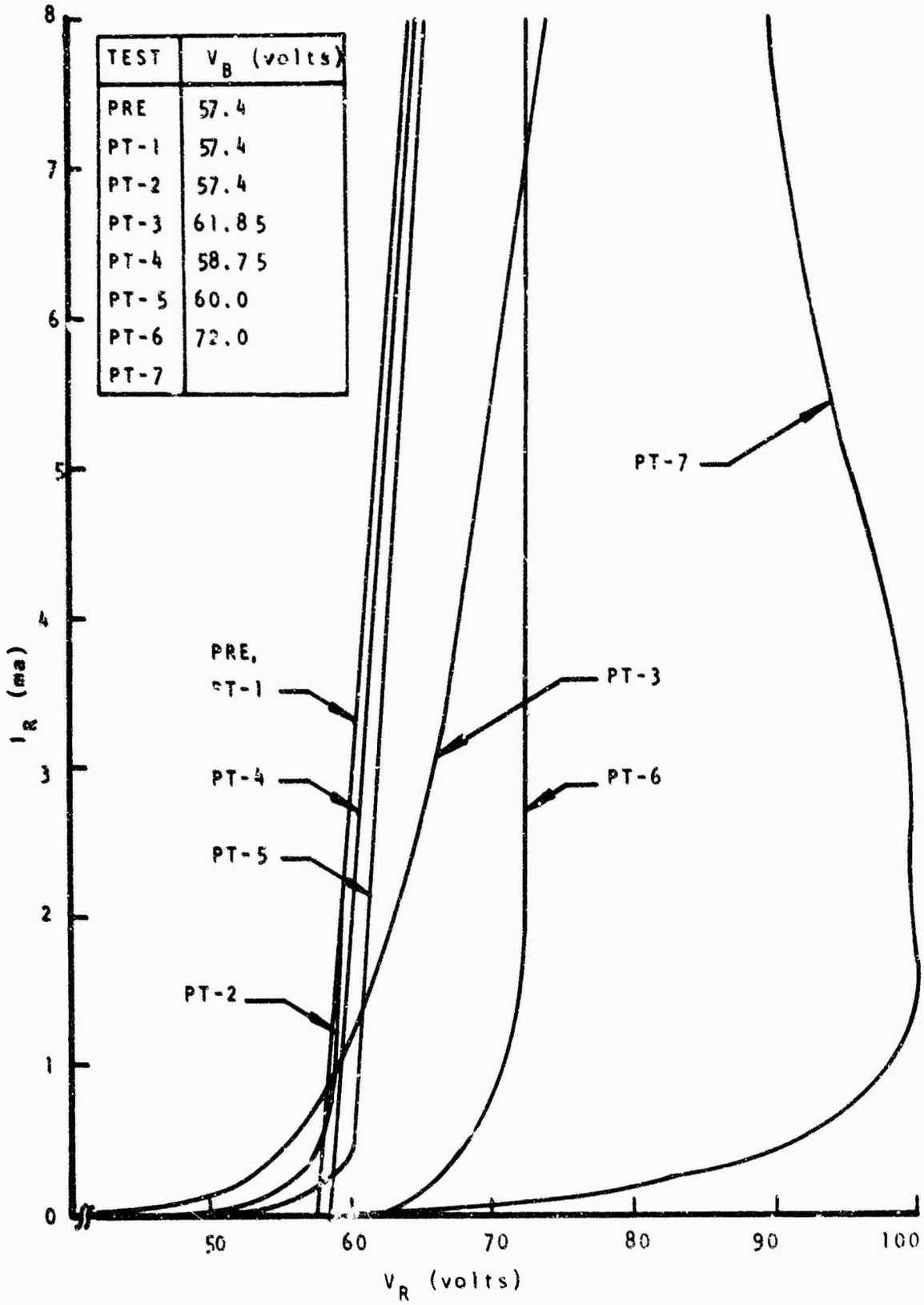

Figure 61. I_R versus V_R for CD5171-21 at Different NVT Exposures

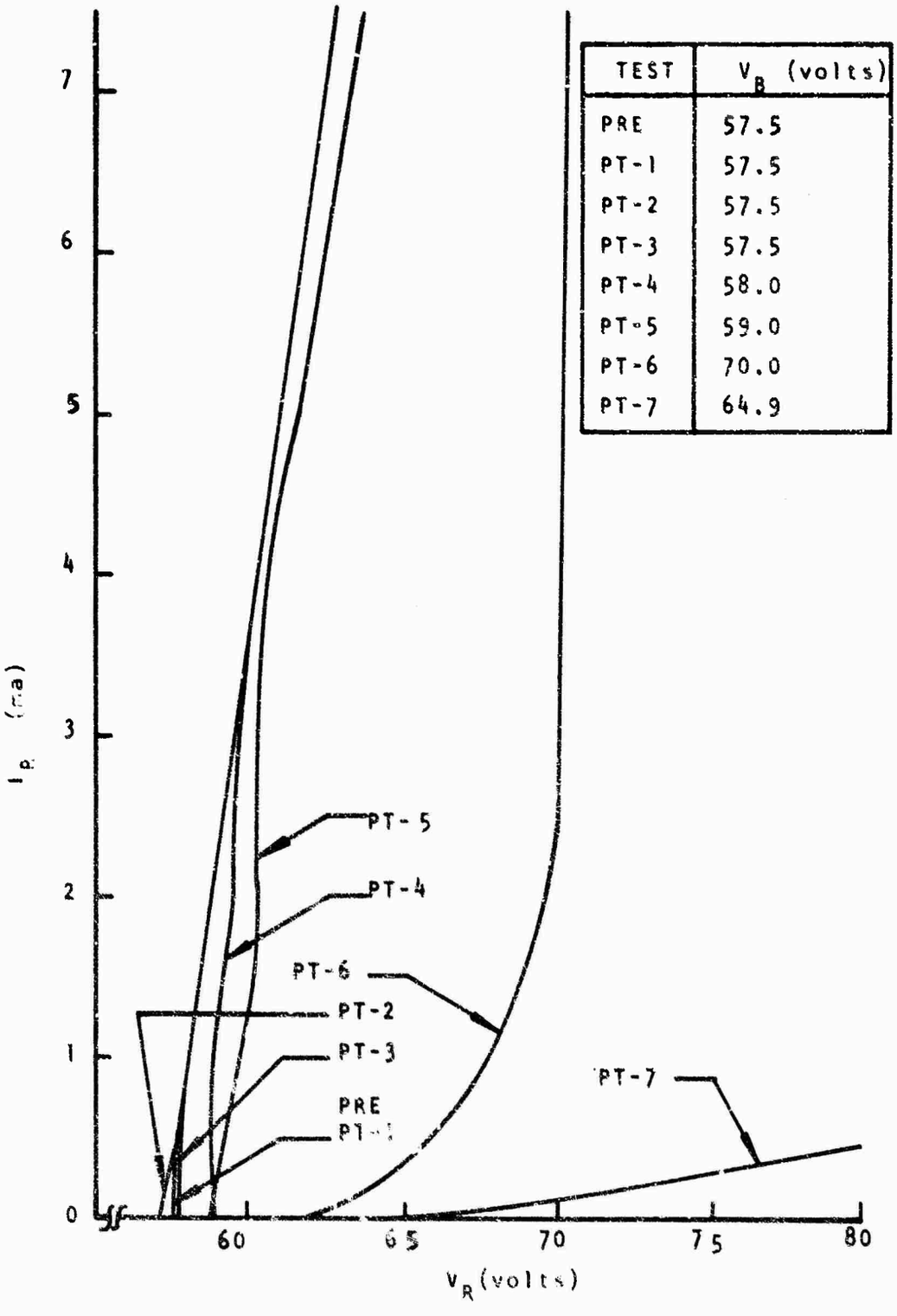

Figure 62. I_R versus V_R for CD5171-22 at Different NVT Exposures

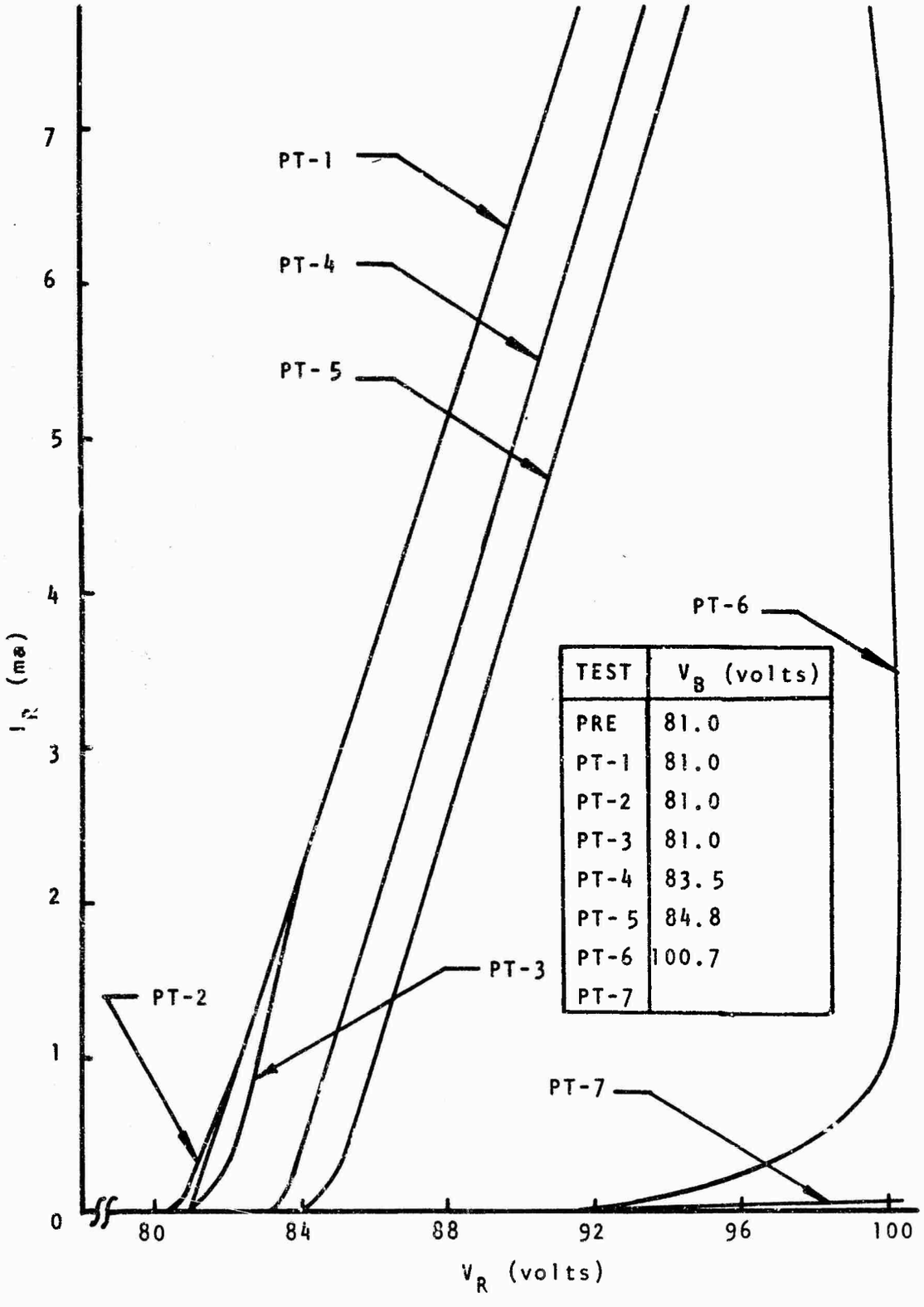

Figure 63. I_R versus V_R for CD3174-26 at Different NVT Exposures

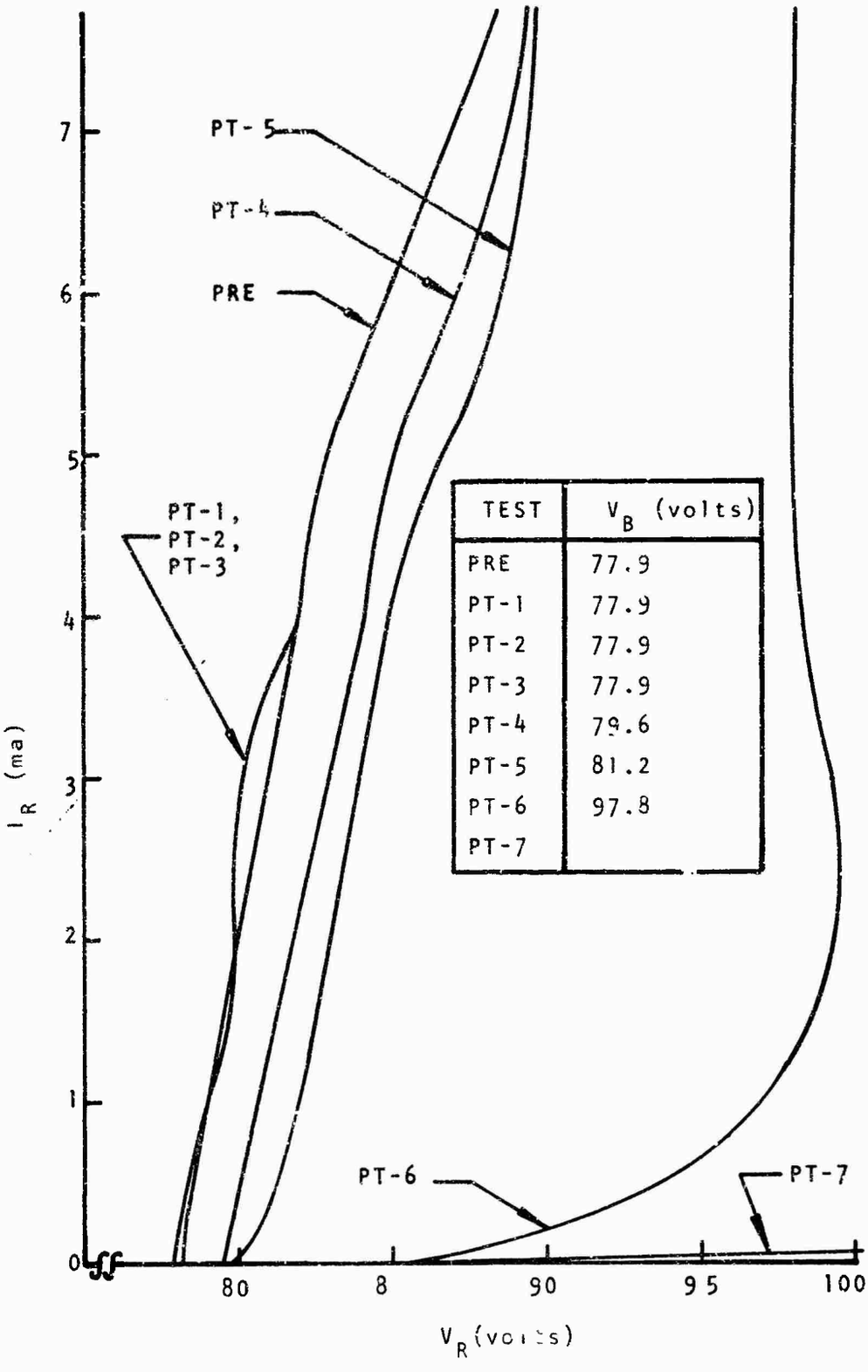

Figure 64. I_R versus V_R for CD3174-27 at Different NVT Exposures

2. Degradation of Avalanche Transistors

Five each of Texas Instrument types 2N3033, 2N3034, and 2N3035 were irradiated with the avalanche diodes in the neutron environment. These transistors were n-p-n epitaxial mesa silicon transistors designed for extremely high-speed, high-current, avalanche mode switching applications. The BV_{CBO} for the different units varied between approximately 50 and 160 volts, and the minimum output response was in the range of 20 to 45 volts for the circuit shown in figure 65.

Delay time, t_d, rise time, t_r, peak output pulse amplitude, V_p, pulse shape, and the minimum input voltage required to trigger the circuit, V_T, shown in figure 66, were determined before irradiation and after each irradiation. This was done by using a Hewlett-Packard sampling scope and recording the data on film by using a Polaroid camera.

Pre- and post-testing of the following electrical parameters were also made using the Fairchild 500:

1. V_F versus I_F, and V_R versus I_R for both the base-emitter diode and collector-base diode.

2. LV_{CEO} and $LV_{CER}(R_{BE} = 50\ \Omega)$ at various levels of current from 10 ma to 199 ma.

3. h_{fe} and h_{ie} for the range of collector dc current from 10 μa to 9 ma at $V_{CE} = 10$ V.

4. V_{CE} SAT for collector current varying from 10 μa to 9 ma.

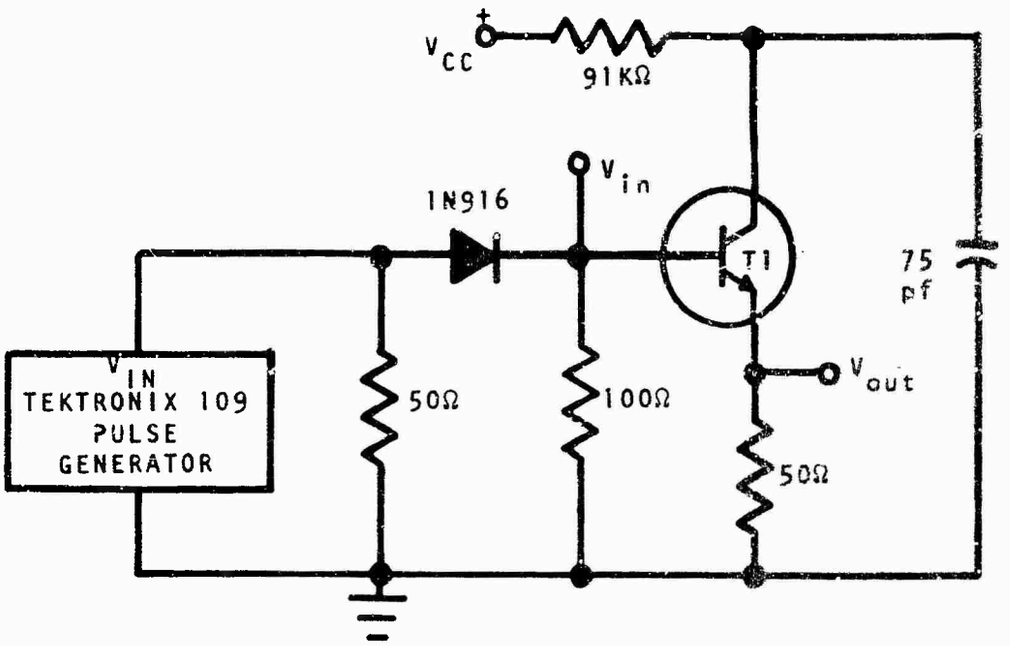

Figure 65. Circuit Used for Observing Neutron Degradation of Avalanche Transistor Switching Characteristics

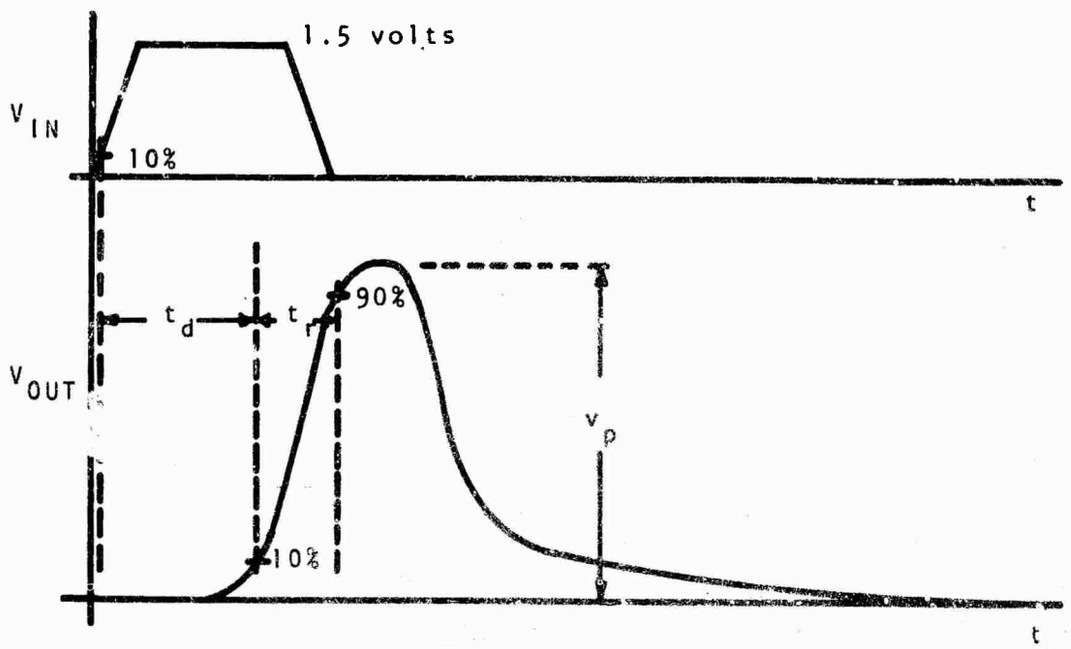

Figure 66. Waveshapes Observed in Circuit of Figure 65

The results for the transistor switching tests of figure 65 are given in tables IV, V. and VI. The following general trend in the experimental data can be observed.

1. V_T tends to decrease and then increase with total exposure. This can be related to the diode results in which minority-carrier-lifetime effects predominate at low flux levels; at higher exposure levels the conductivity modulation suppresses the effect because of the lifetime change. The exact extent to which the forward voltage of a diode for a constant current will change with neutron exposure depends mainly on device structure, fabrication techniques, initial impurity concentrations, the width of the p- and n-regions, injection level, lifetime damage constant, carrier removal rate, temperature, neutron energy spectrum, etc.

2. V_p generally increased with increasing neutron exposure. At low flux levels V_p did not change much or at all due to the small percentage of carriers removed.

3. The rise time, t_r, showed a decrease and the delay time, t_d, showed an increase with increasing neutron exposure. The reason for the decrease in t_r can be explained by considering how current builds up to move operation from points A to C of figure 9. The input voltage causes an injection of a number of carriers, c, from the emitter into the base

TABLE IV

SWITCHING CHARACTERISTIC DATA FOR 2N3033

SAMPLE	nvt neutrons/cm^2	V_T volts	V_P volts	t_d nsec	t_r nsec	V_{CC} volts
1	Pre	1.16	30.0	3.75	2.00	190
1	0.986×10^{13}	1.10	31.5	3.75	2.00	190
1	4.756×10^{13}	1.14	31.0	4.00	1.75	190
1	0.9316×10^{14}	1.20	31.5	4.50	1.50	190
1	4.008×10^{14}	1.20	32.5	4.50	1.50	190
1	0.8408×10^{15}	1.10	32.5	4.25	1.50	190
1	4.1378×10^{15}	1.40	27.0	7.50	1.25	190
1	0.8612×10^{16}	- - - - -	- F a i l e	d - - - -	- - - - -	- - - - -
2	Pre	1.18	34.0	4.5	2.00	190
2	0.986×10^{13}	1.12	34.5	4.5	2.00	190
2	4.756×10^{13}	1.08	35.0	4.5	2.00	190
2	0.9316×10^{14}	1.13	35.0	4.5	2.00	190
2	4.008×10^{14}	1.20	37.0	4.5	1.75	190
2	0.8408×10^{15}	1.20	37.0	4.5	1.50	190
2	4.474×10^{15}	1.20	39.0	5.5	1.50	190

TABLE V

SWITCHING CHARACTERISTIC DATA FOR 2N3034

SAMPLE	nvt neutrons/cm^2	V_T volts	V_P volts	t_d nsec	t_r nsec	V_{CC} volts
1	Pre	1.16	18.50	4.00	2.00	190
1	0.986×10^{13}	1.14	18.50	4.50	1.75	190
1	4.756×10^{13}	1.22	18.75	4.50	1.75	190
1	0.9316×10^{14}	1.10	18.75	4.50	1.50	190
1	4.008×10^{14}	1.20	20.50	4.50	1.50	190
1	0.8408×10^{15}	1.20	20.50	4.50	1.25	190
1	4.1378×10^{15}	0.70	24.00	3.25	1.25	130
1	0.8612×10^{16}	1.24	20.00	3.75	2.00	90
2	Pre	1.19	21.00	4.50	2.0	190
2	0.986×10^{13}	1.18	22.00	4.50	1.5	190
2	4.756×10^{13}	1.19	21.75	4.75	1.5	190
2	0.9316×10^{14}	1.08	22.00	4.50	1.5	190
2	4.008×10^{14}	1.08	26.00	4.00	1.5	190
2	0.8408×10^{15}	0.70	24.00	2.50	1.5	120
2	0.8408×10^{15}	1.24	22.00	6.00	1.5	90
2	4.1378×10^{15}	0.84	18.00	4.00	2.0	90
	0.8612×10^{16}	- - - - -	Failed	- - - - -	- - - - -	- - - -

TABLE VI

SWITCHING CHARACTERISTIC DATA FOR 2N3035

SAMPLE	nvt neutrons/cm^2	V_T volts	V_P volts	t_d nsec	t_r nsec	V_{CC} volts
1	Pre	1.00	17.5	3.0	2.0	190
1	3.77×10^{13}	0.80	18.0	3.0	2.0	190
1	0.833×10^{14}	0.60	18.0	3.2	1.5	190
1	3.909×10^{14}	0.48	13.5	3.2	1.5	90
1	0.8309×10^{15}	0.40	14.0	3.2	1.7	75
1	4.1378×10^{15}	- - - - -	F a i l e	d - - - -	- - - - -	- - - - -
2	Pre	0.80	17.0	3.0	2.00	190
2	0.986×10^{13}	0.90	17.5	3.0	2.00	190
2	4.756×10^{13}	0.96	17.5	3.2	1.75	190
2	0.9316×10^{14}	0.88	17.5	3.2	1.50	190
2	4.008×10^{14}	1.20	17.5	4.5	1.50	90
2	0.8408×10^{15}	1.20	18.0	4.5	1.50	90
2	4.1378×10^{15}	1.28	18.0	4.5	1.20	90
2	0.8612×10^{16}	1.28	18.0	4.5	2.00	90

which reach the collector depletion region after a transit time T_b. The transit time T_b is approximately equal to $(w_T)^{-1}$ where $w_T = 2\pi f_T$, the current gain-bandwidth product (reference 9). In crossing the collector depletion region, multiplication occurs and Mc carriers leave the collector. If the base current is constant, these Mc carriers must flow into the emitter. They flow across the base to the collector with a resulting M^2c flowing out of the collector after another interval T_b. This process keeps repeating, producing a regenerative buildup whose rate depends upon the transit time T_b and M. The base transit time T_b is related to the minority carrier diffusion coefficient D and the base thickness W_b by

$$T_b = \frac{W_b^2}{2Dm} \tag{96}$$

where m is a factor which accounts for built-in fields affecting the motion of minority carriers (references 29 and 30). The diffusion constant D is not truly a constant but is a function of the impurity concentration. Using the Einstein relation, D can be related to the carrier mobility u by

$$D = u \frac{\kappa T}{q} \tag{97}$$

Since u is a function of doping, D is a function of doping. In general, as N (acceptor or donor concentration) gets

smaller, u (hole or electron mobility) gets larger. This would tend to increase D as doping concentration decreases. Thus, as carrier removal starts decreasing the doping in the base region, D should tend to increase with a resulting decrease in T_b.

As carriers are removed from the collector and base region due to neutron degradation, the collector-base diode depletion region spreads further and further into the collector and base regions. This would tend to make the base thickness look smaller and thus require less transient time. A finite time is taken for the carriers to drift across the depletion region, but this time can be neglected for all practical purposes. However, it should be noted that if the depletion layer widens with the voltage held constant there will be a tendency for M to decrease. This would tend to make the rise time increase.

4. For some of the devices, V_{CC} had to be decreased at the higher nvt; otherwise, the device tended to fire without any input signal. This is probably caused by the increase in leakage currents because of neutron damage.

Some of the significant test results after each neutron run using the Fairchild 500 are summarized in figures 67 to 75. Figures 67 to 69 show representative results of β degradation with increased neutron damage. As expected, β

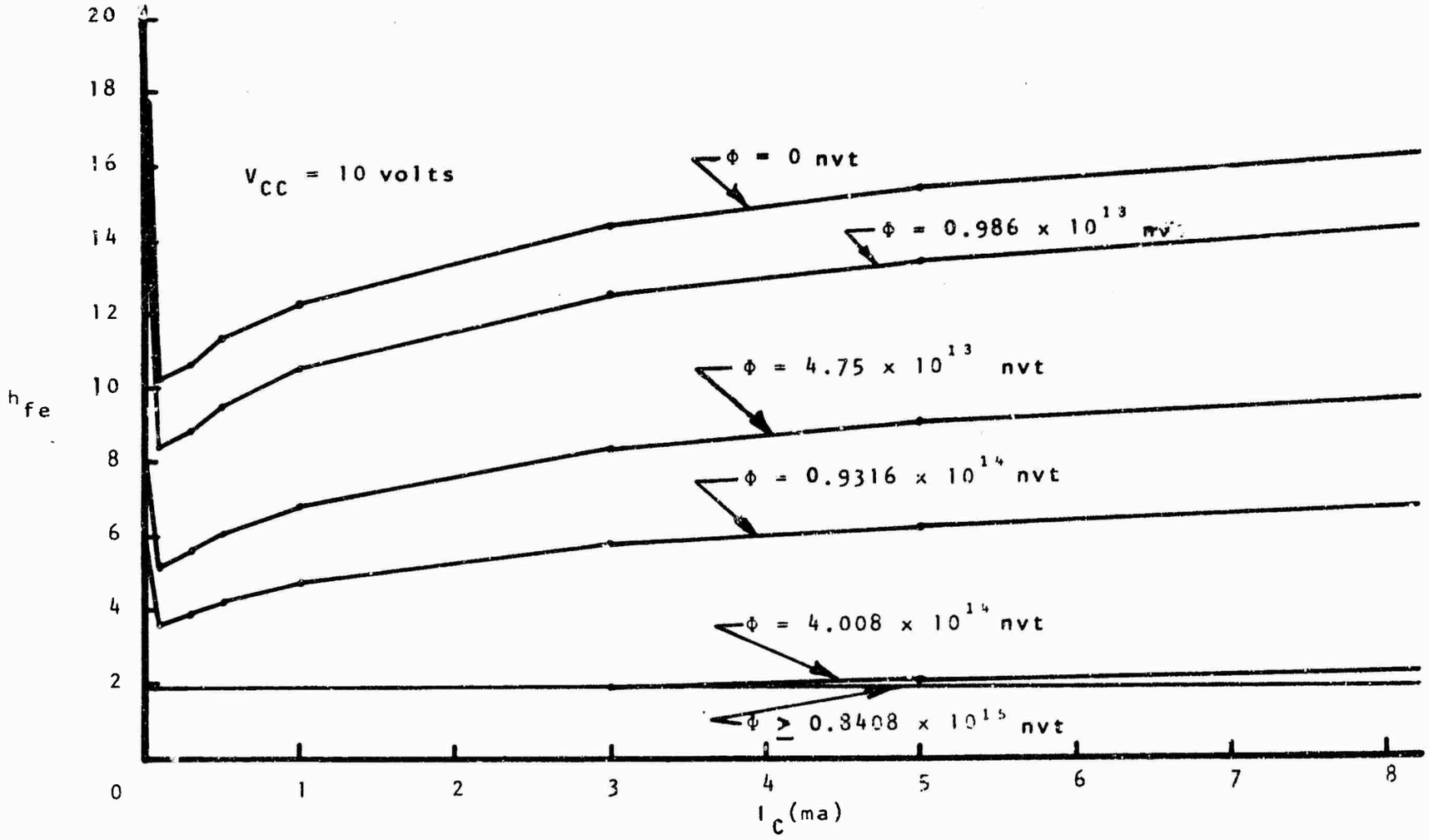

Figure 67. h_{fe} versus I_C at Different NVT Exposures for Avalanche Transistor 2N3033, Sample #2

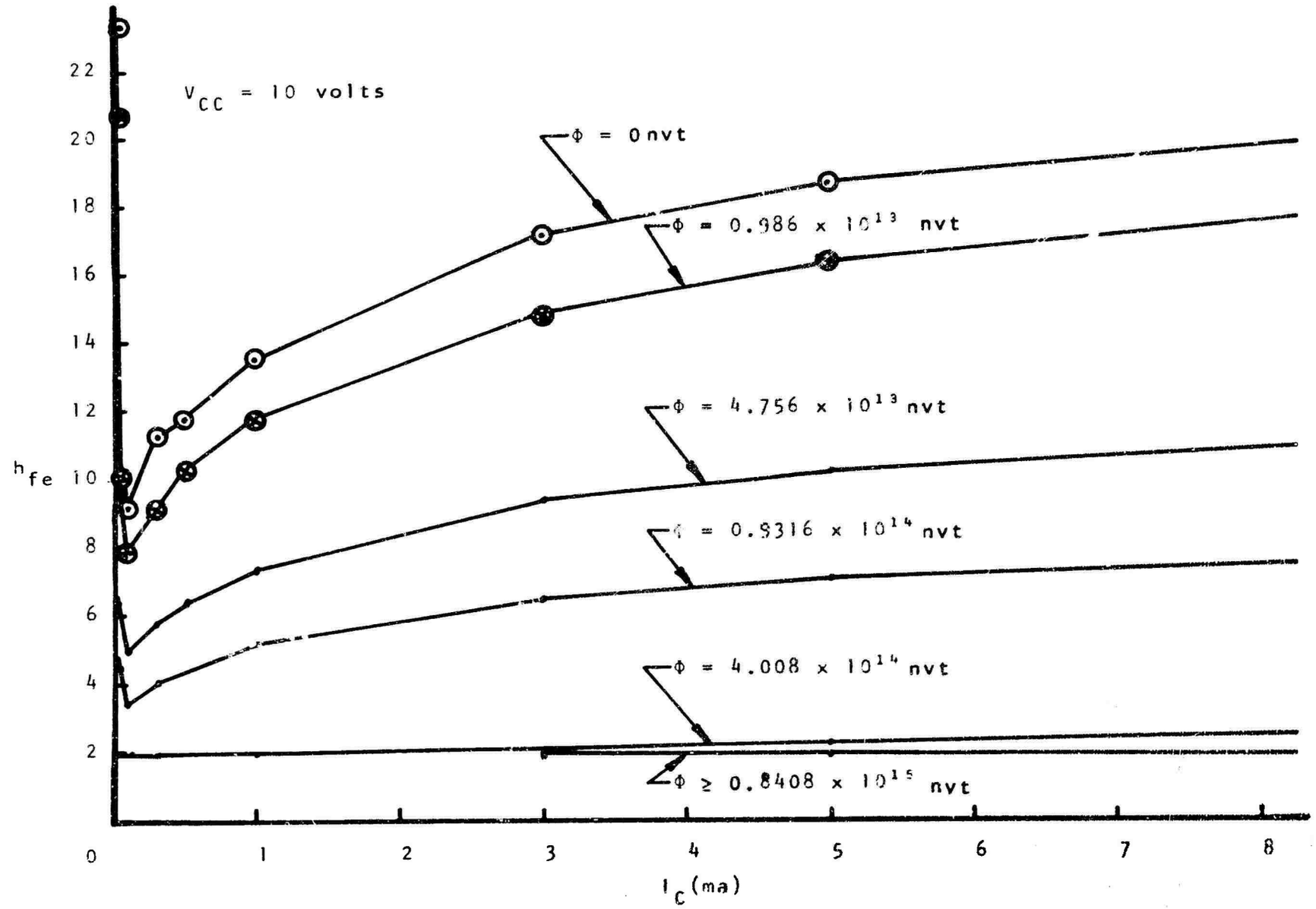

Figure 68. h_{fe} versus I_C at Different NVT Exposures for Avalanche Transistor 2N3034, Sample #2

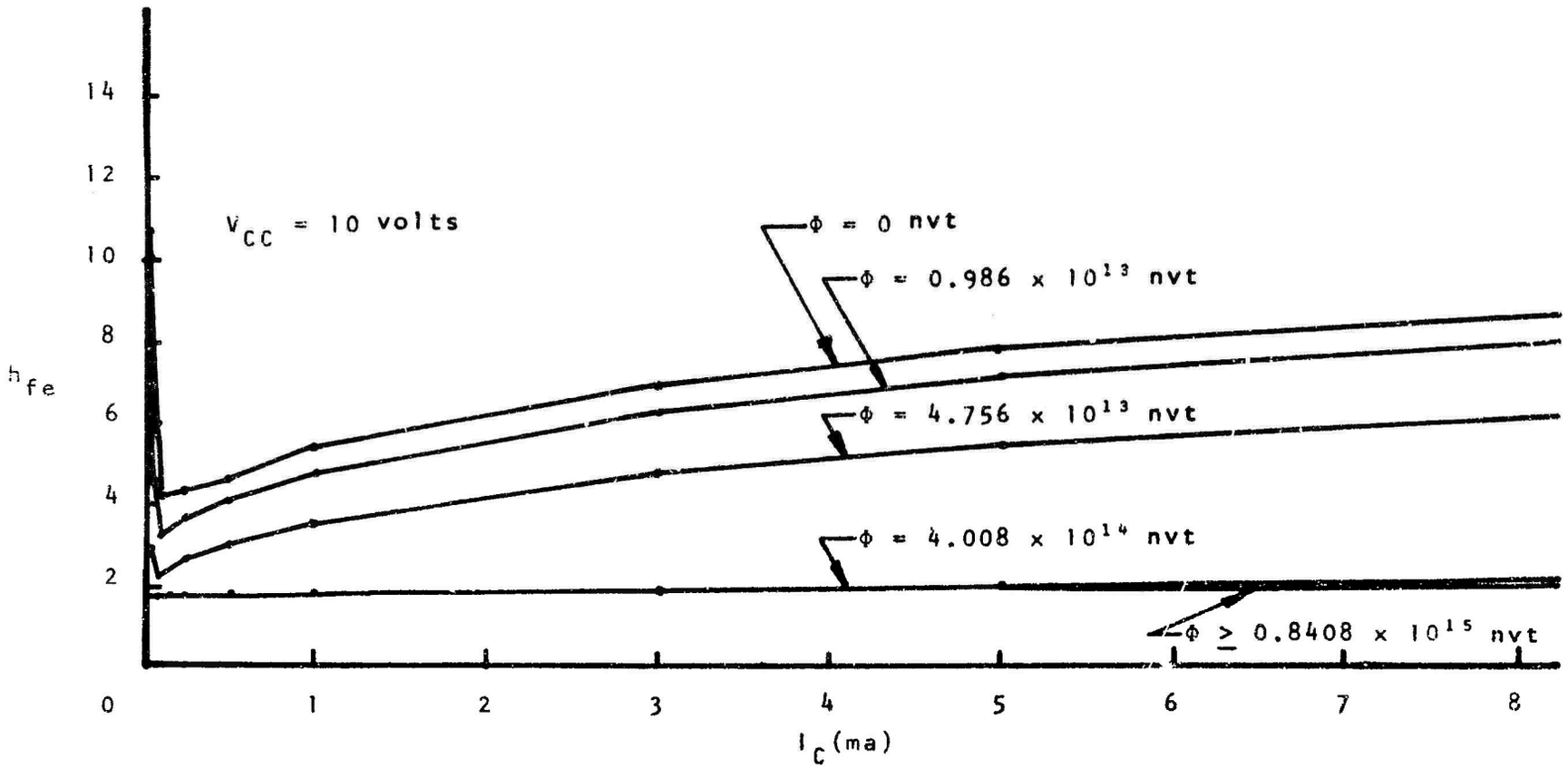

Figure 69. h_{fe} versus I_C at Different NVT Exposures for Avalanche Transistor 2N3035, Sample #2

decreased with neutron fluence. When the measured value of β approached 1.9, the usefulness or interpretation of the Fairchild 500 test data becomes questionable, due to the limitations of the machine. At this level a Tektronix 575 Transistor Curve Tracer was also employed to observe the transistors' characteristics and determine β. At the higher neutron flux levels, the measured values of β approached 1 (a few values of β were less than 1), but the devices continued to fire.

As previously discussed (see page 26, equation 25), the statement $\alpha M = 1$ or

$$\beta_M = \frac{\alpha M}{1-\alpha M} \tag{98}$$

is the condition for the onset of avalanche. If in equation (98) α was only 1/2, the required value for avalanche would be an M of 2. From the X-ray results, values of $M > 2$ are easily obtained by varying the voltage across the junction depletion region. That is, as the voltage V_{CB} is increased, the value of α necessary for avalanche is reduced. It is apparent that what one would like to do is maintain the highest value of M across the junction, so that the smallest value of α necessary for avalanche is required, to minimize β neutron degradation effects on the transistor. This was the approach taken in exposing the devices to a neutron environment, and some of the devices still fired after fluence of 8.612×10^{15} nvt even with a beta of one.

In the process of using the Fairchild 500, many of the transistors were destroyed because of instrumentation problems. One problem was that the Fairchild 500 was not operating properly at times and sometimes the program tape reader would read erroneous information off the prepared tape program. This resulted in the maximum rating of the transistor being exceeded, with possible thermal destruction, and an over-range signal appearing on the Fairchild program panel. Another problem was the author's unfamiliarity with the machine. After a few pre- and post-test sequences, only two to three of each type of transistor were left.

The results of I_R versus V_R for the collector base diode and I_F versus V_F for the emitter base diode at different exposures for some of the transistors are shown in figures 70 to 75. The breakdown voltage, V_B, increased with increasing neutron fluence as shown in figures 70 to 72. The maximum change in V_B was observed in the transistor with lowest doping (2N3033). The results of LV_{CEO}, LV_{CER}, h_{ie}, and V_{CE} SAT are not given, due to the random fluctuation of the data and insufficient time to properly analyze the tremendous amount of experimental data.

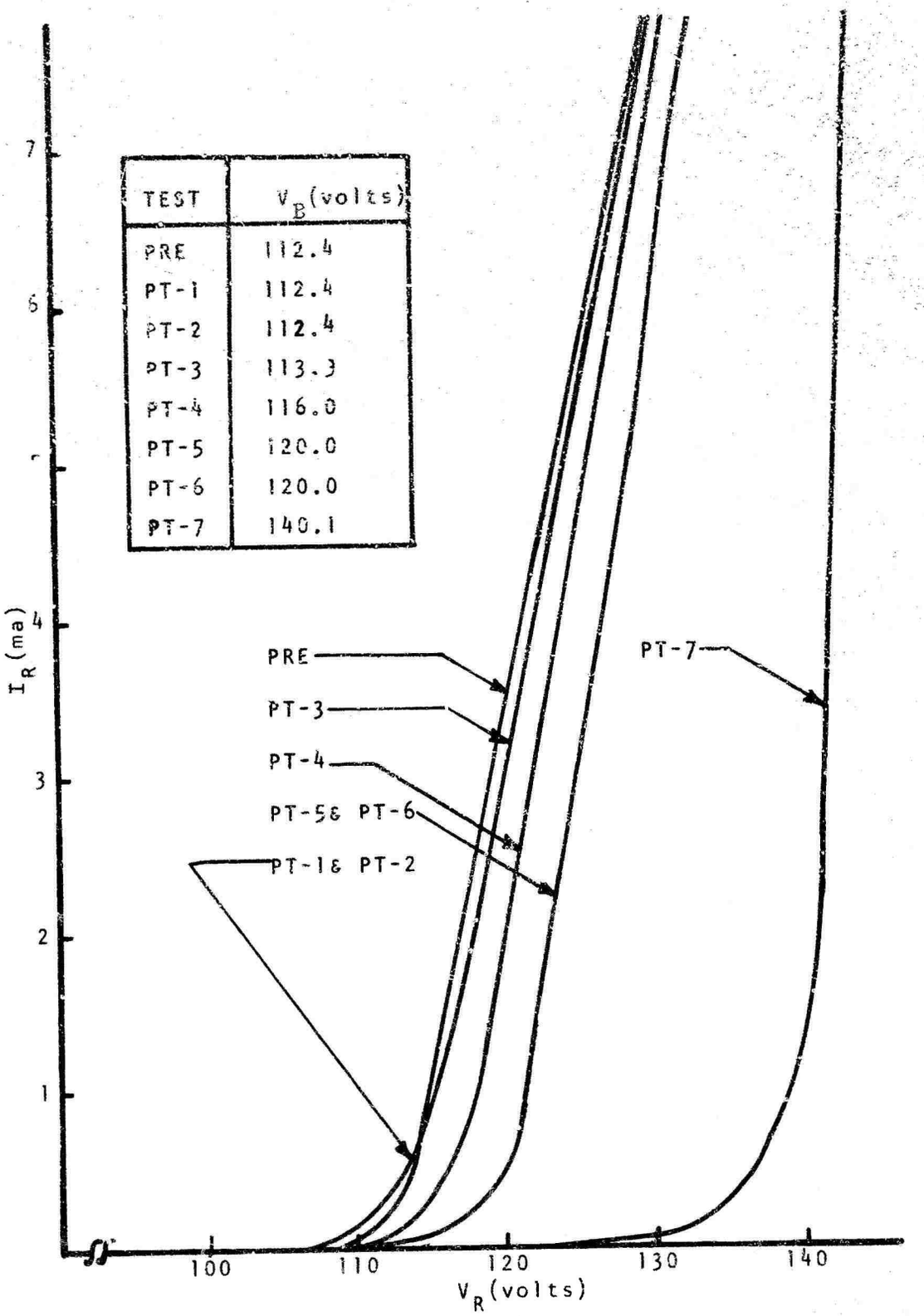

Figure 70. I_R versus V_R for the Collector-Base of Avalanche Transistor 2N3033, Sample #2, at Different NVT Exposures

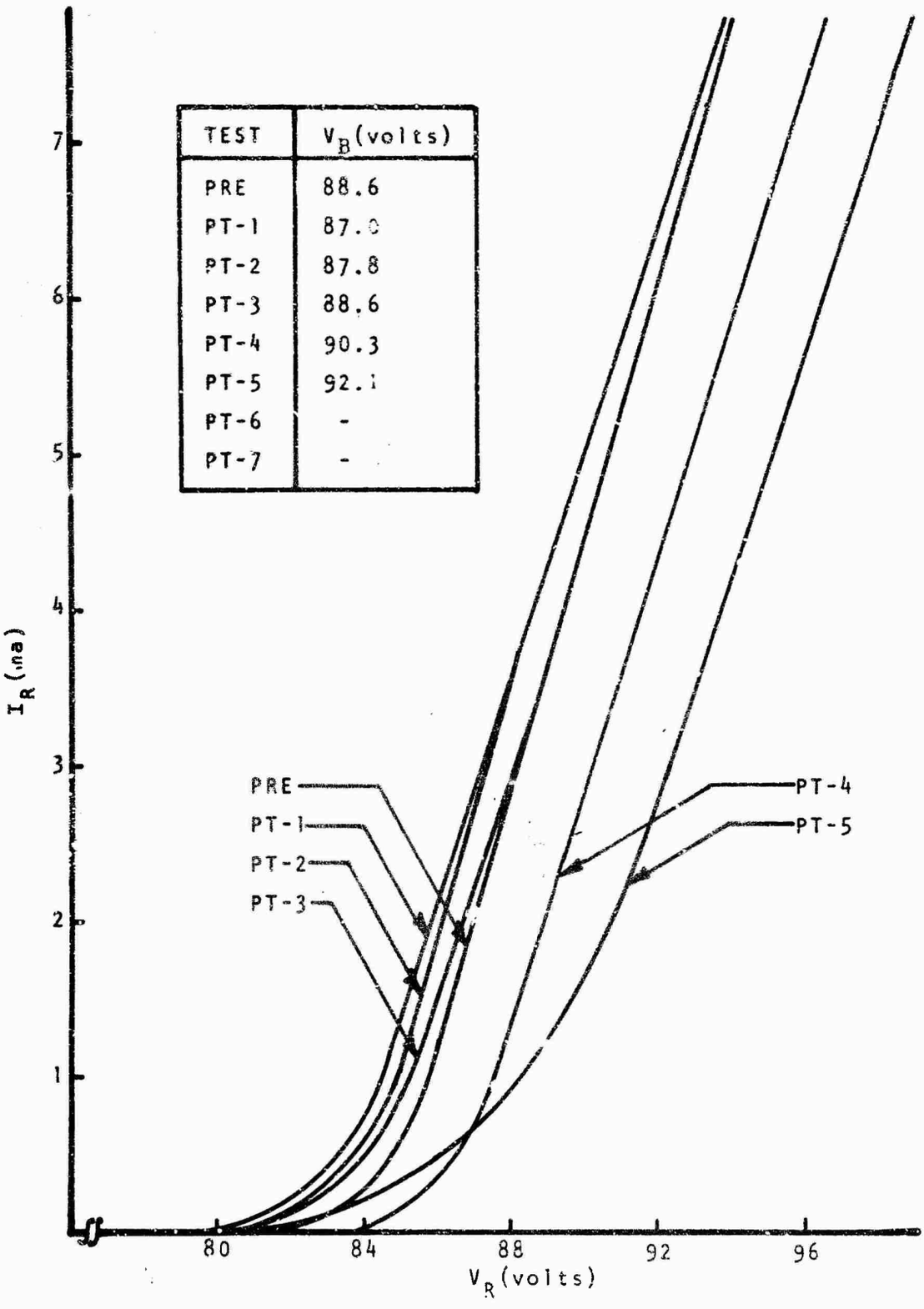

Figure 71. I_R versus V_R for the Collector-Base of Avalanche Transistor 2N3034, Sample #2, at Different NVT Exposures

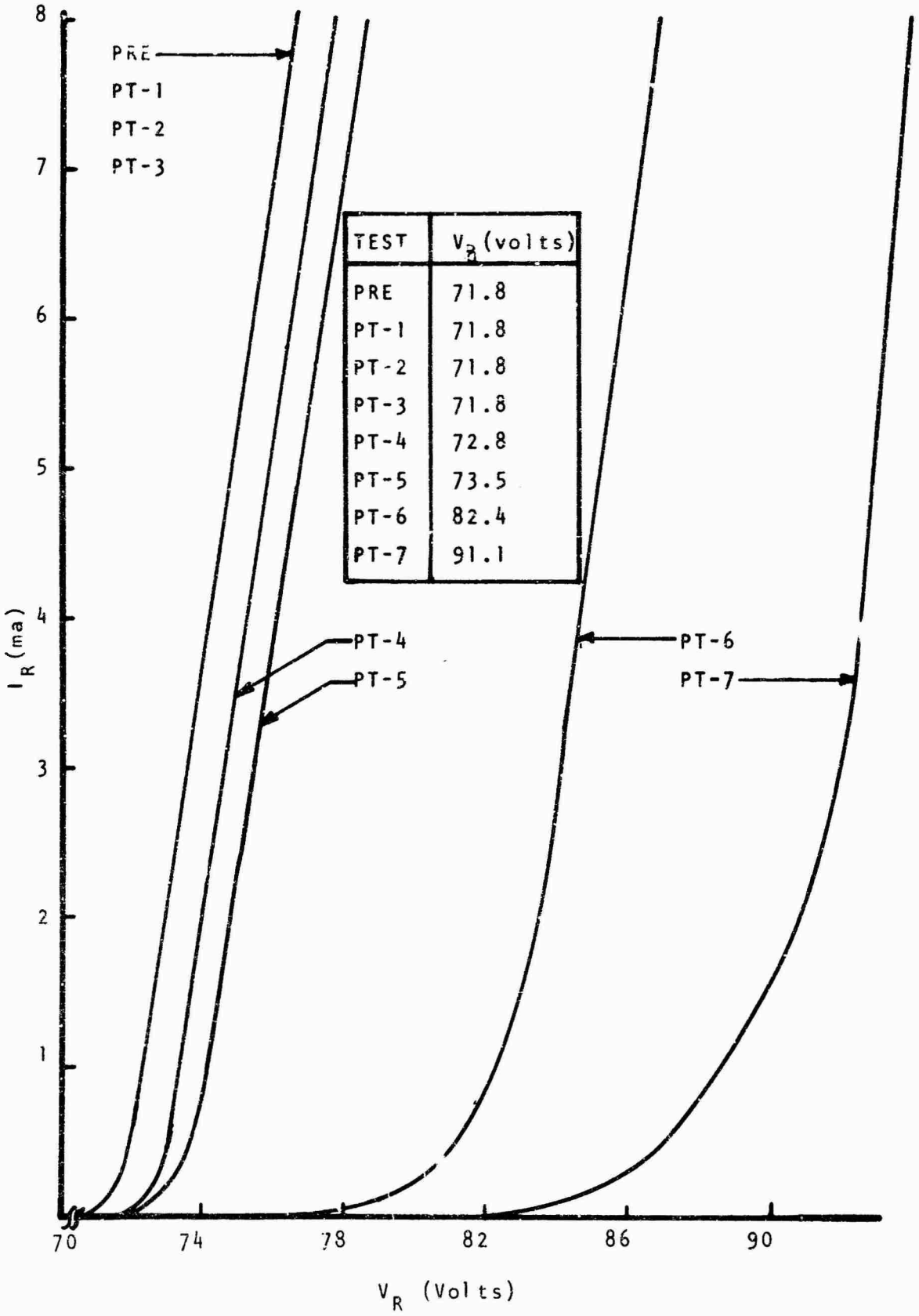

Figure 72. I_R versus V_R for Collector-Base of Avalanche Transistor 2N3035, Sample #2, at Different NVT Exposures

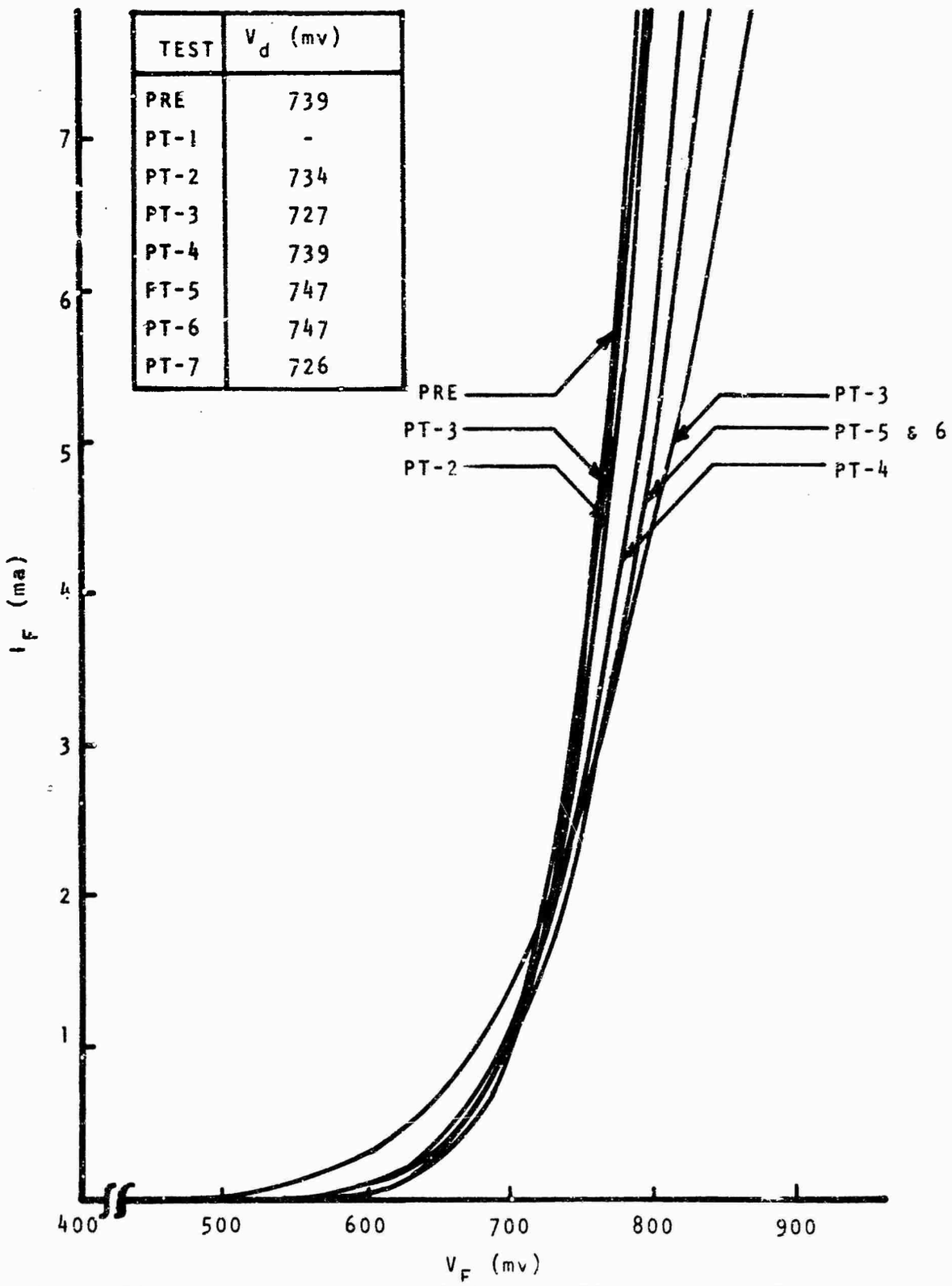

Figure 73. I_F versus V_F at Different NVT Exposures for the Emitter-Base of Avalanche Transistor 2N3033, Sample #2

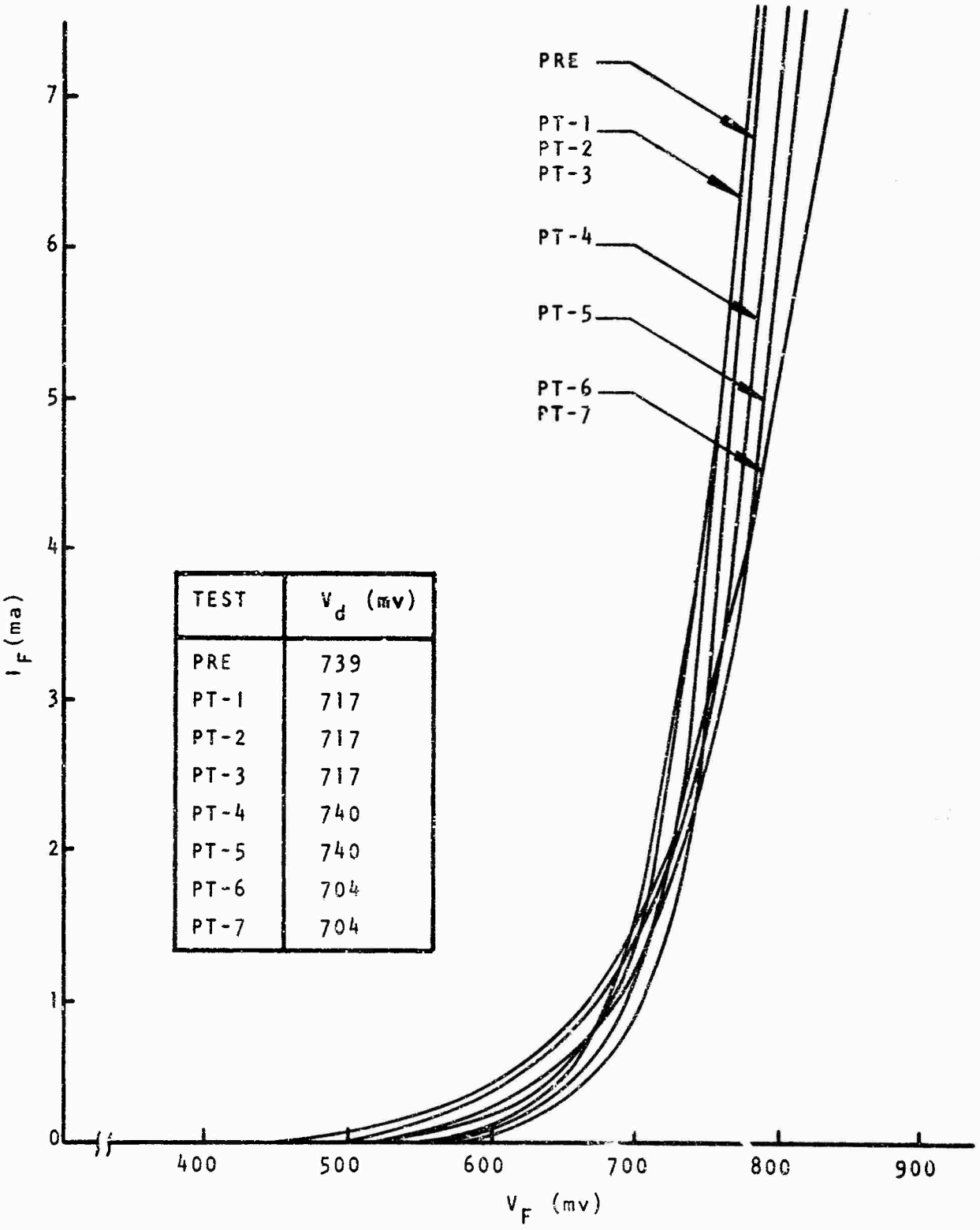

TEST	V_d (mv)
PRE	739
PT-1	717
PT-2	717
PT-3	717
PT-4	740
PT-5	740
PT-6	704
PT-7	704

Figure 74. I_F versus V_F at Different NVT Exposures for the Emitter-Base of Avalanche Transistor 2N3034, Sample #2

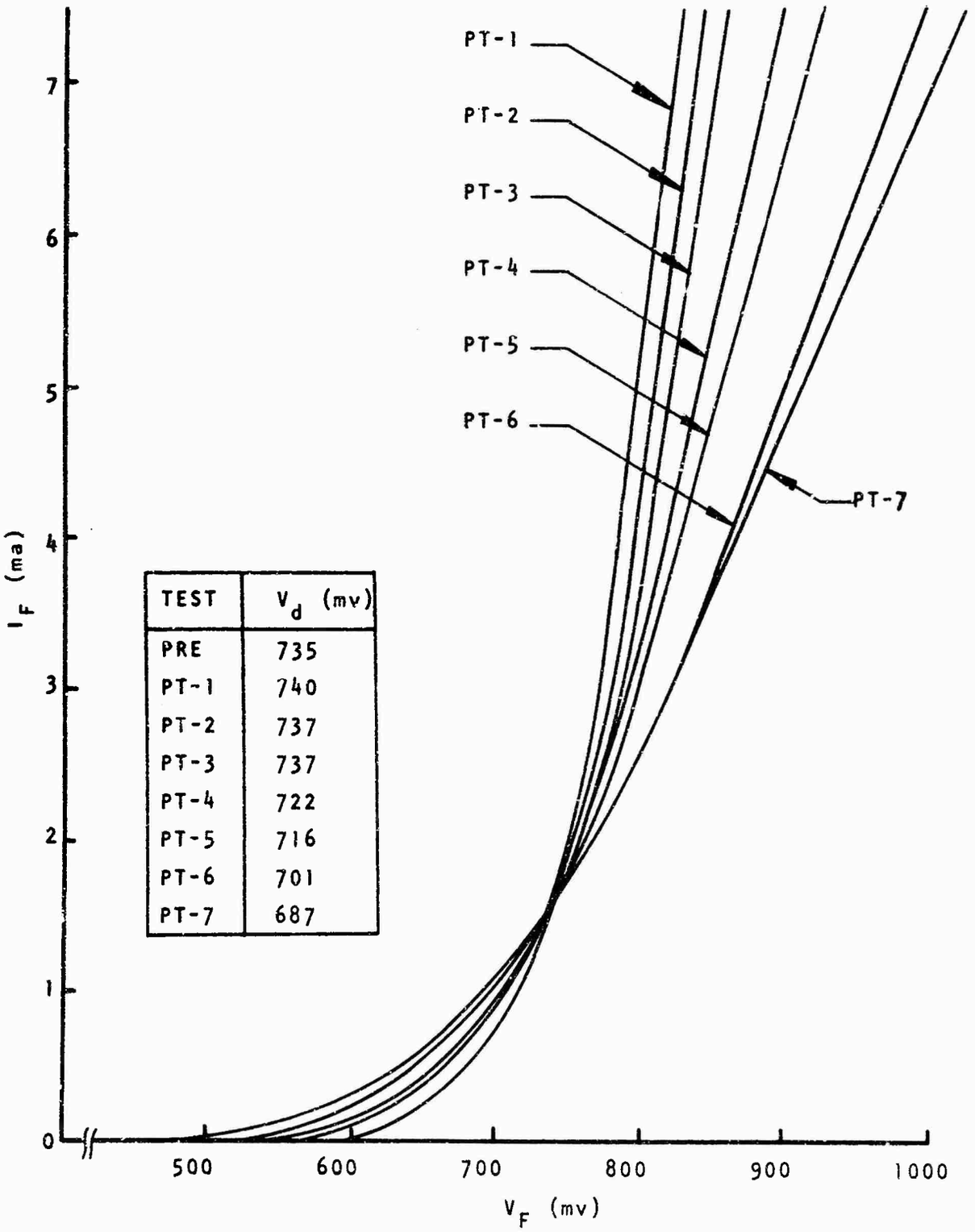

Figure 75. I_F versus V_F at Different NVT Exposures for the Emitter-Base of Avalanche Transistor 2N3035, Sample #2

SECTION VII

SUMMARY AND CONCLUSIONS

An analytical model has been developed in this paper to describe the avalanche multiplication of the photocurrent in a diode. An empirical equation was used to describe avalanche multiplication, which mathematically fits previous experimental results associated with avalanche devices. The avalanche multiplication phenomenon was related to physical parameters of the device, and equivalent circuits under irradiation were developed. These models described the behavior of photocurrent as a function of time when the diode was exposed to ionizing radiation. Both the operations prior to breakdown of the device and after breakdown were included. The parameters of the models were related to measurable diode physical parameters, and hence, were used to develop design requirements for radiation hardening.

An equation was developed which indicated the reason for the observed longer tails on the photocurrent once the device was in breakdown. Experimental results were given for transient radiation effects induced on the alloy p+n diode. The theoretically computed photocurrents compared favorably with the experimentally observed radiation induced photocurrents.

The derivation of the expression for the primary photocurrent indicated the necessity for reduction of the active

volume for radiation hardening since the photocurrent was directly proportional to the active volume. This implied that the smallest possible diode which met the required circuit application and power level should be used. This situation required the minimization of the junction area, depletion area, and minority carrier lifetime. The minority carrier lifetime can be reduced by gold doping, and the depletion widths can be minimized by the use of a lower bias voltage and proper selection of doping profiles. Since all the bulk primary photocurrent was multiplied by the multiplication factor M, this required that the device be operated at low voltage to minimize M. However, the multiplication of the primary photocurrent can be used to an advantage when the device is used as a cancellation diode in a compensation circuit. Although the equation for the diode response did not include the interaction between the device and its external circuitry, the equation can be used in conjunction with the diode model to predict approximate circuit response.

The basic theory of avalanche transistor operation was reviewed and the critical design factors were discussed. Expressions were developed which relate minimum trigger levels, power gains, and output pulse amplitudes to circuit parameters, considering quiescent and transient operating

conditions. Circuit designs were developed for avalanche transistor operation under transient X-ray irradiation.

Since avalanche transistor circuits are normally sensitive to transient ionizing radiation, the following methods of hardening were used: (a) an external base to ground reverse bias source, (b) a collector to base compensation diode, (c) a collector to base compensation diode plus a collector to ground clamping diode, and (d) a base to ground compensation diode. From simplified equivalent circuits, approximate criteria for hardening these avalanche transistor circuits to ionizing radiation were developed. Using these hardening techniques, circuits were fabricated and experimentally tested in a transient radiation environment. The experimental results were consistent with the theoretical predictions. The circuits were tested in the range from 10^6 R/sec to over 10^{10} R/sec, and all of the above techniques increased the hardness of the circuits.

The base to ground diode-compensated circuit, which did not switch at about 4×10^{10} R/sec, theoretically and experimentally, veriries the hardness of avalanche circuits to very high levels of transient X rays. It is felt that with optimally designed circuits, radiation hardening can be achieved to even higher exposure levels.

Avalanche diodes and transistors were also irradiated in a neutron environment, and pre-test and post-test data from the devices were taken. The following fundamental results on the diodes were confirmed or observed as the neutron flux increased: (1) decrease in carrier lifetime, (2) increase in a conductivity modulation, (3) increase in breakdown voltage, and (4) an increase in leakage current. The same results were observed in the transistor with also a reduction in β, a general increase and then decrease in peak output voltage and minimum triggering voltage, and a decrease in rise time with increasing neutron flux. Depending on the dopings, some of the diodes and transistors were still functioning properly after irradiation up to 8.612×10^{15} nvt.

In summary, the avalanche transistor and diode without special design consideration are sensitive to irradiation by transient pulse of X rays. The predominant transient radiation effect in avalanche circuits is the possible switching of the avalanche transistor from the "off state" to the "on state," due to induced transient primary photo-currents. However, by using proper biasing and/or junction compensation, one can harden avalanche transistor circuits so they will not switch at levels of radiation up to

4×10^{10} R/sec. Avalanche design is an effective technique to produce a circuit which is relatively insensitive to a neutron environment. A circuit employing an avalanche transistor has been experimentally determined to function properly after exposure to neutron fluence in excess of 10^{15} n/cm^2.

It is hoped that this research has demonstrated the necessity for future theoretical and experimental work in avalanche devices and the need for extension of the present work to a higher level of sophistication. From this contract work, several areas of investigation need to be further refined and completed.

1. The development of a more sophisticated model of an avalanche transistor and diode for incorporation in computer predictions.

2. The development of techniques for measuring the parameters used in defining an avalanche transistor or diode model.

3. An investigation into the use of avalanche circuits for the replacement of presently used circuits or circuit functions.

4. An investigation into the optimization of the circuits presented in this report.

5. The development of better techniques for observing transient or permanent damage in an avalanche transistor circuit exposed to a nuclear environment.

APPENDIX I

DERIVATION OF p-n JUNCTION TRANSIENT CURRENT

To evaluate an expression for the transient response of a p-n junction, several assumptions have to be made. These assumptions are as follows:

1. The diode has a one-dimensional carrier flow.
2. The voltage applied externally across the diode is assumed to occur mainly across the depletion region up to the breakdown voltage of the device. The field available for drift within the main body of the p-region or n-region is therefore very weak.
3. When the external voltage across the device exceeds the breakdown voltage, the additional voltage is assumed to be dropped uniformly across the lightly doped side.
4. The diode is uniformly doped.
5. Diffusion theory holds for predicting transient effects.
6. The contact on the lightly doped side is greater than several diffusion lengths from the junction.
7. The ionizing radiation uniformly produces excess electron-hole pairs. These excess electron-hole pairs produced are assumed to be in sufficient

amount to significantly alter only the minority carriers in each region as shown in figure 15.

When considering the transient response of a p-n junction, one runs into the problem of hole injection into an n-region, or electron injection into a p-region (reference 16). If holes injected into an n-region are considered, one can express in words the conservation of holes at a fixed point in space as

$$\begin{bmatrix}\text{time rate of}\\ \text{increase in}\\ \text{hole density}\end{bmatrix} = \begin{bmatrix}\text{thermal generation}\\ \text{rate of holes}\end{bmatrix} - \begin{bmatrix}\text{recombination}\\ \text{rate of holes}\end{bmatrix} - \begin{bmatrix}\text{outflow}\\ \text{of holes}\end{bmatrix} + \begin{bmatrix}\text{radiation}\\ \text{generation}\\ \text{rate of holes}\end{bmatrix} \tag{99}$$

The first term on the right-hand side of the above equation is equal to rn_i^2 and the second term is equal to rnp where r is a constant. If it is assumed that only the minority carrier density is altered appreciably in excess of the equilibrium densities p_{no} and n_{no} due to hole injection, one can write

$$p_n = p_{no} + \delta p_n \tag{100}$$

and

$$n_n \approx n_{no} \tag{101}$$

Hence, if one neglects momentarily the radiation term, the first two terms on the right-hand side of equation (99) can be written

$$\frac{d(\delta p_n)}{dt} = rn_i^2 - rnp = rn_i^2 - rn_{no}\,(p_{no} + \delta p_n) \qquad (102)$$

Since rn_i^2 is equal to $rn_{no}p_{no}$, equation (102) becomes

$$\frac{d}{dt}(\delta p_n) = rn_{no}\delta p_n \qquad (103)$$

Solving for δp_n gives

$$\delta p_n = (\delta p)_o e^{-rn_{no}t} = (\delta p)_o e^{-t/\tau_p} \qquad (104)$$

where one defines $rn_{no} = 1/\tau_p$, and $(\delta p)_o$ is the value of δp_n at $t = 0$. Solving for δp_n out of equation (100) and putting it into equation (103) one obtains

$$\frac{d}{dt}(\delta p_n) = rn_{no}(p_n - p_{no}) = \frac{p_{no} - p_n}{\tau_p} \qquad (105)$$

The outflow of holes can be found by examining a cube of widths Δx, Δy, Δz. Net inflow into cube =

$$-\left[\frac{1}{q}\frac{\partial j_z}{\partial y}\Delta y + \frac{1}{q}\frac{\partial j_z}{\partial z}\Delta z + \frac{1}{q}\frac{\partial j_x}{\partial x}\Delta x\right] \qquad (106)$$

On considering a unit cube, one can rewrite equation (106) as

$$-\frac{1}{q}\left[\frac{\partial j_\cdot}{\partial y} + \frac{\partial j_z}{\partial z} + \frac{\partial j_x}{\partial x}\right] = -\frac{1}{q}\nabla \cdot \vec{j}_p \qquad (107)$$

where $\vec{j}_p$ is the current density.

The continuity equation for holes injected into an n-region becomes, from the above derivation,

$$\frac{\partial p_n(x,t)}{\partial t} = \frac{p_{no} - p_n(x,t)}{\tau_p} - \frac{1}{q} \nabla \cdot \vec{j}_p + g(t) \qquad (108)$$

where g(t) is the carrier generation rate due to radiation. Similarly the continuity equation for electrons can be written

$$\frac{\partial n_p(x,t)}{\partial t} = \frac{n_{po} - n_p}{\tau_n} + \frac{1}{q} \nabla \cdot \vec{j}_n + g(t) \qquad (109)$$

The change in signs arises because of the negative charge of electrons.

The electron and hole-current density arises from drift of carriers in an electric field and diffusion of carriers from a concentration gradient. If we assume that both processes go on independently. we can add the current densities to obtain

$$j_p(x,t) = qu_p pE - q D_p \nabla p \qquad (110)$$

and

$$j_n(x,t) = qu_n nE + q D_n \nabla n \qquad (111)$$

where the direction of the current densities is in each case the conventional direction.

The transient response of a diode is made up of two components, which are the depletion component and the diffusion-electric field component. The depletion component is normally referred to as a prompt photocurrent, which is produced by carriers generated in the junction depletion region. Since this component is collected in a few nanoseconds, it can essentially be treated as having no time delay with respect to the radiation pulse, i.e.,

$$i_p(t) = qAW_t g(t) \tag{112}$$

The diffusion-electric field component is a delayed component of photocurrent, $i_d(t)$, developing from the diffusion and drift of carriers generated in the bulk material. If we use a p+n junction, most of the delayed component originates in the lightly doped n-material. Using this assumption, the delayed photocurrent is given by

$$i_d(t) \approx qAu_p E\, p_n(x,t)\Big|_{x=-d_n} \qquad -qA\, D_p \frac{\partial p_n(x,t)}{\partial x}\Big|_{x=-d_n} \tag{113}$$

where the field and x direction are shown in figure 76.

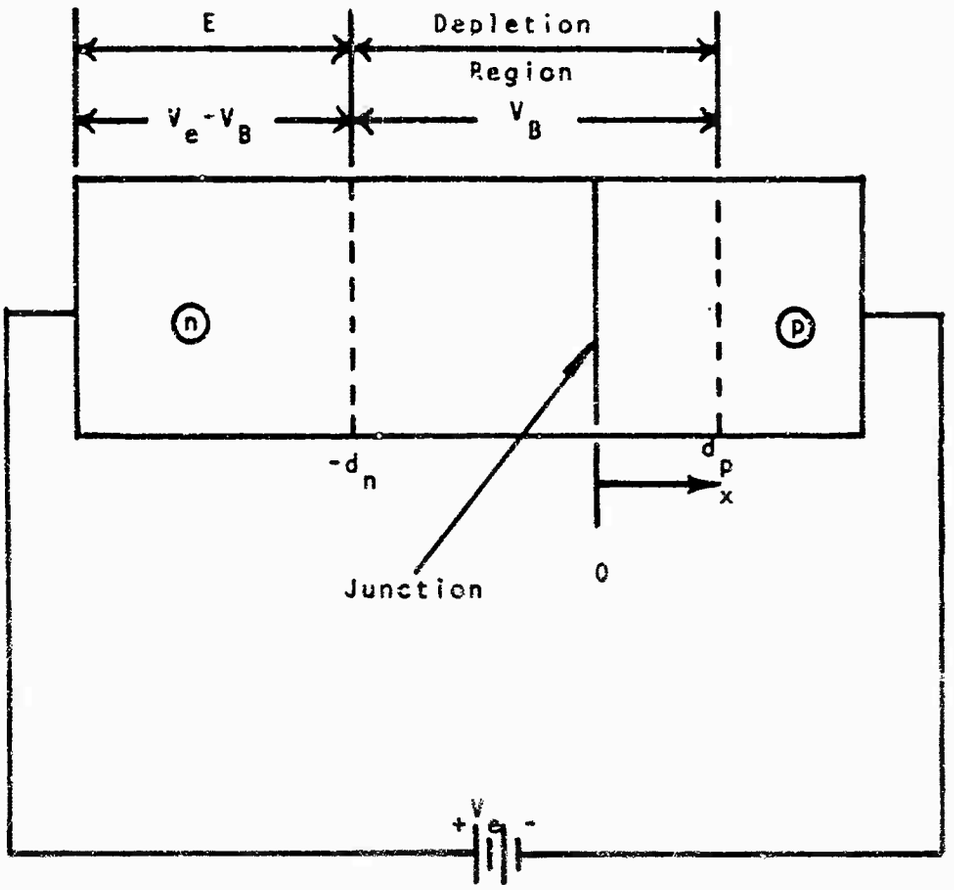

Figure 76. Physical Layout of a p-n Junction.

If one uses the boundary conditions

$$p_n(-d_n, t) = p_{no} e^{qv/kT} \approx 0 \tag{114}$$

and

$$\lim_{x \to -\infty} |p_n(x,t)| < \infty \tag{115}$$

equations (108) and (109) can be solved by use of Laplace transforms for a constant voltage V and an electric field E.

By using equation (110) one can write equation (108) as

$$\frac{\partial p_n(x,t)}{\partial t} = g(t) - \frac{p_n(x,t)-p_{no}}{\tau_p} - u_p E \frac{\partial p_n(x,t)}{\partial x} + D_p \frac{\partial^2 p_n(x,t)}{\partial x^2} \tag{116}$$

Taking the Laplace transform of equation (116) and rearranging terms, one obtains

$$\frac{\partial^2 P_n(x,s)}{\partial x^2} - \frac{u_p E}{D_p} \frac{\partial P_n(x,s)}{\partial x} - \frac{1}{D_p}\left(s + \frac{1}{\tau_p}\right) P_n(x,s) =$$

$$- \frac{1}{D_p}\left(p_n(x,0) + \frac{p_{no}}{s\tau_p} + G(s)\right) \tag{117}$$

By solving the auxiliary equation, one can solve for the complementary solution P_{nc}:

$$P_{nc}(x,s) = C_1 \exp\left(\frac{u_p E}{2D_p} + \sqrt{\left(\frac{u_p E}{2D_p}\right)^2 + \frac{1}{D_p}\left(s + \frac{1}{\tau_p}\right)}\right)(x+d_n) +$$

$$C_2 \exp\left(\frac{u_p E}{2D_p} - \sqrt{\left(\frac{u_p E}{2D_p}\right)^2 + \frac{1}{D_p}\left(s + \frac{1}{\tau_p}\right)}\right)(x+d_n) \tag{118}$$

Since $p_n(x,0) = p_{no} + p_{no}\left(\exp \frac{qV}{kT} - 1\right) \exp\left(\frac{x + d_n}{L_p}\right) \simeq$

$p_{no} - p_{no} \exp \frac{x + d_n}{L_p}$ for reverse bias (reference 16)

the particular solution $P_{np}(x,s)$ was assumed to be of the form

$$P_{np}(x,s) = C_3 + C_4 \exp\left(\frac{x + d_n}{L_p}\right) \tag{119}$$

Putting equation (119) into equation (117) and solving for C_3 and C_4, the particular solution can be written as

$$P_{np}(x,s) = \frac{P_{no}}{s} + \frac{G(s)}{s + \frac{1}{\tau_p}} - \frac{P_{no}}{s + \frac{u_p E}{L_p}} \exp\left(\frac{x+d_n}{L_p}\right) \tag{120}$$

The general solution can then be obtained as the sum of the particular and complementary solutions (equations 120 and 118). Applying the boundary condition given in equation (115) to the general solution, we find that C_2 is zero. Applying the boundary condition given in equation (114) to the general solution, we can solve for C_1 and obtain that

$$C_1 = \frac{-P_{no}}{s} - \frac{G(s)}{s + \frac{1}{\tau_p}} + \frac{P_{no}}{s + \frac{u_p E}{L_p}} \tag{121}$$

Retaining only the terms in the general solution that correspond to the radiation induced densities, one can show that the excess density due to radiation $\hat{P}(x,s)$ is given by

$$\hat{P}(x,s) = \frac{G(s)}{s + \frac{1}{\tau_p}} \left[1 - e^{\left(\frac{u_p E}{2D_p} + \sqrt{\left(\frac{u_p E}{2D_p}\right)^2 + \frac{1}{D_p}\left(s + \frac{1}{\tau_p}\right)}\right)(x + d_n)}\right] \tag{122}$$

Substituting equation (122) into the Laplace transform of equation (113) and adding the prompt photocurrent, we obtain

$$I_{pp}(s) = qAG(s)\left[W_t + \frac{u_p E}{2\left(s + \frac{1}{\tau_p}\right)} + \frac{\sqrt{D_p}\left(s + \frac{u_p^2 E^2}{4D_p} + \frac{1}{\tau_p}\right)^{1/2}}{\left(s + \frac{1}{\tau_p}\right)}\right] \tag{123}$$

where $I_{pp}(s)$ is referred to as the primary photocurrent. By assuming some form of the carrier generation rate, the inverse transform of $I_{pp}(s)$ can be solved. If we assume a pulse of magnitude g and duration t_o, $i_{pp}(t)$ is obtained as shown below, by neglecting the prompt component,

$$i_{pp}(t) = qAg\left[\frac{u_p E \tau_p}{2}\left(1 - e^{-t/\tau_p}\right) - \frac{u_p E \tau_p}{2} e^{-t/\tau_p} \operatorname{erf}\sqrt{\frac{u_p^2 E^2}{4D_p} t} + \sqrt{D_p \tau_p}\sqrt{\left(\frac{u_p^2 E^2}{4D_p} \tau_p + 1\right)} \operatorname{erf}\sqrt{\left(\frac{u_p^2 E^2}{4D_p} + \frac{1}{\tau_p}\right) t}\right]$$

$$0 \leq t \leq t_o \tag{124}$$

$$i_{pp}(t) = qAg\left[\frac{u_p E\tau_p}{2}\left(e^{-\left(\frac{t-t_o}{\tau_p}\right)} - e^{-t/\tau_p}\right) - \frac{u_p E\tau_p}{2}\right.$$

$$\left(e^{-t/\tau_p}\,\mathrm{erf}\sqrt{\frac{u_p^2E^2}{4D_p}\,t} - e^{-\left(\frac{t-t_o}{\tau_p}\right)}\,\mathrm{erf}\sqrt{\frac{u_p^2E^2}{4D_p}(t-t_o)}\right)$$

$$+\sqrt{D_p\tau_p}\,\sqrt{\left(\frac{u_p^2E^2}{4D_p}\,\tau_p + 1\right)}\left(\mathrm{erf}\sqrt{\left(\frac{u_p^2E^2}{4D_p} + \frac{1}{\tau_p}\right)t}\right.$$

$$\left.\left. - \mathrm{erf}\sqrt{\left(\frac{u_p^2E^2}{4D_p} + \frac{1}{\tau_p}\right)(t-t_o)}\right)\right] \quad t \geq t_o \ . \qquad (125)$$

If we let E = 0, equations (124) and (125) reduce to the previous result given by equation (47).

Using equation (123), a computer program was written to determine $i_{pp}(t)$ for different values of τ and E. The assumed values for the empirical constant were as follows: $A = 1 \times 10^{-3}$ cm^2 , $D_p = 6.5$ cm^2/sec , $u_p = 250$ cm^2/v sec $q = 1.6 \times 10^{-19}$ coulomb, and $g = 6 \times 10^{22}$ pairs/cm^3-sec. The generation rate g can be approximately calculated from the relation $g = 100\,\rho\dot{D} + 1.6 \times 10^{-12}\,\bar{e}$, where $\dot{D}$ = absorbed dose in R/sec, ρ = mass density in gm/cm^3 = 2.42 for silicon, and $\bar{e}$ is the average energy to form one electron-hole pair. Using these assumed parameter values, the theoretical results are plotted in figures 77 through 79.

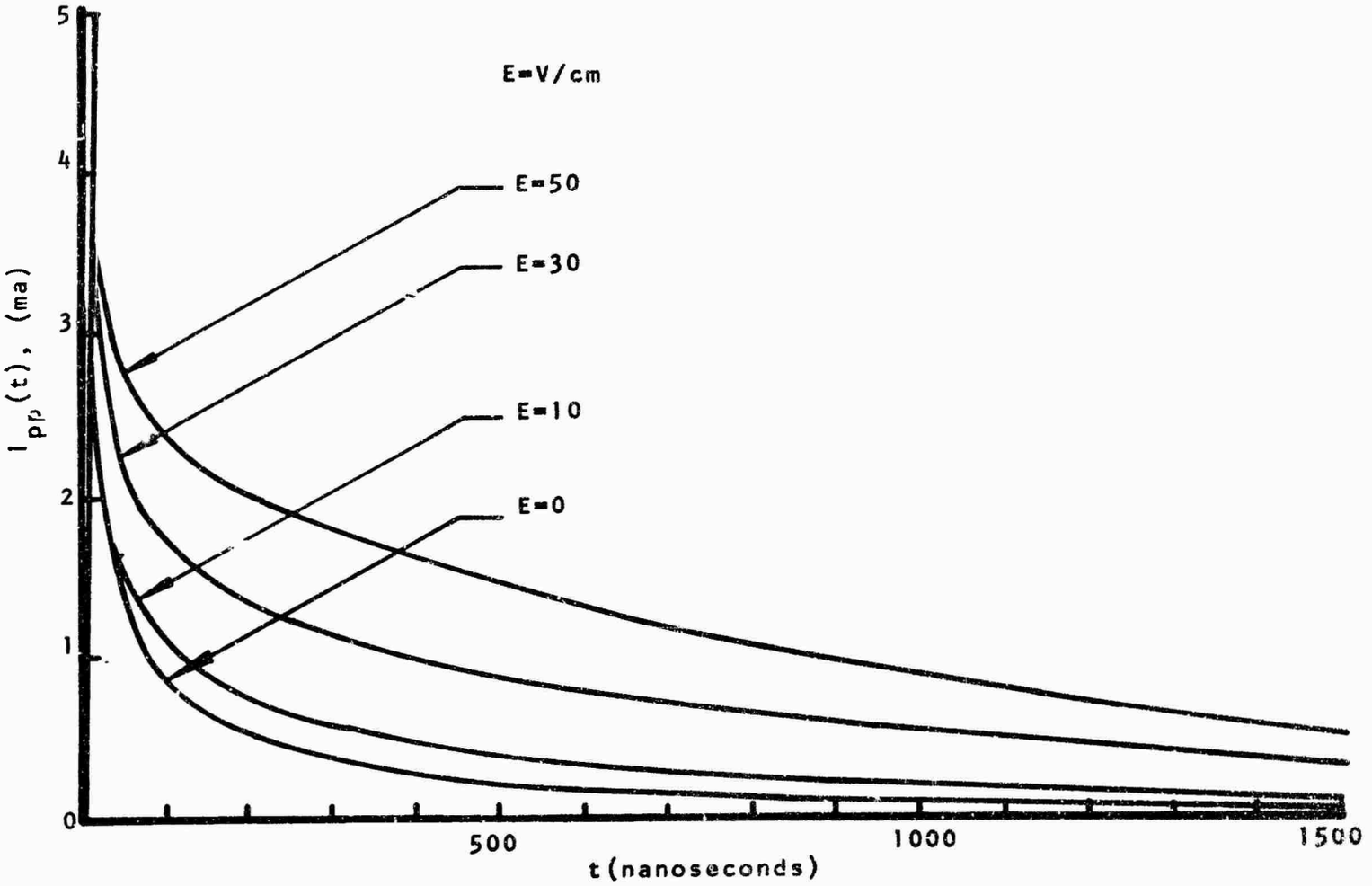

Figure 77. Theoretical Diode Primary Photocurrent for τ = 1,000 Nanoseconds

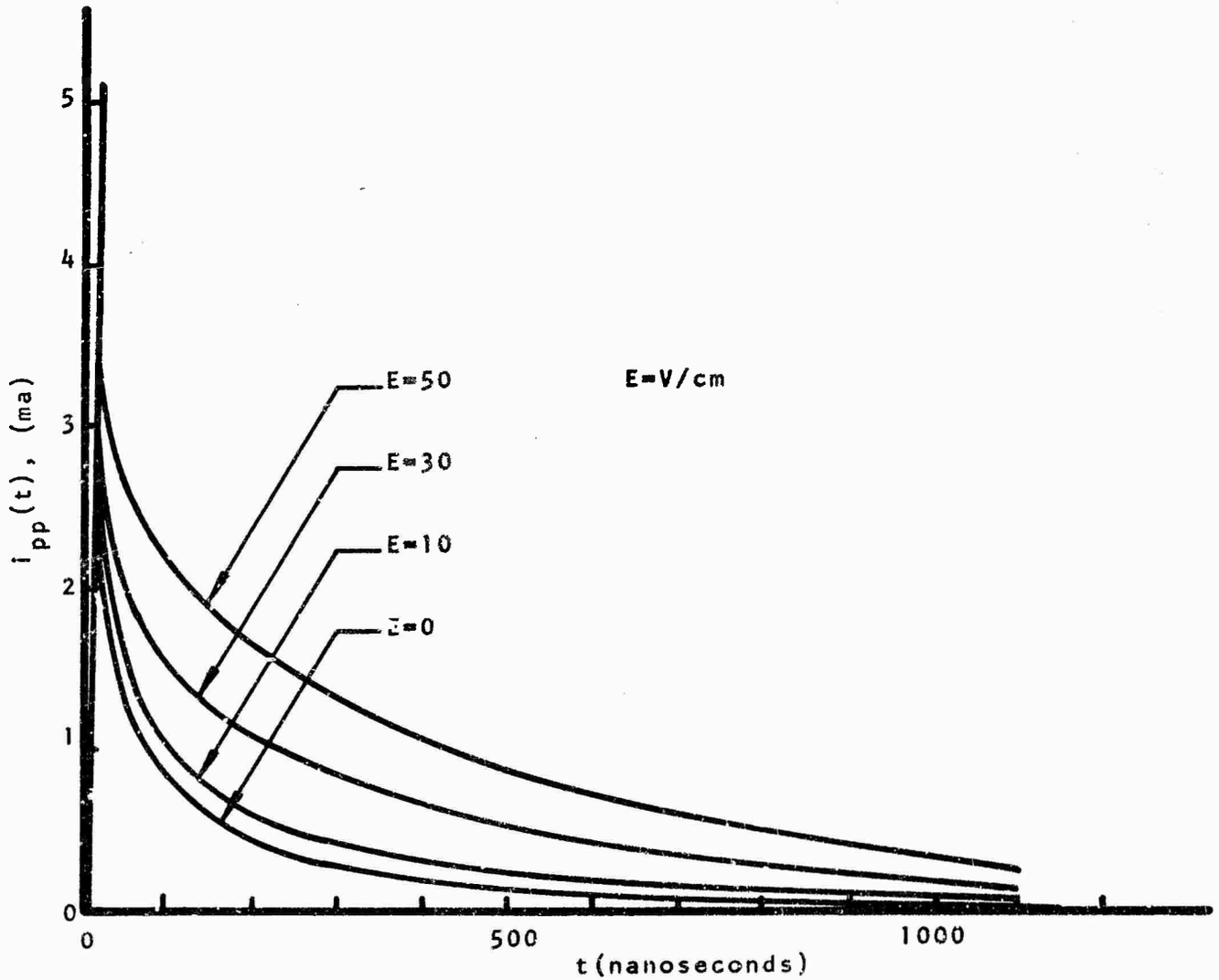

Figure 78. Theoretical Diode Primary Photocurrent for τ = 500 Nanoseconds

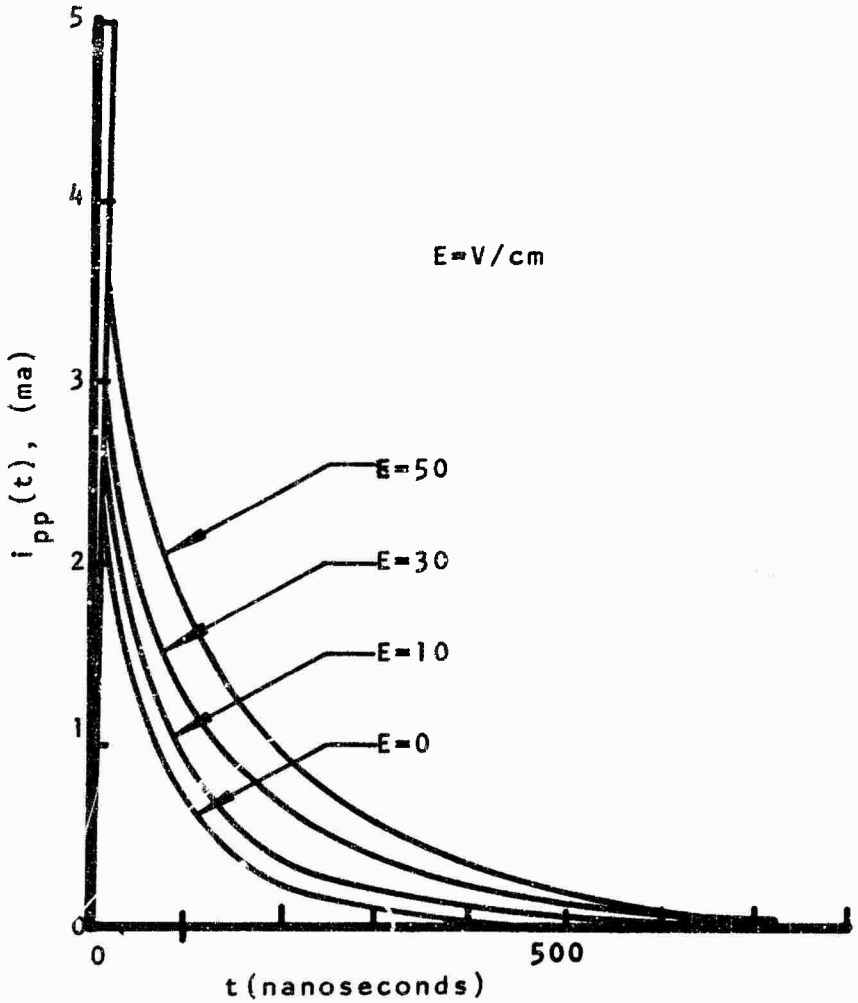

Figure 79. Theoretical Diode Primary Photocurrent for τ = 200 Nanoseconds

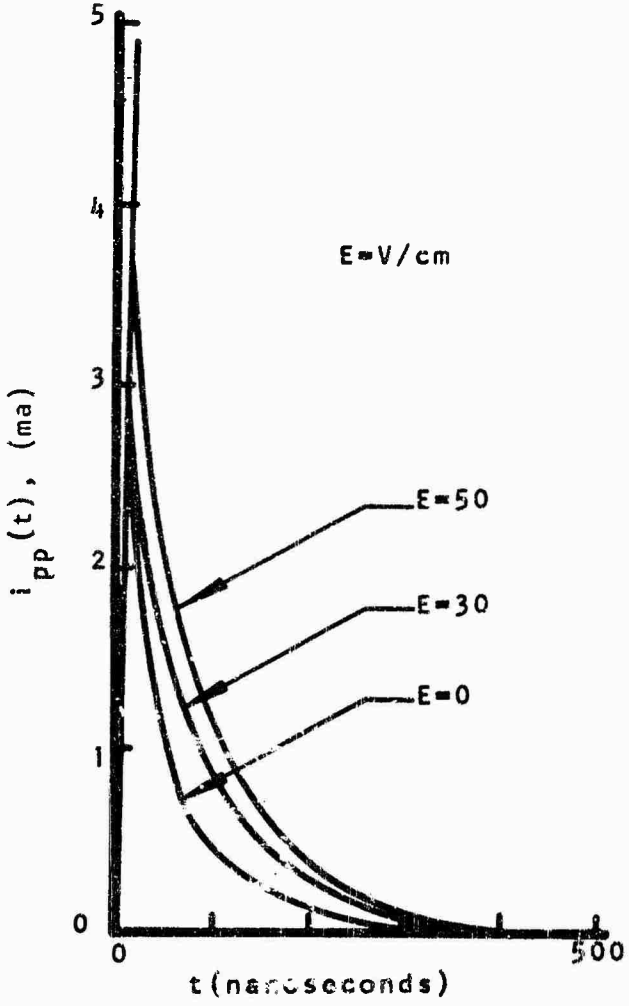

Figure 80. Theoretical Diode Primary Photocurrent for τ = 100 Nanoseconds

APPENDIX II

p-n JUNCTION DEPLETION CAPACITANCE

When a p-type material comes into intimate contact with an n-type material there is a transition region where the impurity concentration changes from one type to another. The behavior of this transition region is different for grown and fused types of construction.

If a p-type material and n-type crystals are brought into contact, there is a diffusion of holes near the junction into the n-type crystal due to the large concentration gradient for both carriers. However, the flow is only temporary and the diffused carriers recombine. But as the diffusion and recombination process continues, the diffusing electrons leave behind immobile, positively-charged acceptors. The tendency here is a buildup of an electric field. However, the electric field that develops from the diffusing of carriers is in a direction that opposes further carrier drainage. This field sets up a drift component of carriers that are in an opposite direction to the diffusion component. An equilibrium is finally reached so that the drift and diffusion components of both electrons and holes are equal and opposite.

Before the two regions were brought into contact, there was no net charge in either region. When the two regions are put together, the bulk region remains electrically neutral and a space charge region develops near the junction. If we

assume there is no voltage field in the bulk material, then all of the electric field lines must terminate in the depletion area. Thus the negative and positive charge volumes must be equal: that is

$$qAN_D d_n = qAN_A d_p \qquad (126)$$

where

q = the electronic charge

A = junction area

N_D = donor concentration in n-region

N_A = acceptor concentration in p-region

d_n = depletion width in n-region

d_p = depletion width in p-region

In figure 81, we have shown the impurity concentration, net charge density, electric field, and the electrostatic potential developed across the transition region for a p+n alloy junction (abrupt junction). As depicted in figure 81b, the space charge areas are equal and opposite with magnitudes N_A and N_D and widths d_p and d_n, respectively. These widths are an approximation, as we expect the space charge to gradually diminish, but the approximation closely describes the real case. The electric field as shown in figure 81c as a function of distance has a maximum at the junction, as the junction is between all the positive and negative charges (that is, the greatest number of field lines cross the junction). From the above discussion we see that upon the

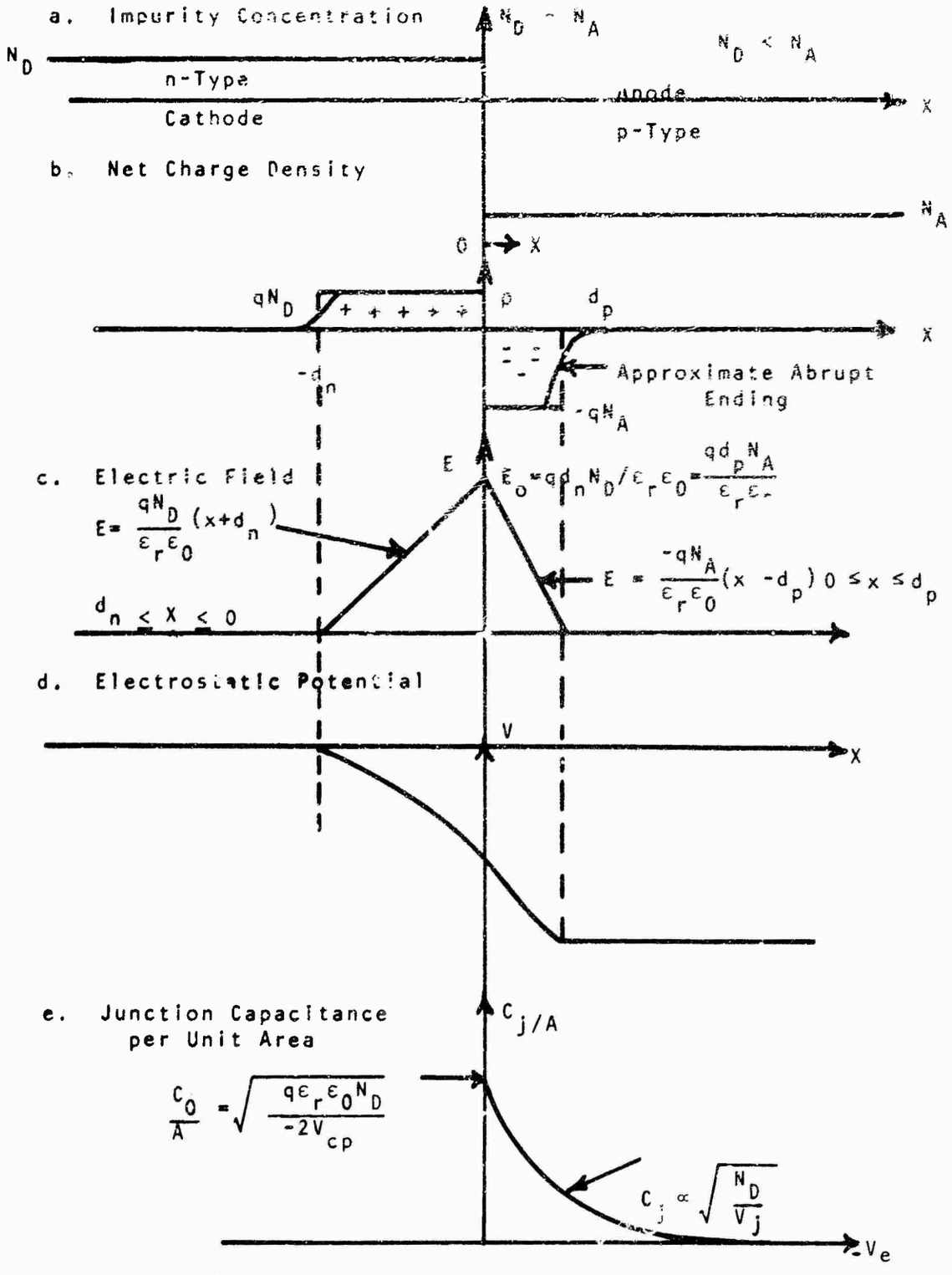

Figure 81. Abrupt Junction Capacitance Characteristics

forming of a junction there arises inherently a space charge region, an electric field, and a potential, and therefore the junction is pre-biased from its built-in contact potential. We know from the current equation that

$$j_n = \sigma_n E + qD_n \frac{\partial n}{\partial x} = nqu_n E + qD_n \frac{\partial n}{\partial x} \qquad (127)$$

Under equilibrium conditions this current must equal to zero; solving for E we obtain

$$E = -\frac{D_n}{u_n} \frac{1}{n} \frac{\partial n}{\partial x} \qquad (128)$$

Since the voltage is the negative integral of the field, the contact potential is given by

$$V_{CP} = -\int_{n\ side}^{p\ side} E \cdot dx = \frac{D_n}{u_n} \int \frac{1}{n} \frac{\partial n}{\partial x}\, dx = \frac{D_n}{u_n} \ln(n) \Big|_{n\ side}^{p\ side} = \frac{D_n}{u_n} \ln \frac{n_p}{n_n} \qquad (129)$$

where n_n is the free-electron concentration in the n-region, and n_p in the p-region. We know that at room temperature n_n is very nearly equal to the doping level N_D in the n-region and p_p is very nearly equal to doping level N_A in the p-region. We can therefore say that $n_p = \frac{n_i^2}{p_p} = \frac{n_i^2}{N_A}$. Using this expression for n_p and the Einstein relation $\frac{D_p}{u_p} = \frac{D_n}{u_n} = \frac{kT}{q}$, equation 129

can be written as

$$V_{CP} = - \frac{kT}{q} \ln \frac{N_D N_A}{n_i^2} \qquad (130)$$

where k = Boltzmann's constant = 1.38×10^{-23} joule/°K, T = temperature in degrees Kelvin, and q is the electronic charge = 1.60×10^{-19} coulomb. As we can see from equation (130), the contact potential depends on the impurity concentration and on the type of semiconductor ($n_i = 2.4 \times 10^{13}$ cm^{-3} for Ge and $n_i = 1.4 \times 10^{10}$ cm^{-3} for Si). It is also a negative value with reference to the n-side and its magnitude for silicon ranges from 0.5 to 0.7 volt at room temperature.

When we apply a reverse bias across the junction (it will be in the same direction as V_{CP}), we upset the bulk equilibrium condition, and the space charge region must widen further depending on the impurities concentration and the voltage applied. Employing Poisson's equation, we can interrelate the electric field, the potential, and the space charge density by

$$\frac{d^2V}{dx^2} = - \frac{dE}{dx} = \frac{- \text{ space charge density}}{\epsilon_r \epsilon_o} \qquad (131)$$

where ϵ_r is relative dielectric constant of the semiconductor, ϵ_o is permittivity of free space = 8.85×10^{-14} farad/cm, and we assume one-dimensional analysis. Since we are assuming that the concentration changes abruptly from a donor to an

acceptor, we can use constant impurity concentration on either side of the junction for calculation purposes. We can therefore carry the derivation in two columns (one for negative x and one for positive x) around x = 0 and add the resulting potentials together to get the total potential across the junction.

Negative x	Positive x	(132)
$\frac{d^2V}{dx^2} = \frac{-qN_D}{\epsilon_r \epsilon_o}$	$\frac{d^2V}{dx^2} = \frac{qN_A}{\epsilon_r \epsilon_o}$	

Integrating with respect to x, we obtain the electric field E as

$$\frac{dV}{dx} = -E = \frac{-qN_D}{\epsilon_r \epsilon_o} x + C_1 \qquad \frac{dV}{dx} = -E = \frac{-qN_A}{\epsilon_r \epsilon_o} x + C_2 \tag{133}$$

where C_1 and C_2 are integration constants. Since the electric field must go to zero at the edge of the depletion region, C_1 and C_2 can be evaluated and the equations above rewritten as

$$\frac{dV}{dx} = -E = \frac{-qN_D}{\epsilon_r \epsilon_o} (x + d_n) \qquad \frac{dV}{dx} = -E = \frac{qN_A}{\epsilon_r \epsilon_o} (x - d_p) \tag{134}$$

This equation for E gives the characteristic for E as shown in figure 81c, where the bulk of the n-type region is used as a reference. The electrostatic potential can be obtained by integrating once more and expressed as

$$V = \frac{-qN_D}{\epsilon_r \epsilon_o}\left(\frac{x^2}{2} + d_n x\right) + C_3 \qquad V = \frac{qN_A}{\epsilon_r \epsilon_o}\left(\frac{x^2}{2} - d_p x\right) + C_4 \tag{135}$$

Since the voltage must be continuous across the junction, C_3 must equal to C_4. The voltages, V_n and V_p, evaluated at $-d_n$ and d_p are given by

$$V_n = \frac{qN_D d_n^2}{2\epsilon_r \epsilon_o} + C_3 \qquad V_p = \frac{-qN_A d_p^2}{2\epsilon_r \epsilon_o} + C_3 \tag{136}$$

The total voltage across the junction V_j with reference to the bulk n-region is found by subtracting V_p from V_n and can be written as

$$V_j = V_p - V_n = \frac{-q}{2\epsilon_r \epsilon_o}\left(N_A d_p^2 + N_D d_n^2\right) \tag{137}$$

where V_j is composed of the contact potential V_{CP} and the externally applied voltage V_e (i.e., $V_j = V_{CP} + V_e$). Using the relation given in equation (126) and equation (137) we can solve for d_n and d_p;

$$d_n = \sqrt{\frac{-2\epsilon_r \epsilon_o V_j}{q}\left(\frac{N_A/N_D}{N_A+N_D}\right)} \tag{138}$$

and

$$d_p = \sqrt{\frac{-2\epsilon_r \epsilon_o V_j}{q}\left(\frac{N_D/N_A}{N_A+N_D}\right)} \tag{139}$$

Since the full width w of the depletion area is the sum of d_n and d_p we obtain

$$w = d_n + d_p = \sqrt{\frac{-2\epsilon_r\epsilon_o V_j}{q(N_A+N_D)}}\left(\sqrt{\frac{N_A}{N_D}} + \sqrt{\frac{N_D}{N_A}}\right) \qquad (140)$$

Equation (140) shows that when the bias is negative, the depletion region widens across the junction with respect to the bulk n-region (that is, the junction depletion region widens if reverse biased and narrows when the junction is forward biased). In a special case of doping as encountered in a p+n junction, $N_A >> N_D$, and equation (140) reduces to

$$w \approx \sqrt{\frac{-2\epsilon_r\epsilon_o V_j}{q}\frac{N_A}{N_D(N_A+N_D)}} \approx \sqrt{\frac{-2\epsilon_r\epsilon_o V_j}{qN_D}} \qquad (141)$$

This implies that in a p+n junction, the depletion region expands almost entirely into the lightly doped side as illustrated in figure 81. The depletion can be visualized as a parallel plate capacitor. That is, for small changes in bias voltage we are just adding charges at the boundary. The incremental junction capacitance C_j per unit area $(\frac{dQ}{dV_T})$ can be expressed with use of equation (140) as

$$\frac{C_j}{A} = \frac{1}{A}\frac{dQ}{dV_j} = \frac{\epsilon_r\epsilon_o}{w} = \sqrt{\frac{\epsilon_r\epsilon_o q(N_A+N_D)}{-2(V_e+V_{CP})}}\Bigg/\left(\sqrt{\frac{N_A}{N_D}} + \sqrt{\frac{N_D}{N_A}}\right) \qquad (142)$$

or for a p+n junction $(N_A >> N_D)$,

$$\frac{C_j}{A} \approx \sqrt{\frac{q\epsilon_r\epsilon_o(N_A+N_D)N_D}{-2(V_e+V_{CP})N_A}} \approx \sqrt{\frac{q\epsilon_r\epsilon_o N_D}{-2(V_e+V_{CP})}} \qquad (143)$$

where V_e and V_{CP} are measured with respect to the n-side. With this terminology, V_{CP} will always be negative and V_e is negative for a reverse biased junction and positive for a forward biased junction. However, in a forward biased case, V_e will not exeed V_{CP}, and therefore w will not go to zero or C_j to infinity. From equations (142) and (143) it would seem possible to plot $1/C_j^2 = 0$. However, this is not possible, as in any electrical measurement there is the problem of stray capacitances. In reality the junction capacitance is given by

$$C_m = A\sqrt{\frac{\epsilon_r\epsilon_o qN_D}{-2(V_e+V_{CP})}} + C_s \qquad (144)$$

where C_m is the small signal measured capacitance and C_s is the stray capacitance. In equation (144) there are four unknowns, A, N_D, V_{CP}, and C_s. If we let $k = -2/\epsilon_r\epsilon_o qN_D$, equation (144) reduces to three unknowns. By measuring the junction capacitance at three d-c bias voltages, equation (144) represents three equations given by

$$\frac{1}{(C_{m_1}-C_s)^2} = k(V_{e_1} + V_{CP}) \qquad (145)$$

$$\frac{1}{(C_{m_2}-C_s)^2} = k(V_{e_2} + V_{CP}) \qquad (146)$$

$$\frac{1}{(C_{m_3}-C_s)^2} = k(V_{e_3} + V_{CP}) \tag{147}$$

After subtracting equation (145) from (146) and equation (147) from (146) we obtain, after rearranging,

$$\frac{\frac{1}{(C_{m_2}-C_s)^2} - \frac{1}{(C_{m_1}-C_s)^2}}{V_{e_2} - V_{e_1}} = k = \frac{\frac{1}{(C_{m_3}-C_s)^2} - \frac{1}{(C_{m_2}-C_s)^2}}{V_{e_3} - V_{e_2}} \tag{148}$$

If we require that $V_{e_3} - V_{e_2} = V_{e_2} - V_{e_1}$, then equation (148) reduces to a cubic equation in the stray capacitance expressed as

$$C_s^3 + \left[\frac{(C_{m1}^2 - 2C_{m2}^2 + C_{m3}^2 - 4C_{m1}C_{m2} - 4C_{m2}C_{m3} + 8C_{m3}C_{m1})}{4C_{m2} - 2C_{m1} - 2C_{m3}}\right] C_s^2$$

$$+ \left[\frac{(C_{m1}C_{m2} + C_{m2}C_{m3} - 2C_{m3}C_{m1})(C_{m1} + C_{m2} + C_{m3})}{2C_{m2} - C_{m1} - C_{m3}}\right] C_s$$

$$+ \frac{2C_{m1}^2C_{m3}^2 - C_{m1}^2C_{m2}^2 - C_{m2}^2C_{m3}^2}{4C_{m2} - 2C_{m1} - 2C_{m3}} = 0 \tag{149}$$

The solution to the cubic equation was solved in a computer program for the various diodes, and the root which satisfied physical considerations was chosen (reference 28).

Knowing C_s, k can be evaluated from equation (148). With this value of k, V_{CP} is computed from equation (145), that is,

$$V_{CP} = \frac{1}{k(C_{m_1} - C_s)^2} - V_{e_1} \qquad (150)$$

By making a plot of the reverse current versus the reverse voltage across the diode past breakdown, the breakdown voltage V_B can be obtained by extrapolating the value of voltage to zero current. Using this value of V_B, the impurity concentration N_D can be obtained from the data of McKay and Miller (references 5,6,7, and 8). For voltages greater than 10 volts, the impurity concentration can be related to the avalanche breakdown voltage by the equation

$$N_D = \frac{3.49 \times 10^{18}}{V_B^{1.43}} \qquad (151)$$

Using the above obtained value of N_D (from equation 151) and k (from equation 148), the value of A can be computed. The results obtained by the above methods compared favorably with those obtained from a destructive measurement.

REFERENCES

1. International Rectifier Corp., International Rectifier Corporation Zener Diode Handbook, El Segundo, California, May 1961.

2. Gibbons, James F., Semiconductor Electronics, McGraw-Hill Co., Inc., New York, 1966.

3. Phillips, Alvin B., Transistor Engineering and Introduction to Integrated Semiconductor Circuits, McGraw Hill Co., Inc., New York, 1962.

4. Miller, S. L. and Ebers, J. J., "Alloyed Junction Avalanche Transistors," Bell System Technical Journal, Vol. 34, No. 5, September 1955, pp. 883-902.

5. McAfee, K. B. and McKay, K. G., "Electron Multiplication in Silicon and Germanium," Physical Review, Vol. 91, No. 5, September 1, 1953, pp. 1079-1084.

6. McKay, K. G., "Avalanche Breakdown in Silicon," Physical Review, Vol. 84, No. 4, May 15, 1964, pp. 877-884.

7. Miller, S. L., "Ionization Rates for Holes and Electrons in Silicon," Physical Review, Vol. 105, 1957, p. 1246.

8. Miller, S. L., "Avalanche Breakdown in Germanium," Physical Review, Vol. 99, No. 4, August 15, 1955, pp. 1234-1235.

9. Motorola, Inc., "High Speed Switching Transistor Handbook," Semiconductor Products Division, Phoenix, Arizona, 1963.

10. Millman, Jacob and Taub, Herbert, Pulse Digital and Switching Waveforms, McGraw-Hill Co., Inc., New York, 1965.

11. Hamilton, D. J., Griffith, P. G. and Saver, F. H., "Avalanche Transistor Circuit for Generating Rectangular Pulses," Electronic Engineering, December 1962, pp. 808-812

12. Bell, Brian, H., Avalanche Circuits are More Versatile Than You Think, National Semiconductor Corp., June 8, 1964.

13. Battelle Memorial Institute, TREES Handbook, D.C.Jones, ed., Prepared for DASA, February 28, 1964.

14. van Lint, V. A. J., Mechanisms of Transient Radiation Effects, GA-4320, General Atomics, San Diego, 1963.

15. Shockley, Wm., Electron and Holes in Semiconductors, D. Van Nostrand Co., Inc., New York, 1963.

16. Middlebrook, R. D., An Introduction to Junction Transistor Theory, John Wiley and Sons, Inc., New York, 1965.

17. Cates, H. T., Transient Radiation Effects on Resistors, Report EE-118, University of New Mexico Bureau of Engineering Research, November 1964.

18. Byatt, W. J. and Cates, H. T., Transient Gamma Radiation Effects on Resistive and Insulating Materials, Report EE-112, University of New Mexico Bureau of Engineering Research, 1964.

19. Rogers, S. C. and Wirth, J. L., The Transient Response of Transistors and Diodes to Ionizing Radiation, SC-R-64-194, Sandia Corporation, July 1964.

20. Brown, W. L., Nuclear Electronics Effects Program Fifth Triannual Report, Bell Telephone Laboratories, Inc., November 1960.

21. van Lint, V. A. J., et al., The Effects of Pulsed Gamma Radiation on Dynamic Electronic Components, RTD TDR-63-3110 General Atomics, San Diego, 1964.

22. Caldwell, R. S., Gage, D. S. and Hanson, G. H., The Transient Behavior of Transistors Due to Ionizing Radiation Pulses, D2-90171, Boeing Co., 1962.

23. Keister, G. L., et al., Manual for Circuit Analysis and Design, TRE WL-64-60, Vol. 1, Boeing Co., July 1964.

24. Warner, R. M., Jr. and Fordemwalt, J. N., eds., Integrated Circuits, McGraw-Hill Co.,Inc., New York, 1965.

25. Lindmayer, Joseph and Wrigley, Charles Y., Fundamentals of Semiconductor Devices, D. Van Nostrand Co., Inc., Princeton, New Jersey, 1965.

26. Keister, G. L., et al., Analytic Methods for Predicting Transient Nuclear Radiation Effects on Electronics Circuits and Devices, RTD TDR-63-3007, Boeing Co., July 1963.

27. Shockley, William, "Problems Related to p-n Junctions in Silicon," Solid State Electronics, Vol. 2, January 1961.

28. Hood, Jerry A., The Effect of Nuclear Radiation on Oxidized Silicon Surface, Technical Report EE-138, University of New Mexico Bureau of Engineering Research, December 1966.

29. Hood, Jerry A., Predicting Current Gain Degradation in n-p-n Silicon Transistors after Irradiation by High-Energy Neutrons, Report No. SC-TM-64-69, Sandia Laboratory, Albuquerque, New Mexico, March 1964.

30. Gregory, B. L. and Smits, F. M., "A Comparison of Radiation Tolerance of Field Effect and Bipolar Transistors," IEEE Transactions on Electron Devices, Vol. ED-12, No. 5, May 1965, pp. 254-258.

UNCLASSIFIED

Security Classification

DOCUMENT CONTROL DATA - R & D

(Security classification of title, body of abstract and indexing annotation must be entered when the overall report is classified)

1. ORIGINATING ACTIVITY (Corporate author) University of New Mexico Bureau of Engineering Research Albuquerque, New Mexico 87106	2a. REPORT SECURITY CLASSIFICATION UNCLASSIFIED 2b. GROUP

3. REPORT TITLE

COMPENSATION AND AVALANCHE TECHNIQUES FOR TREE HARDENING, Vol II, Nuclear Damage on Avalanche Transistors and Diodes

4. DESCRIPTIVE NOTES (Type of report and inclusive dates)

15 November 1966-14 September 1967

5. AUTHOR(S) (First name, middle initial, last name)

Harold T. Cates; W. W. Grannemann; L. T. Boatwright; Goebel Davis, Jr.

6. REPORT DATE April 1969	7a. TOTAL NO. OF PAGES 220	7b. NO. OF REFS 30
8a. CONTRACT OR GRANT NO F29601-67-C-0017 b. PROJECT NO. 5710 c. Subtask No. 16.027 d.	9a. ORIGINATOR'S REPORT NUMBER(S) AFWL-TR-67-95, Vol II 9b. OTHER REPORT NO(S) (Any other numbers that may be assigned this report)	

10. DISTRIBUTION STATEMENT This document is subject to special export controls and each transmittal to foreign governments or foreign nationals may be made only with prior approval of AFWL (WLDE), Kirtland AFB, NM, 87117. Distribution is limited because of the technology discussed in the report.

11. SUPPLEMENTARY NOTES	12. SPONSORING MILITARY ACTIVITY AFWL (WLDE) Kirtland AFB, NM 87117

13. ABSTRACT

(Distribution Limitation Statement No. 2)

An analytical model to describe the behavior of a forward biased or reverse biased (including avalanche breakdown) diode in a transient X-ray environment is developed. The calculated results are compared with experimental results. The avalanche multiplication phenomenon is related to the physical parameters of the device. Equivalent circuits for the device under irradiation are developed. The basic theory of avalanche transistor operation is reviewed and the critical design factors for operation of an avalanche circuit in a radiation environment are discussed. The circuits were tested in the range from 10^6 R/sec to over 10^{10} R/sec. Circuits were tested with and without different types of junction compensations. Avalanche diodes and transistors were also irradiated in a neutron environment. Some of the diodes and transistors were still functioning properly at doses of 8.6×10^{15} nvt. An avalanche circuit was shown to be relatively insensitive to a neutron environment after exposure to neutron fluence in excess of 10^{15} n/cm^2.

DD FORM 1 NOV 65 1473

UNCLASSIFIED

Security Classification

14 KEY WORDS	LINK A		LINK B		LINK C	
	ROLE	WT	ROLE	WT	ROLE	WT
Radiation effects on electronics Avalanche diodes Avalanche transistors Circuit hardening to radiation Hardening of electronic components						